Validation of the Use of Low Enriched Uranium as a Replacement for Highly Enriched Uranium in US Submarine Reactors

by

Brendan Patrick Hanlon

B.S., Physics (2013)
United States Naval Academy

Submitted to the Department of Nuclear Science & Engineering
in partial fulfillment of the requirements for the degree of

Master of Science in Nuclear Science and Engineering

at the

MASSACHUSETTS INSTITUTE OF TECHNOLOGY

June 2015

Author .....
Department of Nuclear Science & Engineering
May 19, 2015

Certified by .....
R. Scott Kemp
Assistant Professor, Department of Nuclear Science & Engineering
Thesis Supervisor

Certified by .....
Benoit Forget
Associate Professor, Department of Nuclear Science & Engineering
Thesis Reader

Accepted by .....
Mujid S. Kazimi
TEPCO Professor of Nuclear Engineering
Chair, Department Committee on Graduate Students

Validation of the Use of Low Enriched Uranium as a Replacement for Highly Enriched Uranium in US Submarine Reactors

by

Brendan Patrick Hanlon

Submitted to the Department of Nuclear Science & Engineering
on May 19, 2015, in partial fulfillment of the
requirements for the degree of
Master of Science in Nuclear Science and Engineering

Abstract

The US Navy has long used highly enriched uranium (HEU) in naval reactors for a variety of technical reasons. In a series of studies, the Department of Naval Reactors determined that switching to low enriched uranium (LEU) was impossible using current fuel designs, but may be possible with a dedicated program to investigate new fuel materials. This thesis simulated an HEU fueled submarine reactor using a uranium oxide-zirconium dispersion fuel, and compared it to an LEU reactor using a uranium-molybdenum alloy fuel. The required energy output of an attack submarine was used to set the burnup requirement of the HEU (333 MWd/kg) and LEU (93.5 MWd/kg) fueled reactors, and each reactor was depleted to the end of life. The results showed that naval reactors could be switched to LEU without sacrificing the lifetime submarine core or increasing reactor volume. Even if unstudied technological details render this impossible, an LEU core would require only a single refueling over the life of an attack submarine. This would necessitate a 3.25% increase in submarine fleet size, which is small compared to the average Department of Defense project cost overrun.

Thesis Supervisor: R. Scott Kemp
Title: Assistant Professor, Department of Nuclear Science & Engineering

Thesis Reader: Benoit Forget
Title: Associate Professor, Department of Nuclear Science & Engineering

Acknowledgments

Primarily, I would like to thank R. Scott Kemp, my thesis adviser, for not only starting me on the road that led to this thesis, but for his constant and consistent encouragement, patience, and support that have helped me to accomplish something I am truly proud of. I can't imagine having a better mentor and adviser for a research project.

I'd also like to thank Benoit Forget for providing more guidance than has ever been required of a thesis reader. It was his constant push to add "just one more thing" that, I think, made this thesis complete.

Thanks are also due to Stephanie MacDougall for reading my thesis, "Just one more time, I promise!" Her work catching my myriad errors and insisting I use real words was an unanticipated but invaluable aid to creating a readable document.

I would never have been able to make it to this point without the unending support of professors, teachers, and mentors at the MIT Nuclear Engineering Department, the United States Naval Academy Physics Department, and Lake Oswego High School. Thank you for keeping my curiosity alive, and always challenging me to reach for the next step.

Finally, I'd like to thank my family. My parents, Roger and Jacinta, for their bottomless love and endless sacrifices, which have made me the person I am today. And my brother, Dónal, for (in the early years) putting up with me and (later) for refusing to allow me to become complacent with what I've achieved. I can't wait to read your thesis in a few years.

Disclaimer

The opinions expressed herein are those of the author, and are not necessarily representative of official policies or positions of the Department of Defense, the United States Navy, or any other affiliate of the United States Government.

The information contained herein is derived entirely from open source material. No aspect of this project was informed by access to classified information of any level.

Contents

List of Figures

List of Tables

Chapter 1

Introduction and Background

The United States Navy has been using nuclear power since the earliest days of the technology. The first US commercial nuclear power plant at Shippingport was a scaled up version of the pressurized water reactor that had been installed on the USS Nautilus a few years earlier [1, p.50]. In the years since, the Navy has operated over 100 nuclear reactors to steam over 130 million miles. The Navy has fully embraced nuclear powered aircraft carriers and submarines [2, p.1]. However, the United States is no longer producing the highly enriched uranium (HEU) that it uses to fuel naval nuclear vessels. Current estimates put the Navy's HEU stockpile around 152 MT [3, p.11]. The estimated lifetime of this stockpile is debatable due to the classified nature of many nuclear fuel details. By estimates covered in section 1.2.1, the Navy has already allocated approximately 100 MT of fuel to current shipbuilding programs. If this is the case, it will be vital for the Navy to pursue options for fueling future nuclear ships. There are significant technological and international concerns with the renewed production of HEU. Any solution that the Navy chooses to embrace should address both the Navy's fuel requirements and the international community's desire to reduce stockpiles of weapon-usable fissile material and prevent new enrichment of HEU. Provided it is technologically feasible, the best way that the Navy can address all parts of this issue is through the development of a low enriched uranium (LEU) fuel for naval reactors.

1.1 History

The US Navy initially became interested in nuclear power for its applications in submarines [1, p.45]. Nuclear power eliminated endurance issues faced by diesel submarines. Nuclear power also allowed submarines to be optimized for underwater performance [1, p.45]. The Navy initially investigated both sodium cooled fast reactors (SFR) and pressurized water reactors (PWR) submarines [4, p.2]. While the fast reactor offered advantages due to sodium's

superior thermal properties, the chemistry challenges of using sodium coolant caused the Navy to abandon fast reactors by 1957 [5, p.272-274]. Other than the prototype USS *Seawolf* (SSN-575),[1] all US nuclear powered naval vessels have used PWRs [1, p.48].

The Navy's choice of the PWR was motivated by the design's inherent compactness. To further reduce reactor size and extend lifetime, the Navy chose to use HEU fuel [6, p.1]. Nuclear refueling overhauls are a long, costly process, lasting one to two years for a submarine or three to four years for an aircraft carrier [6, p.4].[2] Over the last 60 years, the Navy has been able to extend reactor lifetimes from 2 to 33 years. The reactor on the Ohio Replacement class ballistic missile submarine is planned to last for the entire 40-year life of the boat [7, p.ii].

While the nuclear aircraft-carrier program had a rocky start, the first was delivered in 1961 and the Navy has built almost exclusively nuclear carriers since [1, p.50].[3] Experiments with other nuclear powered surface ships were less successful. Most were retired early because they were not cost effective [8, p.36]. Otherwise, the Navy has been satisfied with nuclear power over the last 60 years. Testifying before Congress in 2003, then Director of Naval Reactors Admiral Frank Bowman said that nuclear power provides "high speed, virtually unlimited endurance, worldwide mobility, and unmatched operational flexibility" [9].

The Navy's initial decision to use HEU was based on optimizing core size and lifetime [1, p.47]. In the 1950/60s, this was a technological choice with few political implications. Since then, nuclear nonproliferation has become a major international concern, bringing scrutiny to large stockpiles of plutonium and HEU. For example, the Navy's stockpile of 150 MT of HEU represents thousands of potential warheads to non-proliferation experts, as only about 25 kg of HEU is required to make a simple, first-generation nuclear weapon [10, p.78]. As the United States and Russia slowly reduce their nuclear weapons arsenals, the potential weapon applications of naval fuel grow in relative significance, as it could be used to manufacture a large number of weapons in violation of treaty obligations. This capability has led policymakers to focus on eliminating naval HEU stockpiles in recent years.

International concern over the spread of nuclear weapons led to the signing of the Treaty on the Non-Proliferation of Nuclear Weapons in the late 1960s. As a compromise with non-nuclear-weapons states, the treaty explicitly left many nuclear activities in its category of "acceptable uses," including civi nuclear power. In return, the International Atomic Energy

[1]The *Seawolf* used an SFR, but experienced so many problems that it was converted to a PWR early in its service life [1, p.49].

[2]Part of the reason that the process is so long is that it usually coincides with major refit periods. Section 6.2 attempts to estimate how much of this time is spent on refueling the reactor.

[3]The original nuclear aircraft carrier program was canceled under President Eisenhower, and reincarnated as the Shippingport reactor project in 1954 [1, p.50]. The program was eventually restarted with the USS *Enterprise* (CVN-65).

Agency (IAEA) would have the obligation and authorization to safeguard these activities [11, p.108]. However, the treaty left open a loophole that allows non-nuclear-weapons states to withdraw HEU from IAEA safeguards for "military purposes other than weapons" [12, p.2]. The continued normative use of HEU in military naval reactors provides a pathway for nations to produce HEU outside of safeguards, which could then be used for nuclear weapons. While no nation has used this strategy, the possibility worries non-proliferation experts [13, p.1]. Iran's recent interest in naval nuclear power has convinced some that this is another attempt for Iran to obtain nuclear weapons [13, p.1]

The Fissile Material Cutoff Treaty (FMCT) pursued by many in the international community could close this loophole, while addressing other concerns. The treaty could impose more stringent controls on fissile material to restrict the ability of nations to assemble nuclear weapons [14, p.43]. However, an example draft of an FMCT, submitted by the US in 2006, explicitly stated that HEU produced for military purposes in the past would not be subject to international safeguards [14, p.42]. Nations such as the United States that use HEU fuel in naval vessels are concerned that international inspections of naval reactors would compromise classified design information. An FMCT proposal drafted by the International Panel on Fissile Materials (IPFM) in 2009 eliminated the safeguards loophole entirely. As a compromise, the IPFM attempted to develop a safeguards inspection method that would satisfy treaty requirements while maintaining state secrets, similar to methods used to inspect nuclear weapons [10, p.77]. There has been little progress on an FMCT since then, despite President Obama's nominal support of the treaty during his time in office [15].

1.2 Navy HEU Stockpile Concerns

The United States began uranium enrichment in the 1940s. In total, it enriched about 850 MT of HEU, mostly in the mid 1960s [16, p.28]. Weapons enrichment ended then, but the US continued producing HEU for naval fuel until 1992 [16, p.9]. In an attempt at transparency, the US published a series of inventory reports from 1996 through 2004 containing official histories of production and use of HEU [16, p.28]. These reports combined HEU used for nuclear explosions and naval fuel into a single "military" category. When nuclear testing stopped in 2004, the government stopped publishing the reports, as it would have revealed specifics of Navy fuel utilization [16, p.31].

Since the government stopped providing information on the HEU stockpile, the IPFM has attempted to track it in their yearly Global Fissile Material Report, shown in table 1.1. In 2005, the United States declared 200 MT of HEU excess to military purposes, and began blending down to LEU. Some of this was placed in reserve for naval fuel instead [16, p.34].

Table 1.1. International Panel on Fissile Materials Estimates of the United States' HEU Stockpile

	US HEU Stockpile (MT)						
	Military	Naval (Fresh)	Naval (Spent)	Civilian Material	Excess	Eliminated	Total
2006 [14, p.15][1]	310	180	-	-	100	-	590
2007 [17, p.10][2]	250	228	-	30	146	-	654
2008 [10, p.11]	250	128	100	30	137	96	741
2009 [18, p.13]	250	128	100	30	109	124	741
2010 [16, p.12]	260	130	100	20	104	131	745
2011 [19, p.9]	260	130	100	20	100	135	745
2013 [3, p.11]	260	152	100	20	63	141	736

[1] In 2006, the IPFM reported United States HEU stockpiles in only three categories: Weapons, Naval+, and Excess.

[2] In 2007, the IPFM reported United States HEU stockpiles in only four categories: Weapons, Naval (fresh and irradiated), Civilian Material, and Excess.

[3] The IPFM did not publish a Global Fissile Materials Report for 2012 or 2014.

In response to the availability of excess weapons material, the Navy transitioned from its traditional use of 97.3% enriched HEU to the 93% enriched HEU available from weapons stocks [7, p.ii][16, p.30][20, p.91]. Between the transfer of excess HEU and fuel enriched for the Navy, naval reserves of HEU are estimated at 152 MT as of 2013 [3, p.18]. Judging from the past, it is likely that the Navy could also acquire a portion of the 63 MT of the excess HEU remaining for blending down (depending on how much is enriched highly enough), or more of the military stocks that may be declared excess in the future [3, p.18].

The Navy currently has four programs drawing significant amounts of fuel from the stockpile: the refueling of the final five Nimitz class carriers, construction of Virginia class fast attack submarines, construction and eventual refueling of Gerald Ford class carriers, and planned construction of the Ohio Replacement ballistic missile submarines [21, p.10]. There are also smaller projects such as fuel testing and prototype reactor construction that consume fuel, but for this analysis they will be ignored, as they require much less fuel than active shipbuilding programs.

1.2.1 Estimating HEU Consumption

The exact weight of HEU in a naval reactor core is a debated topic in the open source literature. The Navy's keeps this information classified. There is general agreement on the size of a fast attack submarine core at roughly 0.5 MT of HEU [10, p.78][20, p.92]. Additionally, the core of an Ohio class ballistic missile submarine is estimated to contain roughly 1 tonne of HEU [10, p.78][16, p.32].[4] There is much less agreement on the core size

[4]Though both estimates of 900 kg and one tonne come from the IPFM, they are calculated using two different methods. In one case, the weight is calculated from shaft horsepower utilized over the course of

of a Nimitz class carrier. Estimates vary wildly from two to five MT of HEU use over the life of the ship [10, p.78][16, p.32].[5]

Due to this disagreement, it is useful to estimate the weight of a carrier core as a factor multiplier of submarine core size. Throughout these calculations, estimations will err towards lower HEU usage. This way the final values will represent the longest possible life for the Navy's nuclear programs. If this still shows that the Navy faces an HEU shortage, then the Navy has a problem to deal with.

The basis for estimating energy requirements in a naval reactor core is detailed in a 2014 MIT Masters thesis by Cameron McCord [22]. The four required parameters are the core's power rating and lifetime along with the vessel's deployment cycle and duty cycle (or capacity factor). For a Virginia class submarine, these numbers can be estimated as 150 MW, 33 years, 6/12 months, and a 0.25 duty cycle [22, p.44].[6] For an aircraft carrier, all of these values are very different, though they carry varying levels of uncertainty. They will be discussed in order from least uncertain to most uncertain.

The deployment cycle of a US aircraft carrier has historically been about 9/36 months [23, p.1]. The two current aircraft carrier classes (the Nimitz and Gerald Ford class) have core lifetimes of 22.5 and 25 years respectively [6, p.10][7, p.2]. For the Nimitz class, the reactor power can be estimated by comparing to the USS *Enterprise* (CVN-65). The Enterprise used eight A2W submarine reactors to generate 960 MW of power [20, p.91]. The Nimitz class carriers are of a similar "generation" as the *Enterprise*, and so each of the Nimitz class's two A4W reactors can be estimated as 480 MW. This number can be checked by comparing the ratio of thermal power to horsepower in past naval reactors for which information is readily available.[7] This ratio would give the Nimitz class a power of 512 MW per reactor. An average of 500 MW is used for this analysis.

The Ford class carriers should have similar power requirements to the Nimitz class, though it will be slightly higher. It is reported to have three times the electrical generation of the Nimitz class [24, p.6].[8] Each of the Ford's two cores provides the same 140,000 hp as the

---

the submarine's lifetime. In the other, the total weight of used naval fuel is distributed among naval vessels proportionally to their horsepower.

[5]Because US carriers have two reactors, with the exception of the USS *Enterprise* (CVN-65), and undergo a nuclear refueling at midlife, some sources choose to discuss the total amount of HEU removed from the stockpile over the course of the ship's life rather than the size of a core.

[6]The estimate of reactor power used in this thesis is different from that used by McCord. For an explanation of the 150 MW value, see section 2.1.1.

[7]The paper "Ending the Production of Highly Enriched Uranium for Naval Reactors" provides information for the reactors used to power the Los Angeles class (S6G), Ohio class (S8G), Seawolf class (S6W), and USS *Enterprise* (A2W) [20, p.91]. From these reactors, the Navy averages a ratio of 3.66 MW/shp. Each of the Nimitz class's two A4W reactors delivers 140,000 shaft horsepower.

[8]The increased electrical generation is due to the installation of electromagnetic aircraft launch systems, improved radar and communications systems, and improved air conditioning among other variables [25,

Nimitz class's [20, p.91]. Therefore, equation 1.1 provides the basis for splitting the reactor's available power into both electrical generation and propulsion. The Nimitz can be calculated to require 38 MW of electrical generation.[9] Tripling this number and backing out the other factors gives the Ford class 1280 MW of thermal power, or 640 MW per reactor.

$$\text{Thermal Efficiency} \cdot \text{Thermal Power} = \frac{\text{Shaft Horsepower}}{\text{Motor Efficiency}} + \text{Electrical Generation} \quad (1.1)$$

Estimating the duty cycle of an aircraft carrier is a much more qualitative argument. In order to sustain flight operations, the carrier must be moving fast enough to generate a significant amount of wind over the bow. Because drag power scales as the velocity cubed, 50% power output should put the ship around 80% of its rated maximum speed.[10] Therefore, anytime the carrier is engaged in flight operations, the capacity factor is likely at least 0.50. Anytime the carrier is transiting from one location to another, it is also likely moving quickly. It is note common to spend significant amount of time loitering at low speeds as this precludes flight operations. Operations that take place at lower speeds, such as underway replenishment, would account for a small portion of the carrier's sea time compared to transit and flight operations. Therefore, an estimate of a 0.50 duty cycle for carriers should be low, but close to accurate.

$$\begin{aligned} \frac{\text{\# Virginia Cores}}{\text{\# Carrier Cores}} &= \frac{\text{Carrier Energy Required}}{\text{Virginia Energy Required}} \\ &= \frac{\text{Carrier}}{\text{Virginia}} \left[\frac{\text{Power}}{\text{Power}} \cdot \frac{\text{Life}}{\text{Life}} \cdot \frac{\text{Deployment Cycle}}{\text{Deployment Cycle}} \cdot \frac{\text{Duty Cycle}}{\text{Duty Cycle}} \right] \end{aligned} \quad (1.2)$$

Equation 1.2 can be used to scale the total energy requirements of an aircraft carrier to that of a submarine.[11] This allows for the estimation of the HEU usage of an aircraft carrier as a multiple of the HEU usage in a Virginia class submarine. The results of this calculation are shown in table 1.2. In total, this shows that current shipbuilding programs account for 127 MT of the Navy's stockpile of 152 MT of HEU.

p.9,23]. Because both ships have the same shaft horsepower, the Ford class requires a larger reactor.

[9]The Nimitz class has 1000 MW of thermal power available from its two 500 MW reactors. Assuming a thermal efficiency of 0.27, judging from [20, p.91], gives the ship 270 MW of usable energy. The ship requires 280,000 shp of propulsion. Assuming a motor transmission loss of 10% along the shaft gives the ship just over 38 MW of electrical generation.

[10]The cubic relation gives the ratio: power level/max power=$(v/v_{max})^3$. The actual speed will be less than this, as electrical generation will be a constant load on the reactor independent of speed.

[11]This assumes that carrier and submarines have equivalent power densities, as well as a similar discharge burnup.

Table 1.2. Summary of Current Naval Reactor Projects

	Current Nuclear Navy Projects			
Reactor Properties	Virginia Class	Ohio Replacement	Nimitz Class	Ford Class
Type	S9G	S1B	A4W	A5W
Life (Years)	33	40	22.5	25
Thermal Power (MW)[1]	150[2]	220[3]	500[4]	640[5]
Number of Reactors	1	1	2	2
Number of Refuelings	0	0	1	1
Future Construction (Total)[21, p.4][6]	47(57)	12(12)	5(10)[7]	10(11)
Required Cores	47	12	10	42
VA Cores per Core X[8]	1	4	2.3	3.2
VA Equivalent Cores	47	48	23	136
VA Cores per Core X (lowered)	1	4	1.8	2.2
VA Equivalent Cores (lowered)	47	48	18	91
Required HEU (MT)[9]	23.5	24	11.4	68.0
Required HEU (MT) (lowered)[10]	23.5	24	9.1	45.5

[1] Thermal power is given as a per reactor quantity.

[2] The estimation of the Virginia class power requirement is shown in section 2.1.1.

[3] Assumes that the Ohio Replacement submarine will have the same power requirements as the Ohio class. Ohio class power requirement retrieved from [20, p.91].

[4] Estimation of the A4W reactor power level is summarized in section 1.2.1.

[5] Estimated using equation 1.2. Parameters are discussed in section 1.2.1.

[6] The Navy's shipbuilding plan submitted in 2014 does not cover the last four Gerald Ford class carriers to be constructed between 2044 and 2063, but the Navy plans on building a fleet of 11 carriers [26].

[7] All 10 of the Nimitz class carriers have been constructed, but only five still have upcoming refuelings.

[8] For the Ohio Replacement class, HEU consumption is assumed to be on par with the original Ohio class. Because the replacements will have a 40 year life as opposed to the Ohio's 20 year core life [27, p.1], the Ohio Replacement should require two MT of HEU in its core as opposed to the Ohio's one tonne. This is the equivalent of four Virginia class submarine cores per Ohio Replacement core. The calculation for carriers is discussed in the body of the paper.

[9] Calculated by multiplying the number of equivalent Virginia cores by 0.5 MT per core.

[10] Required weight of HEU using more conservative estimates of carrier parameters.

The uncertainty in the values used to calculate aircraft carrier fuel usage is very large. Therefore, it is worthwhile to investigate the sensitivity to changing initial parameters. To show that stockpile lifetime concerns are a significant issue, all estimated parameters were changed by 5% in the direction that would lower HEU use in carrier reactors.[12] Even after applying the more conservative estimates, the Navy would still have over two thirds of its remaining fuel stockpile allocated to current programs.[13]

These calculations suggest that Navy shipbuilding is guaranteed at least until 2043, the far end of the Navy's current shipbuilding plan submitted to Congress, shown in table 1.3 [21, p.10]. However, it provides a problem for the next generation of nuclear ships. The first Ford class carrier will reach the end of her planned service life in 2063. When the Navy designs a replacement for the Ford class, it will not have sufficient HEU stockpiled to fuel the entire class. Additionally, the Ohio Replacement class will begin retiring at the end of their 40 year lives in 2061. Finally, the Virginia class will be a continual drain of 0.5-1.0 MT of HEU per year through the 2040s under the Navy's plan. Because new designs would need to begin soon, the Navy should soon consider whether it could shift to an LEU design to address HEU stockpile limitations.

The Navy should also acknowledge the national security and political implications of HEU use. The Navy is one of the most internationally visible arms of the US Government. It has bases all over the world, makes port calls in dozens of countries with little other American contact, and responds to humanitarian crises worldwide. Whether they like it or not, any actions taken by the Navy reflect visibly on the United States as a whole. Because of this, the Navy should be concerned with how their actions regarding HEU affect international discussions about the right to produce HEU and corresponding proliferation potential. Any long-term fueling options the Navy considers must therefore address both the technical aspects of how the Navy can guarantee a fuel source for the indefinite future as well as the political aspects of HEU use.

[12]These changes reduce the A4W reactor's power to 475 MW and thermal efficiency to 0.256. The motor transmission loss is increased to 10.5%. This gives the A5W reactor a thermal power of 510 MW. The reactor's duty cycle is then decreased to 0.475, and the deployment cycle is reduced to the Navy's ideal plan of 8/36 months [23, p.1].

[13]The calculation is most sensitive to thermal efficiency and duty cycle. Small changes in thermal efficiency radically alter the estimation of electricity generation for the Nimitz class. This can cause large changes in the estimate of the Ford's A5W reactor power. Because the duty cycle is directly multiplied into the core ratio a 5% change in duty cycle is automatically a 5% change in fuel requirement. Deployment cycle is a fairly well known value, and has the least uncertainty.

Table 1.3. Yearly Navy Shipbuilding Plan for Nuclear Vessels

	Fiscal Year[1]										
Ship Type	'14	'15	'16	'17	'18	'19	'20	'21	'22	'23	
Ford Class					1					1	
Virginia Class	2	2	2	2	2	2	2	2	2	2	
Ohio Replacement Class								1			
Nimitz Class Refueling (estimated)[2]				1				1			
	'24	'25	'26	'27	'28	'29	'30	'31	'32	'33	
Ford Class					1					1	
Virginia Class	1	2	1	2	1	1	1	2	1	1	
Ohio Replacement Class	1		1	1	1	1	1	1	1	1	
Nimitz Class Refueling (estimated)		1				1				1	
	'34	'35	'36	'37	'38	'39	'40	'41	'42	'43	Total
Ford Class					1					1	6
Virginia Class	1	1	1	2	2	1	2	1	2	1	47
Ohio Replacement Class	1	1									12
Nimitz Class Refueling (estimated)											5

[1] Table adapted from [21, p.4].
[2] Estimated by projecting forward from the year the Nimitz class carriers were constructed.

1.3 Potential Solutions to the Fuel Shortage

The simplest way for the Navy to prolong its supply of HEU is to continue acquiring excess weapons material as it becomes available. This process could be accelerated if the Navy were to convince Congress and US Strategic Command (STRATCOM) that the current nuclear weapons HEU stockpile is unnecessarily large for national security. This could free up approximately 135 MT of HEU for naval use.[14]

By taking HEU from the military stockpile in this manner, the Navy could almost double its supply of fuel.[15] While this does not solve the fuel limitation problem, it pushes the time line for a long term solution another fifty to one hundred years down the road. However, this

[14]Assuming the United States' entire 5,000 warhead nuclear arsenal is made up of two-stage, medium-yield weapons in the 300–500 kt range (which use 4 kg of plutonium and 25 kg of HEU [19, p.27]), weapons account for about 125 of the 260 MT of HEU set aside for military use [3, p.50]. This would leave about 70 MT of the United States' 87.6 MT stockpile of plutonium as a military reserve, equivalent to 14,000 single stage weapons in the 40-80 kt range (which use 5 kg of plutonium [19, p.27])[3, p.18]. While the "right" number of nuclear weapons a nation may need is a matter for national debate, it is conservative to estimate that 20,000 is enough. This arsenal would be four times larger than what the US currently maintains under treaty requirements. It is also roughly two thirds of the arsenal the US maintained at the height of the Cold War [3, p.51]. Given the international move towards nuclear disarmament, it is unlikely that the US would need an arsenal this large anytime in the future.

[15]This is assuming that the entire weapons stockpile of HEU is enriched to a sufficient level for Naval Fuel (90%+). This is likely, as that is also the requirement for weapons material.

fails to address the geopolitical concern of naval fuel supplies becoming weaponized. If, after moving HEU stockpiles to Navy control, the US continues the process of nuclear disarmament then the Navy's stockpile would represent an even larger fraction of the United States' weapon usable fissile material. This could potentially limit Russian willingness to cooperate with the United States on further nuclear disarmament. So while this solution addresses the Navy's medium term fuel supply problem, it does not address long term concerns or the issues of non-proliferation and arms control.

A more permanent solution to the fuel stockpile issue is to resume uranium enrichment for the Navy. The year-to-year HEU requirement for the Navy is small, as shown in table 1.4. With an active, reliable enrichment program the Navy would be able to maintain a relatively small fuel stockpile, and continuously use and replenish it every year. The United States does not currently have a facility capable of naval enrichment. The two gaseous diffusion plants (Paducah and Portsmouth) that produced the majority of the United States' HEU stockpile have both closed [28, p.B1]. The civilian enrichment market in the United States is currently dominated by Urenco's enrichment plant in Eunice, NM and Areva's new plant in Eagle Rock, Idaho. Both of these plants technically have the capacity to fulfill the Navy's enrichment requirement as shown in table 1.5 [3, p.24]. However, both Urenco and Areva are bound by a 2011 treaty between the United States, France, Britain, Germany, and the Netherlands only to enrich uranium for peaceful purposes [29, p.4]. This prohibits them from supplying the Navy. The only enrichment option available is through Centrus, formerly the United States Enrichment Corporation (USEC), which recently declared bankruptcy after failing to receive a $2 billion loan guarantee from the United States Department of Energy [28, p.B1]. Regardless of the bankruptcy, Centrus's current centrifuges, based on a 1980s design and updated in the 2000s, have faced significant setbacks and challenges [10, p.44][14, p.60]. The amount of time USEC has spent developing the American Centrifuge Program without anything to show for it leaves little confidence in its success.

While enrichment prospects currently appear bleak in the United States, the Navy could easily afford to wait the short amount of time it would take to establish a successful centrifuge program. The potential HEU shortage is decades away, and a focused effort on behalf of the Navy could lead to a mass-producible, high reliability centrifuge, independent of the complex AC100 design [31, p.14]. The US has been through many centrifuge designs varying in length from 0.305 m to 12 m [30, p.4]. If encouraged by the Navy to abandon the AC100 and revert to an earlier, functional design, a US effort could likely have an operational enrichment plant within a decade.[16] The plant would not even need to be economically competitive with Areva

[16]The same treaty prohibiting Areva and Urenco from supplying the Navy with enriched uranium prohibits them from providing European-designed centrifuges [29, p.4].

Table 1.4. Navy HEU Consumption Rate

	Generational Fuel Requirements		
Year	Virginia Class	Ohio Replacement	Ford Class
Number of Ships in class	57	12	11
Life of ship (Years)	33	40	50
Cores per Ship	1	1	4
HEU / Ship (MT)[1]	0.5	2	6.4
HEU Consumption (MT/year)[2]	0.86	0.6	1.4

[1] Calculated by converting the number of cores per ship into an equivalent number of Virginia class submarine reactors, using the results in table 1.2.

[2] Calculated by multiplying the number of cores per ship by the number of ships, then divided by the life of the ship.

Table 1.5. Uranium Enrichment Requirements

	Uranium Enrichment		
	7.0%	20.0%	93.7%
Plutonium Burnup Fraction[1]	0.28	0.078	≈0
Fuel Weight (MT-HM/year)[2]	27.6	12.4	2.86
tSW/year[3]	308	475	577
AC100 Centrifuges[4]	933	1439	1748

[1] Fraction of burnup due to plutonium was calculated by running a CASMO simulation of an infinite pin lattice using UO_2 fuel and standard PWR conditions to 50 MWd/kg of burnup. All three lattices remained critical at the end of the simulation.

[2] HEU fuel weight retrieved from table 1.4. For lower enrichment levels, fuel weight was calculated as: HEU Weight × 0.937 / new enrichment × (1 - plutonium burnup fraction).

[3] Calculated using standard enrichment work equations, assuming 0.2% tails.

[4] Assumes an average performance of 330 SWU/year [30, p.4].

or Urenco's plants, as its only initial customer would be the Navy. Once completed, the plant could attract customers that would enable an expansion into a competitive civil enrichment program for commercial nuclear power.

While a new enrichment program would solve the Navy's fuel issues indefinitely, it fails to solve non-proliferation concerns and creates a few more. Even if the Navy were to eliminate its HEU stockpile in return for an enrichment plant (or at least limit the stockpile to what is needed to cover ships under current construction), the existence of an enrichment plant producing the equivalent of hundreds of bombs a year would be problematic [19, p.27]. Both the 2010 National Security Strategy and the 2014 Quadrennial Defense Review reaffirm the United States' commitment to reducing both its weapons and HEU stockpiles in accordance with the New START Treaty [32, p.23][33, p.14]. New HEU enrichment is in direct contradiction to both strategies.

An internationally acceptable option would be to limit enrichment to ¡20%.[17] As shown in Table 1.5, by reducing enrichment to either the LEU limit of 20%, or the 7% used by the French Rubis class submarines, the Navy could fund a smaller enrichment plant than if they were to require HEU. This would solve most of the international concerns with the Navy stockpile. The enrichment plant and produced uranium could even be placed under IAEA safeguards without putting military secrets at risk if it was well known that excess LEU was being produced. The material could then be removed from safeguards when it is to be manufactured into fuel. The Navy's excess HEU stockpile could be down-blended to LEU and used for naval cores. Finally, the United States would be setting an international example by moving away from the use of weapons usable fissile material for naval propulsion, removing an excuse other nations could use to produce HEU.

If the Navy were to embrace LEU fuel, it would also open up a second source of fuel. Currently, the Navy has 100 MT of irradiated naval fuel sitting in disposal [3, p.11]. Because this fuel was enriched to over 95% before it was burned, there is still a significant amount of ^{235}U remaining in the waste. While this irradiated fuel is currently not useful to the Navy without re-enrichment capability, it could be used if the Navy were to convert to LEU. With fuel reprocessing, the remaining ^{235}U could be pulled out of the fuel and down blended to LEU for future use as Navy fuel. Additionally, the resulting waste contains less than 0.05% plutonium by weight because the irradiated naval fuel contained very little ^{238}U, so there would be no separated plutonium proliferation concerns.[18] [19]

[17]The feasibility of naval vessels operating with LEU fuel will be the focus of this thesis.

[18]CASMO simulated a single UO_2 fuel pin burned at standard PWR operating conditions in an infinite lattice. PWR conditions are from Appendix K of Nuclear Systems Volume 1 by Todreas and Kazimi [34]. The lattice was burned to 300 MWd/kg.

[19]Though this reprocessing would be proliferation neutral initially, while the Navy was working with its

While reprocessing could be beneficial to the Navy as a fuel source, it would complicate the Navy's waste disposal process. Currently, when ships are defueled the spent fuel is removed from the reactor compartment at Puget Sound Naval Shipyard and sent to the Naval Reactors Facility (NRF) at Idaho National Lab [35, p.1]. The spent fuel is stored at the Expended Core Facility in water basins [36]. The reactor compartments are then (if the ship is being decommissioned) cut out and shipped up the Columbia River to the Navy's reactor compartment disposal site at Hanford in south-central Washington [35, p.1]. Ultimately, the Navy is obligated under a 1995 agreement with the State of Idaho to transfer all spent nuclear fuel to dry storage containers by 2023, and to remove it from Idaho by 2035 [37, p.2]. All spent naval fuel at NRF is currently awaiting the establishment of a national geological depository for storage under the 1982 Nuclear Waste Policy Act [38, p.411]. As of now, the Navy is proceeding with plans to put the fuel into containers and prepare it for shipment. If the Navy were to decide to reprocess their spent fuel, it would likely require an additional agreement with the State of Idaho to resume reprocessing at Idaho National Laboratory, or with another state to begin reprocessing there.

While reprocessing could help the Navy prolong stockpiles in the case of moving to LEU, it would likely be much more expensive than new enrichment. While the H Canyon complex at the Savannah River Site could likely manage some of the reprocessing, it does not solve concerns about the ultimate disposal of high level waste [39, p.1].[20]

If the Navy decides to stick with HEU fuel into the future, their best option is to depend on US Strategic Command to decrease its weapons stockpile and hope that this results in excess HEU being transferred to the naval reserves. However, this option also only delays the fuel shortage the Navy will eventually face. The only way to guarantee a fuel source for the indefinite future, while addressing international proliferation concerns, would be to embrace the use of LEU fuel in naval reactors and begin planning for an enrichment plant dedicated to producing LEU naval fuel.

The switch to LEU in the Navy has long been a contentious issue. When ordered to report on the feasibility of using LEU by Congress in 1995, the Office of the Director of Naval Reactors responded unequivocally that the change would require unacceptable performance compromises [6, p.1]. When ordered to re-investigate the issue in 2013, Naval Reactors responded that with current technology and funding it was not feasible, but that with the

past irradiated fuel, any future LEU irradiated fuel would not be proliferation neutral. LEU irradiated fuel contains a significant amount of plutonium, and so a reprocessing effort would produce a separated plutonium stockpile.

[20]The H Canyon site has been used since March 2003 to down-blend HEU to create fuel for commercial reactors operated by the Tennessee Valley Authority [39, p.2]. Since May 2006, it has been used to recover HEU from used research reactor fuel for use in LEU fuel [39, p.2].

recent development of advanced fuel systems it might be possible [7, p.5]. It appears the Navy is warming to the idea of LEU fueled reactors, perhaps motivated by the choices of other navies and the desire to continue innovative research at Naval Reactors.

1.4 RERTR and the Navy

Since 1978, the Reduced Enrichment for Research and Test Reactors (RERTR) program has been directed towards converting HEU research reactors to LEU fuel [14, p.68]. When nuclear power was still in its infancy, the United States provided HEU fueled research reactors to its allies [40, p.2]. Since then, the RERTR program has attempted to curtail the use of HEU in civilian applications to reduce nuclear proliferation risks [40, p.2]. The United States currently has 20 MT of HEU set aside for civilian use in these research reactors [3, p.11]. While this represents a small portion of the United States' HEU, it is widely dispersed across the country, and under significantly less security than military and naval stockpiles. This makes it a concern for non-proliferation experts.

The main approach to eliminating civil HEU has been to develop LEU fuels with higher uranium densities able to replace the older HEU fuels. Most older HEU fuels have relatively low uranium densities, ¡20% that of uranium metal. The RERTR program has focused on developing new, metal-based fuels that increase the uranium density within the fuel by a factor of five or more to make up for the enrichment decrease to 20%. The program saw many early successes, almost doubling uranium density early on, and tripling it by 1988.[21] Since then, work has focused on gamma phase uranium-molybdenum alloys either as a metal or dispersed in an aluminum fuel matrix. Because the molybdenum can be kept at low levels, 5–10% by weight, the fuel is able to approach the density of natural uranium [42, p.2-4]. Some of these fuels have uranium densities approaching 16 g/cc, a ten-fold increase over the uranium densities of older fuels [42, p.2].

The RERTR program has been very successful at converting research reactors from HEU to LEU. To date, over 40 reactors worldwide have been converted, and analysts believe that up to 41 more could be converted [14, p.68]. At the MIT reactor, a proposed 7% molybdenum dispersion fuel was shown to meet operational and experimental needs [43, p.278-279]. While the replacement required a re-design of many of the fuel assembly parameters (plate spacing, cladding thickness, etc.) it was shown that the replacement would not require restructuring of the reactor's physical internals.

[21] The fuels available going into the RERTR program were uranium aluminum dispersion fuel with uranium densities up to 1.7 g/cc, uranium-oxide aluminum dispersion fuels up to 1.3 g/cc, and uranium zirconium hydride (TRIGA) fuels at 0.5 g/cc. These fuels were requalified up to 2.3, 3.2, and 3.7 g/cc respectively very early on. By 1988, new uranium silicide aluminum dispersion fuels had been qualified up to 4.8 g/cc [41].

The Navy has expressed interest in the so-called "advanced fuel systems" offered by the RERTR program [7, p.5]. If the new fuels were used with the Navy's current HEU, it could allow naval reactors to shrink even smaller or last even longer. However, it is also possible that the large increase in uranium density could make up for a decrease in enrichment. This was investigated in an MIT thesis by Thomas Ippolito in 1990. Ippolito showed that by increasing uranium density within a fuel, fuel enrichment could be lowered with a smaller impact on overall core size [44]. It is possible that with twenty years of advancement in fuel technology, the same methodology could be repeated using the molybdenum alloy fuels being developed by the RERTR program.

The Navy is well positioned to integrate the DOE's work on LEU fuels. In addition to addressing fuel supply and proliferation concerns, switching to high-density fuels could guarantee funding for the Department of Naval Reactors for years to come. With the recent success in designing a lifetime core for the Virginia class submarine, and upcoming completion of work on the Ohio Replacement class core, the Department of Naval Reactors is going to be left with no major programs to guarantee funding [7, p.5]. The current funding allocated to Naval Reactors is not enough to maintain the department's resources such as the Advanced Test Reactor, the Knolls and Bettis Atomic Laboratories, and a highly specialized team of naval-reactor engineers [7, p.5-6]. The development of an LEU fuel could be a project that reinvigorates the department, guaranteeing funding and the preservation of its resources for decades.

1.5 New Work: A Proof of Concept

A strong case has been made for the political, social, and economical reasons for beginning an LEU fuel project within the Department of Naval Reactors. However, what is less clear is whether LEU can meet the technical demands of the Navy. In 1995, Naval Reactors issued a report declaring that the conversion to LEU would require three refuelings for nuclear attack submarines, resulting in a fleet size increase of 8%, increased radiation exposure of shipyard workers, and increased waste storage requirements [6]. They declared that if an LEU core was designed to last the lifetime of the boat, it would require significant, unacceptable compromises in performance [6, p.12]. However, in 2014 Naval Reactors issued a report identifying that the 1995 report overlooked the possibility that a new fuel material could extend the lifetime of an LEU core, and that with a dedicated fuel design program a lifetime LEU core *might* be possible [7, p.4].[22]

[22]The report goes on to stress that success is not guaranteed in the venture, but that the potential rewards would be worth an investment.

This thesis will attempt to determine the thermal and neutronic feasibility of using LEU fuel in a US attack-submarine, with the goal of achieving a lifetime core. Chapters 2 and 3 will discuss the margins and requirements of a US attack-submarine reactor, as well as the physics, thermal-hydraulics, and neutronic considerations applicable to reactor design. Chapter 2 identifies an HEU fuel that may be reflective of that used in modern submarine reactors to establish a baseline case, as well as an LEU fuel that may be able to match burnup and reactivity requirements for a lifetime core. Chapter 4 presents a model and burnup results for an HEU fueled naval reactor. Chapter 5 presents a model and burnup results for an LEU fueled naval reactor. The basis for these simulations will be the Virginia-class fast-attack submarine. Chapter 6 estimates the effects of LEU on shipyard radiation, submarine availability, and required fleet size. Finally, chapter 7 presents the conclusions of the thesis.

Chapter 2

Requirements and Background / Fuel Selection

This chapter discusses the performance requirements and operating margins that a naval reactor must meet, summarizes the materials challenges naval reactors face, and selects materials to be used in the reactor models. A summary of the margins and requirements for the reactor is shown in table 2.4. The HEU fuel to be simulated is described in section 2.5, and the LEU fuel to be simulated is described in section 2.6. Finally, a summary of the materials used in this thesis is shown in table 2.9.

2.1 Margins and Requirements

The first step to designing a full reactor is to determine its operating parameters and performance requirements. These include the power, total energy output, and size constraints, as well as a minimum neutronic and thermal margins for reliable operating. These are developed for an attack submarine similar to the Virginia class.

2.1.1 Power Requirement

Both the thermal and electric power of naval reactors are classified values [45, p.12-6]. In a 2001 article, Chunyan Ma and Frank von Hippel were able to compile a series of open source documents detailing the reactor performances of over 20 classes of nuclear vessels [20, p.91]. Of particular importance from this list are the details of the USS *Enterprise* (CVN-65) and the Los Angeles, Virginia, and Seawolf class submarines. The details of these vessels are

Table 2.1. Comparison of Naval Reactors[1]

Ship or Class	Displacement (tons)	Reactor Power (MW_{th})	Shaft Horsepower (shp)
USS *Enterprise* (CVN-65)	93,970[2]	120	35,000
Los Angeles Class	6,927	130	35,000
Seawolf Class	9,137	220	57,000
Virginia Class	7,700	?[3]	40,000

[1] This information contained in this table is adapted from Table 2: Key Characteristics of Commissioned Nuclear-Powered Submarines and Ships (2000) in [20, p.91].

[2] The USS *Enterprise* (CVN-65) was the first nuclear powered aircraft carrier. To ease pressure on the design team and speed development, it used eight attack submarine sized nuclear reactors. All further US aircraft carriers have used two larger, "carrier-sized," nuclear reactors apiece [46, p.CRS-6]. The values listed for *Enterprise* are per reactor.

[3] There has not been a good open source estimation of the Virginia class's power requirements. The estimation of this value will be covered in section 2.1.1.

shown in table 2.1.[1]

The first step to simulating a Virginia class core is to estimate the maximum power required. The most simple way to do this is to scale up from the Los Angeles class reactor, and down from the Seawolf class reactor. Equations 2.1 through 2.4 show attempts to estimate the Virginia using both shaft horsepower and displacement.[2]

$$\text{Los Angeles-to-Virginia Displacement} = \frac{7,700\,\text{tons}}{6,927\,\text{tons}}\,130\text{MW}_{th} = \ 144.5\,\text{MW}_{th} \tag{2.1}$$

$$\text{Seawolf-to-Virginia Displacement} = \frac{7,700\,\text{tons}}{9,137\,\text{tons}}\,220\text{MW}_{th} = \ 185\,\text{MW}_{th} \tag{2.2}$$

$$\text{Los Angeles-to-Virginia Power} = \frac{40,000\,\text{shp}}{35,000\,\text{shp}}\,130\text{MW}_{th} = \ 149\,\text{MW}_{th} \tag{2.3}$$

$$\text{Seawolf-to-Virginia Power} = \frac{40,000\,\text{shp}}{57,000\,\text{shp}}\,220\text{MW}_{th} = \ 154\,\text{MW}_{th} \tag{2.4}$$

With equation 2.2 as a clear outlier, this points to a reactor power near 150 MW_{th}. As such, that will be taken as the targeted maximum power for both the HEU and LEU reactors in this thesis.[3]

[1] Absent from table 2.1 are the Ohio class submarines. The USS *Ohio* (SSBN-726/SSGN-726) and its sister ships are ballistic missile (and guided missile), as opposed to attack, submarines. Their different mission makes their reactors less useful for comparison, as they have different and less stringent requirements.

[2] Using the *Enterprise* reactors as a scaling factor would be inappropriate. Firstly, the reactors are from a very different era. When the USS *Enterprise* (CVN-65) was constructed, nuclear energy was in its earliest stages, and the reactors were likely of a very different technology. Additionally, the *Enterprise* could have had a very different plant, because of its larger size, affecting the ratios between shaft horsepower, displacement, and reactor power.

[3] There are two other technical theses of note that investigate submarine conversion to LEU. The first, by Thomas Ippolito in 1990, simulated a Rubis class submarine with a reactor rated at 50 MW_{th} [44, p.23]. The second, by Cameron McCord in 2014, estimated a Virginia class submarine to have a thermal power of

2.1.2 Temperatures and Mass Flow Rate

Two other important sizing parameters for the reactor are the mass flow rate of the coolant and the inlet and outlet temperatures of the coolant. While commercial PWRs tend to operate in the range of 280°C to 320°C, these ranges might not be appropriate for a naval reactor [47, p.22]. A 40°C temperature difference is spread over a 3 m tall core in a commercial plant, but a naval reactor is only about 1 m tall. This standard would increase the temperature gradient over the reactor. Instead, the naval reactor model will use a temperature difference of 290°C to 310°C over the reactor. This keeps the same median coolant temperature as a commercial reactor, while only having a slightly higher temperature gradient. This should not affect the thermal efficiency of the reactor, as that is set by the temperature in the secondary loop.[4] The different temperatures may require a slight modification of steam generator design. This, in turn, sets the mass flow rate through the core.

$$Q = \dot{M}\Delta h \tag{2.5}$$

In the equation above, Q is the total power of the reactor (assumed to be 150 MW, calculated in section 2.1.1), $\dot{M}$ is the total mass flow rate through the reactor, and Δh is the enthalpy difference of the coolant between the entrance and exit of the core. This is based on of a one dimensional conservation of energy equation [34, p.143]. Because the enthalpy is fully determined by two state parameters, temperature and pressure, equation 2.5 can be used to solve for the mass flow rate through the core.[5] This gives a mass flow rate of 1370 kg/s.

2.1.3 Total Energy Requirement

The maximum power requirement described in section 2.1.1 set the size of the reactor, but does not give the lifetime required of a core. This will be needed to estimate the required burnup of the fuel.[6] Unlike commercial reactors, naval reactors do not simply start, run at 100% power, and shutdown for refueling. It is necessary to estimate the submarine's lifetime

122 MW_{th} [22, p.76]. McCord's thesis attempted to estimate reactor power using the maximum required speed of the submarine, but did not address "hotel power" requirements of feeding the electrical buses on the submarine.

[4]The boiling temperature of water at 7.5 MPa, the typical secondary side pressure, is about 290°C. Therefore, as long as the median primary loop temperature is higher than this, it should be possible to evaporate the secondary side working fluid.

[5]The pressure used for the reactor is 15.51 MPa, taken from the typical value for a PWR [34, p.971]. Because the pressure drop across the reactor, described in section 3.4, is low, the static pressure will be treated as uniform in the reactor.

[6]Burnup is represented inconsistently in nuclear literature. This thesis will attempt to use MWd/kg, or the equivalent GWd/t, whenever possible. However, when citing certain documents it will be impossible not to refer to either "fission density" or "percent of ^{235}U fissioned."

in actual years, deployment cycle, and duty cycle to determine lifetime energy requirements.

Core Lifetime

One of the primary goals for Naval Reactors over the years has been to achieve a core design that would not need refueling over the life of a submarine [6, p.9]. The resistance from Naval Reactors over the conversion to LEU is in large part owed to the belief that a conversion to LEU would require submarine refueling [7, p.3]. Currently, a Virginia class SSN has an expected lifetime of 33 years, and should not have to refuel over that time period [48, p.CRS-6]. This will be the target lifetime for the reactors modeled in this thesis.

Deployment Cycle

The deployment cycle of a submarine captures a similar effect as the capacity factor of a commercial nuclear power plant. Commercial plants are not able to operate 100% of the time. They must shut down for refueling, maintenance issues, and emergencies. Likewise, submarines shut down the reactor whenever they are moored in port. Commercial plants tend to operate as much as possible, generally pushing their capacity factors over 0.9 [49, p.14]. Submarine deployment and maintenance cycles generally mean that they are operational for only six months out of the year, generating a deployment-cycle factor of 0.5 [22, p.44].

Duty Cycle

In actual operation, it is unlikely that the reactor will often be run at full power. While full power is useful for long transits, it is loud, compromising the stealth that submarines value so highly. Submarines are more likely to be operating at low power during mission essential activities such as intelligence, surveillance, and reconnaissance (ISR), special forces operations, or while awaiting strike missions [22, p.44]. The duty cycle estimates the percent of full power that the submarine would average over the operating time during deployment. An appropriate duty cycle for a US SSN is approximately 0.25 [22, p.44].

Total Energy

With all of the previous factors determined, it is possible to calculate the total amount of energy that must be extracted from the core over its lifetime. This is shown in equation 2.6.

$$\begin{aligned} \text{Energy} &= \text{Power} \cdot \text{Lifetime} \cdot \text{Deployment Cycle} \cdot \text{Duty Cycle} \\ &= 150\,\text{MW}_{th} \cdot 33\,\text{years} \cdot 0.5 \cdot 0.25 \\ &= 618.75\,\text{MW-years} = 225,850\,\text{MWd} \end{aligned} \tag{2.6}$$

2.1.4 Size Limitations / Dimensions

The size limitation on naval reactor compartments is the most unique factor in reactor design. Modern nuclear submarines, such as the Los Angeles class (10 m), Seawolf class (12 m), and Virginia class (10 m), have extremely narrow beams in order to defeat detection methods, increase speed, and operate in shallow water [22, p.77][50, p.3].[7] When the Department of Naval Reactors rejected the use of LEU in 1995, one of the major reasons cited was the fact that submarine reactors would have to increase their volume by a factor of five to maintain core life [6, p.10]. When faced with the same challenge in 2014, Naval Reactors claimed it would still require the core to increase in volume by a factor of three [7, p.4]. Open source studies have claimed that the change to LEU would only require a core volume increase by a factor of two ([44, p.177]) or three ([20, p.96]). However, neither of these scenarios have been deemed acceptable by the Navy.

In their 2014 report, Naval Reactors seemed to concede that all other challenges could be accommodated if a new LEU fuel could provide a reactor of the same size [7, p.6]. Therefore, the size limitations placed on the LEU core in this project will be the same as those currently applied to HEU naval reactors. The target will be a cylindrical core with a height of 1 m and a diameter of 1.1 m.[8]

2.1.5 Reactivity

Reactivity is a measurement of the reactor's ability to maintain criticality. There are a variety of measures used to discuss reactivity and criticality. The first, and most commonly used, is k_{eff}, the effective multiplication factor. It is usually used to describe the static criticality of a geometry. In a Monte Carlo simulation, it can be calculated by a variety of different tallies and their respective ratios.

[7] Even the Ohio class, whose size is set by the Trident II D5 missile, keeps its average beam to 42 feet (12.8 m) despite the fact that the missiles it carries are 44 feet long [51, p.5].

[8] This would fit with a reactor pressure vessel diameter of 66 inches (1.67 m) [22, p.78].

Table 2.2. LWR Reactivity Coefficient Estimates[1]

	Reactivity Coefficient
Fuel Temperature	-3 pcm/K
Moderator Temperature[2]	-150 pcm/K
Soluble Boron Dilution	-9 pcm/ppm
Burnup	-800 pcm/(MWd/kg)

[1] These coefficients are for a typical light water reactor. In any other spectrum, they could shift significantly. Unless otherwise noted, figures are from [52].

[2] The moderator temperature coefficient combines the effect of the moderator's increased temperature and the corresponding density change. The measurement is taken at typical PWR operating conditions. Value taken from [53, p.4].

Reactivity, ρ, is commonly used to measure changes in criticality. The formula for reactivity is shown in equation 2.7.

$$\rho = \frac{k_{\text{eff}} - 1}{k_{\text{eff}}} \tag{2.7}$$

$$\rho \approx k_{\text{eff}} - 1 \tag{2.8}$$

When k_{eff} is close to 1, reactivity can be estimated as equation 2.8.[9] Positive values of reactivity therefore represent changes that increase k_{eff} (such as an increase in moderation or soluble boron dilution) while negative values represent changes that decrease criticality (such as control rod insertion or temperature increases). Reactivity is not measured with units, but can be expressed in "dollars" and "cents," where one dollar of reactivity is a reactivity change equal to the delayed neutron factor.

Another unit for reactivity is "pour cent mille," or "pcm." A single pcm is one thousandth of one percent change in criticality. This is a useful measurement for criticality changes, because it results in intuitive values. A change of -8,000 pcm corresponds to a change from k_{eff} of 1.08 to 1.00. This makes it useful for estimations where the answer is only desired to a low degree of accuracy. Some common pcm estimations and rules of thumb are shown in table 2.2.

A k_{eff} value greater than unity represents a supercritical geometry, while less than unity represents subcriticality. In order to maintain operations, the core must be able to achieve

[9] This version will be used everywhere in this thesis, as it is the most intuitive method of measuring changes in k_{eff}. This version of measuring reactivity is also sometimes referred to as Δk.

k_{eff} value greater than unity at all times, even after the generation of short-lived neutron poisons. This is to ensure that the reactor can start at will. Once this minimum value is reached, the reactor has outlived its useful life and requires either refueling or decommission.

The duty cycle estimation poses a dilemma for reactor simulation. There are two methods that could be used for the simulation. In the first, the reactor is simulated at 25% power for the full 33-year lifetime of the reactor. This has the advantage of being a real simulation of the operational power. However, it also makes margins of temperature, departure from nucleate boiling, and pumping power artificially easy to achieve. The second path is to run the simulation with the reactor at full power. This is the more limiting requirement for thermal hydraulics, as power densities (and thus temperatures) are much higher, pushing the reactor closer to melting and other thermal crises.[10]

In this thesis, the full power condition will be simulated for two reasons. First, it provides the worst-case scenario as far as margins are considered. This makes it a conservative choice. Secondly, it provides the worst case scenario in terms of reactivity. Higher power, and thus higher temperatures, increase Doppler broadening, stealing neutrons from the fission chain reaction. Although this breeds plutonium, increasing core life, this does not fully offset losses in the fission chain. Additionally, higher power increases the steady state concentrations of xenon, samarium, and iodine neutron poisons, decreasing the neutron economy at operation and inserting negative reactivity after shutdown.[11]

The Monte Carlo reactor physics code Serpent can be used to calculate a steady state value of k_{eff} during operation.[12] However, there are two fission product poisons whose transient effects during shutdown must be analyzed. It is these transient effects that set the required startup margin (defined in section 2.1.5) for the reactor. The first is ^{135}Xe and the second is ^{149}Sm. The absorption microscopic cross sections of each are shown in figure 2.1 for reference.

^{135}Xe

^{135}Xe is a product of ^{235}U fission with a very large neutron capture cross section. It also decays with a half-life of about nine hours. However, most of the equilibrium xenon in the reactor is not created from fission, but through the decay of ^{135}Te and ^{135}I [56, p.52].[13] The combination of a large cross section with delayed generation leads to a variety of transient

[10] The margin for fuel melting is discussed in section 2.1.7. The margin for departure from nucleate boiling is discussed in section 2.1.8.

[11] The neutronic effects of these elements and the associated reactivity margins is discussed in section 2.1.5.

[12] Serpent is a three-dimensional continuous-energy Monte Carlo reactor physics burnup calculation code, specifically designed for lattice physics applications [54, p.715].

[13] The isotope ^{135}Te has a half-life of half a minute, while that of ^{135}I is 6.6 hours. Therefore, ^{135}I is usually discussed as the creator of ^{135}Xe, even though it isn't technically the start of the decay chain.

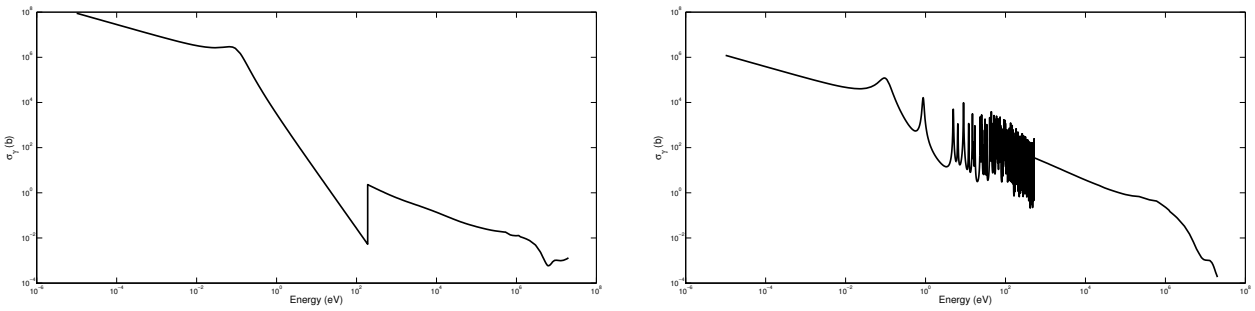

(a) ^{135}Xe Absorption Cross Section (b) ^{149}Sm Absorption Cross Section

Figure 2.1. Above are the absorption cross sections of both major fission product poisons. While the cross section at thermal energies is larger for ^{135}Xe, ^{149}Sm does not radioactively decay. Therefore, xenon has a larger effect immediately after shutdown, while samarium has a larger effect long after shutdown. Both plots use the ENDF/B-VII.1 data set retrieved from the National Nuclear Data Center [55].

effects during both operation and shutdown. The steady-state, full-power effect of ^{135}Xe is fairly straightforward. As operation continues, it builds up to an equilibrium value, balanced between burnoff due to neutron capture and decay and generation due to fission and the radioactive decay of its precursors. However, it is the power maneuvering effect of xenon that is of particular importance to setting reactivity margins.[14]

Because the half-life of ^{135}Xe is greater than that of ^{135}I, the concentration of ^{135}Xe begins to rise when the reactor is shutdown. This leads to an effect commonly referred to as "peak xenon" or the "xenon pit." The spike in concentration of ^{135}Xe, seen in figure 2.2(a), leads to a sharp decrease in the reactivity of the core. At the end of a reactor's life, this reactivity drop can preclude startup after shutdown. The maximum value of xenon poisoning in an LWR is usually capped around 6,000 pcm worth of lost reactivity around 10 or 11 hours after reactor shutdown [57, p.2.2-2.3].[15] After peak xenon has been reached, it takes about 30 hours for ^{135}Xe to decay to its pre-shutdown levels, as shown in figure 2.2(a). The poisoning effect of ^{135}Xe has a large amount of spectral dependence, as will be discussed in section 2.1.5.

^{149}Sm

While ^{149}Sm is also a fission product poison with a large thermal neutron cross section, it behaves very differently than Xe-135. First, the neutron capture cross section is an order of magnitude lower than that of xenon. The reactivity effect can be seen in figure 2.2(b).

[14] Of particular concern in this thesis is the xenon effect due to shutdown. However, any change in power level, and therefore flux, will cause ^{135}Xe transients.

[15] This includes a poisoning effect of about 2,000 pcm present at steady state. Therefore, the net effect of shutdown is an addition of -4,000 pcm to the core.

This figure also shows the second important difference between these two poisons: ^{149}Sm is a stable isotope. Therefore, after shutdown, ^{149}Sm concentration builds up to an equilibrium value, and stabilizes until the reactor starts again, at which point it is burned back to its equilibrium value through transmutation. The timescale that this occurs over is also very different than that for xenon. While xenon builds to its maximum value within a half day, samarium takes roughly 300 hours to build to its maximum. This is because the parent isotope of ^{149}Sm, ^{149}Pm, has a half-life of 53.1 hours. Samarium reaches a peak value of -1,050 pcm, with an operational equilibrium around -600 pcm in a typical light water reactor [57, p.2.2-25].

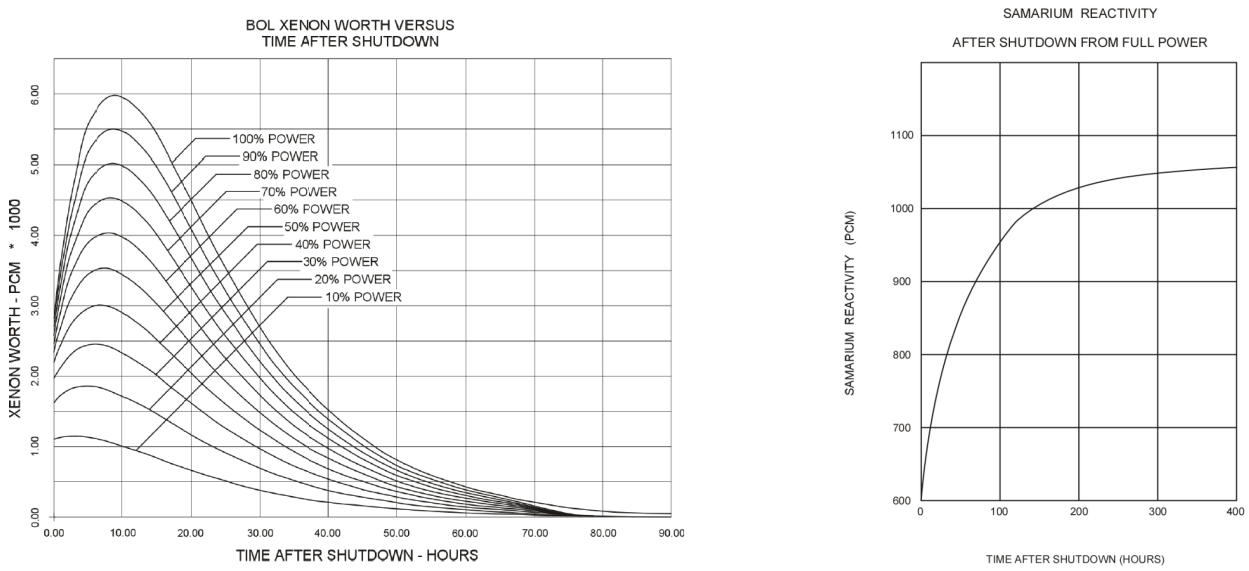

(a) Xenon Negative Reactivity

(b) Samarium Negative Reactivity

Figure 2.2. These figures show the reactivity effects of ^{135}Xe and ^{149}Sm after a reactor is shutdown. Subfigures (a) and (b) are from [57, p.2.2-23, 2.2-25].

Reactivity Margin

One of the design requirements for naval reactors is that they must be able to restart at any time. If a submarine has to SCRAM unexpectedly at sea, it must be able to restart immediately once the situation has improved [22, p.48]. In practical terms, this means that the reactor must be capable of overcoming the effects of both ^{135}Xe and ^{149}Sm at any time.[16]

The reactivity contribution of xenon after shutdown can be estimated with the equation

[16]These are the only two poisons that increase in concentration after shutdown. Other poisons reach their maximum equilibrium points during full power operation, and begin to decay at shutdown. Therefore, xenon and samarium set the requirements for the reactivity margin.

Table 2.3. Xenon Reactivity Required Constants[1]

	^{135}I	^{135}Xe
Decay Constant (λ) (s^{-1})	2.87×10^{-5}	2.09×10^{-5}
Fission Product Fraction (γ)[2]	0.0639	0.00237

[1] The data in this table was taken from [59, p.16-17].
[2] The fission product yields are specific to ^{235}U.

below [58, p.573].[17]

$$\rho(t) = -\sigma_a^{Xe}\phi\frac{\Sigma_f}{\Sigma_a}\left[\frac{\gamma_I + \gamma_{Xe}}{\lambda_{Xe} + \sigma_a^{Xe}\phi}\exp\left(-\lambda_{Xe}t\right) + \frac{\gamma_I}{\lambda_I - \lambda_{Xe}}\left[\exp\left(-\lambda_{Xe}t\right) - \exp\left(-\lambda_I t\right)\right]\right] \quad (2.9)$$

The subscripts I and Xe refer to ^{135}I and ^{135}Xe. The symbols λ and γ refer to the isotopes' decay constants and fission product fraction, the values for which are shown in table 2.3.[18] The reactivity change due to xenon as a function of time is $\rho(t)$, the xenon microscopic absorption cross section is σ_a^{Xe}, and the neutron flux is ϕ.[19]

All cross sections, both macro and microscopic, must be weighted by the appropriate flux spectrum. Most estimations of post-shutdown xenon poisoning assume a xenon absorption cross section on the order of 10^8 b [58, p.572].[20] Early simulations performed for this thesis showed that this is an overestimation of the effective microscopic absorption cross section of ^{135}Xe in a thermal LWR, and the faster spectrum found in the naval reactor simulations led to an even lower effective cross section on the order of 10^3 b. The final flux spectrum in each reactor, as well as the resulting ^{135}Xe cross sections, will be discussed in chapters 4 and 5. This contributes to uncertainty in the exact value of k_{eff} representing the end of core life. Estimates of -4,000 pcm peak xenon, or a $k_{\text{eff}} = 1.04$ end of life cutoff (used by Ippolito [44, p.26]), may be overly conservative. However, it is unknown what amount of conservatism naval reactor designers would require for a lifetime core. For this thesis, 1.04 will be used as a reactivity cutoff to ensure conservatism and account for uncertainty in Naval Reactors proscribed limits.. However, the poisoning due to xenon will also be calculated using equation 2.9 to estimate the actual xenon poisoning.

[17] In Duderstadt, the leading Σ_f/Σ_a term is replaced by $1/(\nu p\epsilon)$. ν, p, and ϵ are easier to estimate by hand, but Serpent is capable of directly calculating one group macroscopic cross sections, correctly weighted by the appropriate flux spectrum. Therefore, the cross sections will be used

[18] In this case, it is important to differentiate the decay constant from the more commonly used half life. The decay constant is equal to $ln(2)/t_{\frac{1}{2}}$.

[19] This assumes no ^{135}I absorption, and instant decay of ^{135}Te.

[20] Though the Duderstadt book does not explicitly state this, substituting the decay constant of ^{135}Xe into equation 15-18 yields this result. This appears to be a value that is not collapsed by an appropriate spectrum.

2.1.6 Burnup

The competitor with reactivity for defining the end of the core's life is burnup. The theoretical maximum burnup of a single gram of ^{235}U is shown in equation 2.10.

$$\text{Burnup} = \frac{1\,\text{mol}}{0.235\,\text{kg}} \cdot \frac{6.02 \times 10^{23}\,\text{atom}}{1\,\text{mol}} \cdot \frac{200\,\text{MeV}}{1\,\text{fission}} \cdot \frac{1.602 \times 10^{-19}\,\text{MJ}}{1\,\text{MeV}} \cdot \frac{1\,\text{day}}{86,400\,\text{s}} \tag{2.10}$$

$$\text{Maximum Burnup} = 950\,\text{MWd/kg} \tag{2.11}$$

The above equations show the maximum *theoretical* burnup.[21] This represents the fissioning of every atom of heavy metal, with no parasitic captures or radioactive decays. Burnup is also sometimes described in terms of fissions per cubic centimeter (fission/cm^3). The conversion from this to MWd/kg is shown in equation 2.12.[22]

$$\frac{n \times 10^{21}\,\frac{\text{fission}}{\text{cm}^3}}{\rho_U[\text{kg/cm}^3]} \cdot \frac{200\,\text{MeV}}{1\,\text{fission}} \cdot \frac{1.602 \times 10^{-19}\,\text{MJ}}{1\,\text{MeV}} \cdot \frac{1\,\text{day}}{86,400\,\text{s}} = n^*\text{MWd/kg} \tag{2.12}$$

Fuel burnup can be limited by either physical effects such as radiation damage, or the loss of criticality discussed in section 2.1.5.

The primary driver of burnup limits is void swelling, discussed in section 2.2.5. At a certain point, fission gases accumulate to pressures that apply too much stress to the fuel and cladding. If, at this point, the fuel maintains a adequate reactivity, it is referred to as "burnup limited" (as opposed to reactivity limited).[23] Physical burnup limits vary widely based on the fuel, cladding, and reactor in question. Most thermal-spectrum, light-water reactors are limited to 50–60 MWd/kg [34, p.27]. Using the same fuel in a fast spectrum can push the maximum burnup to 100–150 MWd/kg, and fast reactors with metal fuels and plenums can average 120 MWd/kg [34, p.27]. The burnup limits of the fuels used in this study will be determined in sections 2.5 and 2.6.

2.1.7 Fuel Blistering and Melting

The most obvious thermal limit of nuclear reactors is to keep the fuel from melting. This ensures that fission products can be kept within the fuel, and is a basic requirement of ensuring fuel integrity. In this thesis, it was quickly discovered that the melting points of the

[21] Equation 2.11 also implies a useful rule of thumb: 10 MWd/kg is roughly 1% fuel burnup. When more precision is required, it can be referenced as 1.05% atomic burnup [60, p.88].

[22] Some data, such as that in figure 2.14, is presented in terms of fissions/cm^3. This equation can be used to estimate an equivalent burnup in MWd/kg.

[23] Beforehand, it is impossible to know whether the fuels used in this study will be burnup or reactivity limited. That will be tested for the individual cases in chapters 4 and 5.

fuels considered was not the most limiting factor. The literature shows that fuel blistering is a more important thermal phenomenon to regulate [61, p.1]. As temperature accelerated creep begins in the cladding, fission gas and thermal swelling in the fuel causes local blistering and pillowing of the fuel plates. This phenomenon is still under study. However, it has been determined that it generally onsets when the fuel-cladding interface reaches 400–500°C [61, p.7].[24] Therefore, a limiting outer fuel temperature of 425°C will be used in this thesis.

Additionally, the centerline fuel temperature will be kept 300°C below its melting point to ensure that blistering is indeed the limiting phenomenon.[25] This requires two separate calculations. The first is an analytical calculation of the temperature distribution within a fuel plate as a function of the average power density.[26] This calculation is covered in detail in section 3.2. The second is a core-wide power peaking factor for finding the hottest region in the core. This value is reported by Serpent during the depletion calculation for each time step. Section 3.6 discusses efforts taken to keep the power peaking factor low. Using the core-wide power peaking factor as a multiplying factor to the average power density, the maximum fuel plate temperature can be found.

2.1.8 Departure from Nucleate Boiling (DNB)

The primary difference between a PWR and a BWR is that the bulk coolant in a BWR is allowed to boil. In a PWR, even the exit temperature of the coolant is well beneath its boiling point. However, boiling still occurs in the coolant channels along the fuel plates. This phenomenon is known as "subcooled nucleate boiling." It is a desirable phenomenon, as it greatly increases heat transfer from the plate to the coolant [34, p.37]. Figure 2.3 shows this effect. However, there is a limit to the amount of subcooled boiling that can be attained. Once a certain critical heat flux (CHF) is achieved, the bubbles from nucleate boiling combine to create a solid vapor film along the plate. This effect can be seen in figure 2.4(b), and causes the outer cladding temperature to jump from point C to point E in figure 2.3, as the only heat removal process is conduction through the gas film. This can quickly cause the temperature of the cladding to rise above the 1200°C limit that prevents the runaway zirconium oxidation reaction discussed in section 2.3. Therefore, it is desirable to enforce a margin to departure from nucleate boiling (DNB).[27]

In PWRs, the critical heat flux limit is referred to as the minimum departure from

[24]This measurement if for uranium-molybdenum alloys in an aluminum cladding. Further research is neccesary to determine if similar patterns exist using a zircaloy cladding.

[25]All materials used in this thesis do not undergo phase changes before melting.

[26]The average power density is equal to the total power divided by the mass of uranium in the core.

[27]In LWRs, the critical heat flux is usually the most limiting of all the thermal limits, and adherence to it usually ensures that fuel centerline temperature is maintained well within its limit [34, p.37].

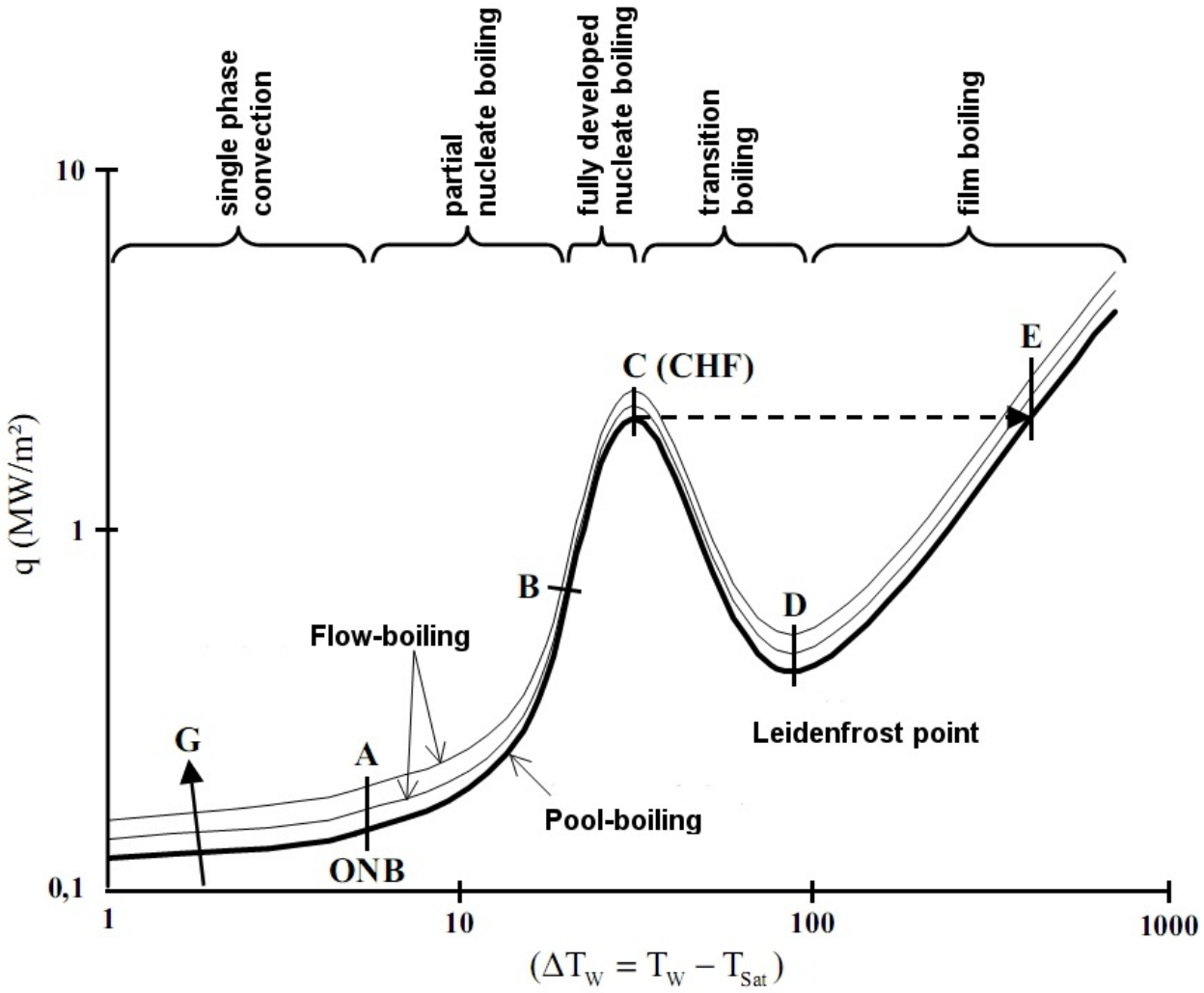

Figure 2.3. This figure shows the relationship between heat flux and ΔT_W. The heavy black line represents the pool boiling case, and coolant mass flux increases moving up to the thinner curves for flow boiling. This figure was taken from [62].

nucleate boiling ratio (MDNBR). The departure from nucleate boiling ratio (DNBR) is defined in equation 2.13, where q''_{actual} is the actual heat flux in the reactor and q''_{DNB} is the heat flux at which departure from nucleate boiling is calculated to occur. The general shape of these two heat fluxes is shown in figure 2.4(a).

$$\text{DNBR} = \frac{q''_{\text{DNB}}}{q''_{\text{actual}}} \tag{2.13}$$

The critical heat flux is calculated from an appropriate correlation. The most common and

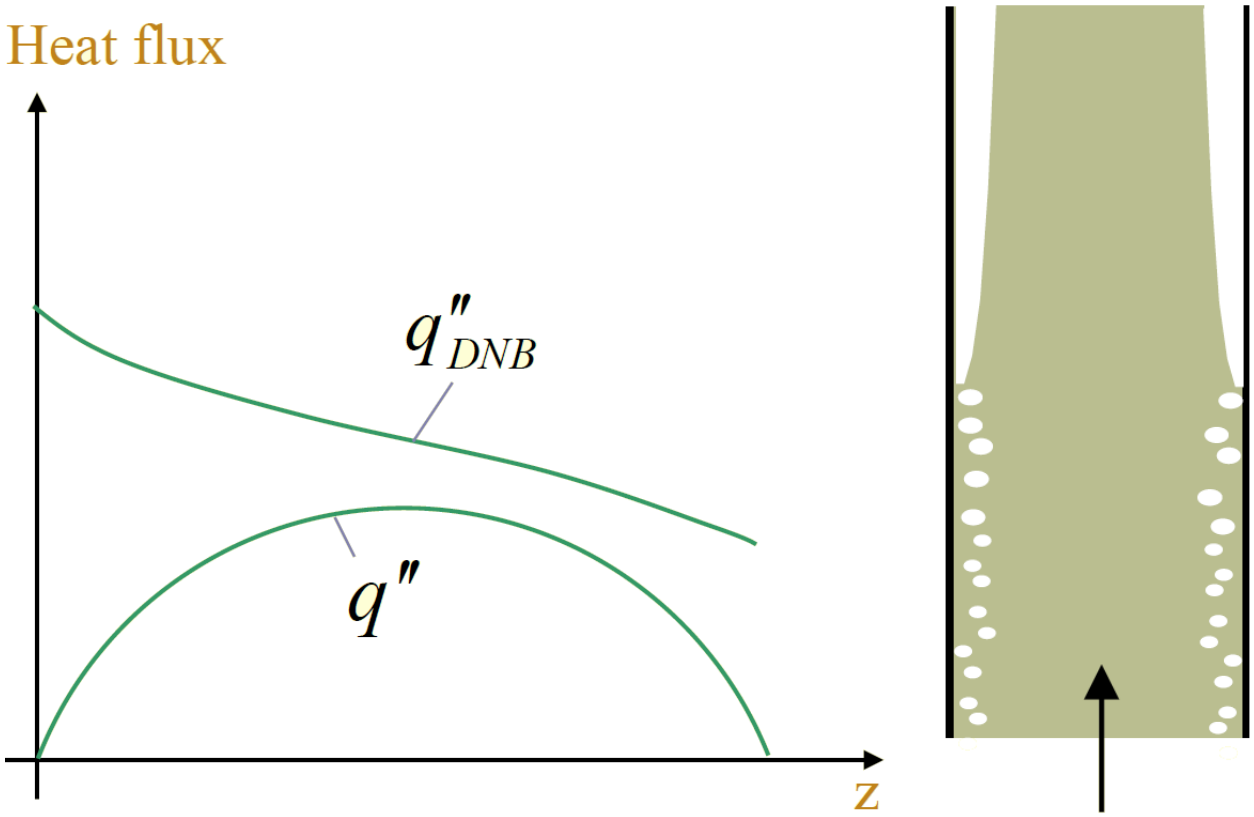

(a) DNB Heat Flux (b) DNB Flow

Figure 2.4. Subfigure (a) shows how the critical heat flux (q''_{DNB}) varies due to a typical axial power profile. It can be seen that the minimum departure from nucleate boiling ratio (MDNBR) will not neccesarily occur at the point of maximum actual heat flux (q''). Subfigure (b) shows how subcooled boiling can collapse to create a continuous vapor film. The figures are taken from [63, p.7,13].

straightforward of these is the Tong-68 correlation, shown in equation 2.14 [63, p.8].[28]

$$q''_{\mathrm{DNB}} = K_{\mathrm{Tong}}\, h_{fg} \frac{\dot{m}^{0.4}\mu^{0.6}}{A^{0.4} D_e^{0.6}} \tag{2.14a}$$

$$K_{\mathrm{Tong}} = 1.76 - 7.433\, x_e + 12.222\, x_e^2 \tag{2.14b}$$

$$x_e = -\frac{c_{p,\ell}\,(T_{\mathrm{sat}} - T_{\mathrm{bulk}})}{h_{fg}} \tag{2.14c}$$

In the Tong correlation, q''_{DNB} is the heat flux at which departure from nucleate boiling will occur. The correlation creates a curve showing the DNB heat flux at each location, as seen in figure 2.4(a). Of the remaining variables in the DNB equation, h_{fg}, μ, $\dot{m}$, A, and D_e, are

[28] More recent, and accurate, correlations are generally proprietary information of the companies that generate them. The Tong correlation is sufficient for the scoping analysis of this thesis.

the specific enthalpy of vaporization and dynamic viscosity of the coolant, mass flow rate, flow area, and equivalent diameter respectively. K_{Tong} and x_e are placeholder variables to simplify the expression of the correlation. Finally, $c_{p,\ell}$ is the isobaric specific heat of the liquid phase of the coolant, T_{sat} is the saturation temperature of the coolant, and T_{bulk} is the bulk fluid temperature as a function of position.

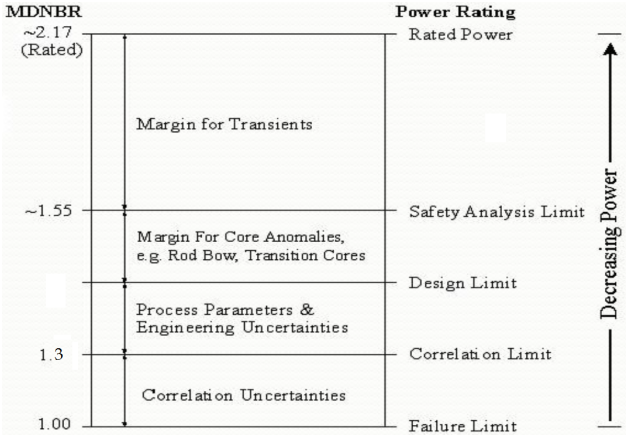

Figure 2.5. There are many considerations when determining the required margin for departure from nucleate boiling. This figure shows some of the considerations that must be taken into account, and their relative contribution to MDNBR. This figure was taken from [64, p.13].

While the Tong correlation allows calculation of the margin to DNB (defined as the DNBR in equation 2.13), it does not provide guidance on the minimum margin to provide safety. Figure 2.5 shows some of the considerations that are currently taken into account when determining the MDNBR requirement for a reactor. A typical DNBR target for a commercial reactor will be around 2.1 or 2.2 at normal operating conditions [64, p.13]. The post-accident limit on MDNBR is 1.3 [64, p.17].

In this thesis, DNBR was quickly determined to be the most limiting of all thermal considerations. Relatively thin fuel plates were easily able to meet targets for fuel and cladding temperature limits. However, the high heat fluxes demanded by a high power density core made reasonable CHF margins difficult to achieve. As a compromise, the MDNBR limit of 1.3 was adopted for steady-state core operations.[29] To determine the MDNBR of the core, the maximum power peaking factor of the core was calculated in the depletion simulation.

[29]This limit does not provide naval reactors with as much margin as commercial reactors. However, there are a few unique methods naval reactors can use to gain more margin. First, the Russian icebreaker core uses twisted cruciform rods in order to increase the turbulence in the core, gaining more margin. Additionally, the small required size of naval reactor pumps (shown in table 4.3) means that larger pumps could be installed.[30] This would allow for a large increase in coolant flow rate (and thus MDNBR) if it were required due to accident conditions. Finally, a transient analysis of fuel and cladding temperature after the onset of film boiling could be calculated as part of a future safety analysis.

A fuel plate with a power density equal to the average times the power peaking factor then used the Tong Correlation to determine MDNBR. An actual core design by naval reactor engineers would have to choose a larger steady state DNBR limit in order to provide protection against all of the considerations shown in figure 2.5.

2.1.9 Plate Thickness

There are a few competing factors when selecting a fuel plate thickness. The first is the thermal characteristics of the core. A thick fuel plate leads to large heat fluxes, and correspondingly high fuel temperatures and low DNB margins. In fact, plates as thin as a half centimeter can have MDNBR values as low as 0.5. Margins for melting are much easier to achieve due to the high thermal conductivity of the fuels used in this thesis. Thermal characteristics of the core encourage thin fuel plates.

The second consideration is the amount of unfilled space within the core. Figure 2.6 shows an example of a core with fuel plates that are half a centimeter wide and plates that are a quarter centimeter wide. Using the thinner plates allows for there to be less "corner space" inside the core barrel, where another fuel assembly could almost be placed but not quite. However, competing with this effect is the fact that as the number of fuels plates increases, the volume of the core taken up by cladding increases. The width of the fuel plate is additionally limited by the "battleshock" condition of 50gs of force [22, p.14].

In the end, a balance between the competing factors was found with a plate thickness of 0.25 cm.[31] This kept the plate thin enough that temperature and DNB margins could be met, yet thick enough not to waste space on cladding or risk the structural integrity of the fuel. This makes the plates roughly the same size as those used by Ippolito in his "thick plate" study [44, p.78].

2.2 Materials Considerations

A nuclear reactor is one of the most challenging material environments to design for. In addition to the factors that everyday materials face such as creep, fatigue, and a variety of corrosion mechanisms, radiation can cause swelling, helium embrittlement, radiation induced segregation, and other phenomena. This section will discuss some of the important materials considerations in the reactors. The most basic factor affecting material selection is the high temperature environment. This will be followed by a description of the corrosion modes that

[31] In this case, "plate width" is actually referring to the width of fuel within the plate. The complete width of the plate, cladding included, is 0.33 cm.

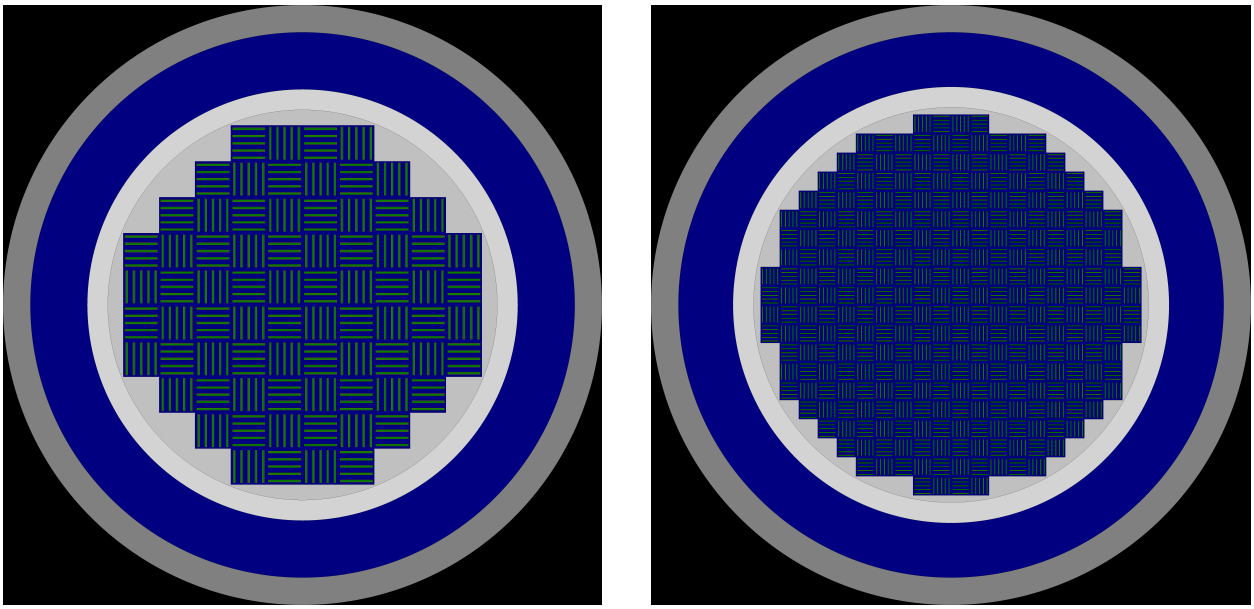

(a) 0.50 cm Fuel Plates

(b) 0.25 cm Fuel Plates

Figure 2.6. Subfigure (a) shows a full reactor core using plates twice as wide as those in subfigure (b). Using thinner plates allows for the space within the core barrel to be filled with a higher volume of fuel, wasting less volume on the core baffle.

exist in a pressurized water reactor. The long term effects of irradiation will be discussed next, and a short section will describe the various compatibility requirements of the materials used in naval reactors. Finally, fission gas swelling will be discussed.

2.2.1 High-Temperature Effects

The high power density of nuclear reactors make high-temperature effects and properties of materials very important. Light water commercial reactors generally have inlet and outlet temperatures of around 280°C and 320°C respectively [47, p.22]. The maximum temperature in the cladding can range from 350°C to 450°C, while fuel centerline temperatures can pass 1750°C during normal operation [34, p.428, p.433]. Even structural components not involved with the power production process will have to meet certain high-temperature requirements.

The most critical thermal property of materials is their melting point. The more specific details of what the melting point must be will depend more on the component in question, but a melting point significantly above operating conditions is desirable in all parts of the reactor. Coupled with the melting point is the thermal conductivity. High thermal conductivities serve to keep steady state temperatures lower, especially in the fuel and cladding where heat

Table 2.4. Reactor Margins and Design Criteria

Margin	Criteria
Power	150 MW
Total Energy	225,850 MWd
Height	1 m
Diameter	1 m ± 10%
Minimum k_{eff}	1.04
Maximum Burnup	-[1]
Maximum Outer Fuel Temperature	425°C
Maximum Fuel Temperature	T_{melt}-300°C
MDNBR	1.3

[1] The maximum burnup will be different for the fuels chosen for the HEU and LEU cores. For details on each, see section 2.5 and 2.6 respectively.

transfer is driven by a combination of thermal conductivity and temperature gradients.[32] High temperatures can also activate and accelerate mechanical creep, leading to material failure if not correctly planned and accounted for.

2.2.2 Corrosion Mechanisms and Consequences

The coolant used in nuclear reactors subjects most of the materials in the reactor to a significant amount of corrosion. The primary effect of this is that the outer layers of many materials in the reactor can either be removed, or suffer detrimental changes to their properties. The pace of degradation can be accelerated by flow assisted corrosion, where the normally protective outer oxide layer is stripped by the fast flowing coolant.[33]

The flow assisted corrosion process also leads to the deposition of CRUD on all revealed surfaces of the reactor.[34] CRUD can then increase the thermal resistance of the cladding, increasing temperatures in the fuel, or produce power level oscillations in the reactor.[35] The effects of CRUD are currently a major research area of CASL in the United States.[36]

[32]The derivation of the exact temperature profile in the fuel and cladding is shown in section 3.2.

[33]This oxide layer is sometimes intentionally stripped away. The oxide layer can inhibit heat transfer from the plates, raising temperatures of the cladding and fuel [6, p.64].

[34]CRUD, originally from "Chalk River Unidentified Deposits," is a catch-all term referring to the deposition of oxides dissolved in the coolant onto fuel rods, control rods, and other locations.

[35]In a PWR, soluble boron can be precipitate out of the coolant onto the fuel, locally depressing reactivity, and therefore power.

[36]The Consortium for Advanced Simulation of Light Water Reactors (CASL) is a US Department of Energy funded research initiative with the goal of simulating all thermal-hydraulic, neutronic, and materials effects of a nuclear reactor at once.

Corrosion can also lead to stress corrosion cracking of the cladding and other materials. In the Davis-Besse incident in 2002, it was discovered that the borated primary coolant had eaten through more than six inches of carbon steel, leaving only the 3/8" stainless steel cladding of the pressure vessel behind to maintain structural integrity [65, p.4]. The NRC later concluded that stress corrosion cracking had caused the event, and issued strict inspection requirements for all other reactors [65, p.8]. Materials chosen for use in nuclear reactors must be able to resist all of these corrosion mechanisms, and degrade in a predictable, steady manner over the life of the reactor.

2.2.3 Radiation Effects

All materials in a naval reactor will encounter a significant amount of radiation of various types over the reactor's life. The most active part of the reactor will be the fuel, due to the transmutation of uranium into higher actinides as well as that of the fission products that build up over the course of the reactor's life. However, all parts of the reactor will encounter a significant amount of neutron bombardment. This causes a number of effects unique to nuclear engineering.[37]

The cause of irradiation damage in materials is the deposition of energy from radiation absorption and slowing down processes.[38] As particles enter a material, they collide with atoms or molecules held within the material's lattice. If the energy exchange is high enough, this can lead to the creation of a "Frenkel Pair," where a displaced atom in the lattice leaves a gap ("vacancy") behind and comes to rest between lattice positions elsewhere (creating an "interstitial") [67, p.x]. These defects can move through the material and recombine or accumulate to create large-scale deformations.

The accumulation of vacancy defects in one area can lead to void swelling of a material. Fluences as low as 10^{22} n/cm^2 can lead to volume changes of 20% in elemental solids [67, p.x]. Irradiation can also lead to growth or creep in a material. Void swelling generally refers to geometry changes that result in an increase in volume, while irradiation growth refers to effects that distort geometry while maintaining a constant volume. For example, a pure uranium metal rod 10 cm in length and 1 cm in diameter exposed to a fluence of 10^{20}

[37] Almost all of these effects are accelerated between 30% and 55% of the material's melting point [66, p.41]. At these temperatures, defects caused by irradiation are mobile enough to concentrate, yet immobile enough to prevent recombination. For more a more detailed discussion of radiation effects on materials, see [67].

[38] In this context, it is useful to think of gamma rays as "particles" of radiation. This is not an entirely accurate description, as the interaction mechanisms of gamma rays are quite different from neutrons or charged alpha and beta particles. However, the effects of these interaction mechanisms are similar in this very broad description of radiation.

n/cm^2 can grow to 30 cm in length and shrink to 0.58 cm in diameter [67, p.x].[39]

The migration of defects can cause the composition of a material to change radically at grain boundaries. As defects accumulate inside a grain, certain elements can be preferentially forced towards or away from grain boundaries [66, p.41]. This can lead to local concentrations of alloying elements 20 to 60 times their bulk value [67, p.x]. This effect is known as radiation induced segregation, and is shown in figure 2.7. The depletion of chromium at grain boundaries of stainless steels has been linked to intergranular stress corrosion cracking in many components [67, p.805]. Furthermore, the enrichment of chromium away from the boundary causes the formation of a variety of intermetallic phases, further embrittling the alloy [66, p.41].

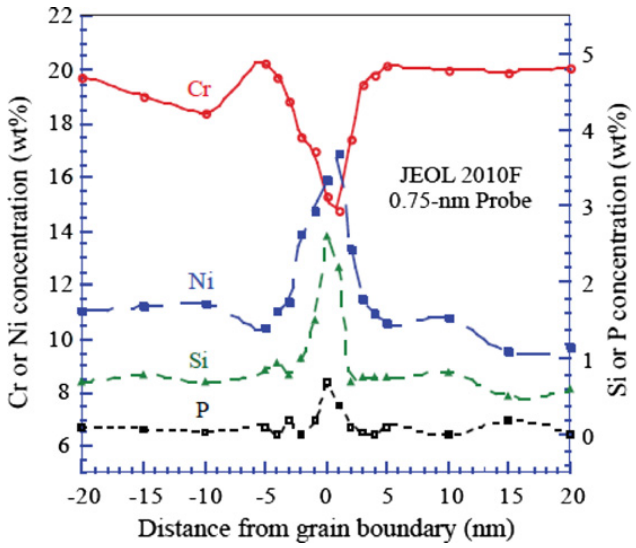

Figure 2.7. The accumulation and movement of defects causes chromium to preferentially migrate away from the grain boundary in many stainless steels, while nickel and other elements become enriched. This can cause embrittlement of the steel and aggravate corrosion mechanisms. Figure reproduced from [66, p.42].

Finally, many of the materials in the reactor can become activated through neutron capture. Activated corrosion products can be carried by the coolant.[40] This results in irradiation of the entire primary loop in addition to the core and its surrounding materials. While this effect will be of a much lower magnitude than the damage accumulated in the core, it means that all parts of the primary system must be designed to cope with irradiation.

[39]The preferential direction seems to be due to the crystal structure of the metal.
[40]The oxygen in the coolant can also become activated, and the hydrogen can form tritium.

2.2.4 Chemical and Nuclear Compatibility

To preserve the integrity of the reactor, all chosen materials must be chemically and metallurgically compatible with the coolant and each other. For example, it would be undesirable to use group-I alkali metals in high concentrations anywhere in the reactor, as they undergo a rapid, exothermic oxidation reaction when exposed to water. One advantage of a PWR is that liquid water coolant is compatible with steels and other common metal alloys.[41] Furthermore, the most common fuel cladding materials (aluminum and zircaloy family alloys) do not interact with most fuels. Future Generation IV reactors incorporating molten salt fuels or gas coolants may have to make design choices based on compatibility issues. However, for the limited aims of this thesis (a modest change in fuel type and enrichment), the current generation family of steel and zircaloy alloys should prove sufficient.

Additionally, all materials chosen for use within the reactor should have low neutron absorption cross sections. This prevents structural and other materials from acting as built-in poisons to the core. Additionally, high absorption cross sections would cause transmutation of the material over the life of the core. This could result in significant changes to material properties.

2.2.5 Fission-Gas Swelling

One of the primary causes of physical changes in fuel with burnup is the accumulation of fission product gases [68, p.3751]. It can cause the fuel to swell, blister, or crack as individual atoms of gas coalesce to form bubbles and apply pressure to the fuel and the interior of the cladding [60, p.90]. In commercial PWRs, the fuel is allowed to crack, and fission gases accumulate in a specially designed plenum that keeps gas pressure low [69, p.1526]. Nevertheless, the fuel cracking leads to a sharp decrease in fuel thermal conductivity, and a resultant rise in temperature [34, p.372]. In metal fuels, the more important effect of fission gas release is the formation of gas bubbles within the fuel, and resulting void swelling [70, p.12]. Most fission-product gases are also radioactively stable, so accumulation will continue over the life of the reactor [68, p.3755].

2.3 Cladding

There are two common cladding materials used in nuclear reactors. The most commonly used cladding in commercial nuclear reactors is a zirconium alloy, usually under the "zircaloy"

[41] While most metals will corrode in water, they generally do so at a predictable rate, precluding their immediate disqualification.

trademark. It is generally composed of about 95% zirconium and less than 2% each of tin, niobium, iron, chromium, nickel, and other metals, added to improve mechanical properties and corrosion resistance. The most commonly used cladding used in research reactors is aluminum metal, due to its low absorption cross section, high thermal conductivity, and low cost.

Aluminum is a popular choice for research reactors that run at low temperatures and pressures. However, it is unsuitable for power reactors due to its relatively low melting point (roughly 650°C) and correspondingly lower creep temperatures. This makes it a poor choice for a power reactor that operates at high temperatures, and may face acute conditions during an accident. The remaining option is zircaloy cladding.

Zircaloy is commonly used in light water reactors due to its combination of neutronic and structural properties. However, the use of zircaloy cladding forces a thermal constraint on the reactor due to the oxidation properties of zirconium. Zirconium undergoes an exothermic oxidation reaction, shown in equation 2.15.

$$\mathrm{Zr} + 2\,\mathrm{H_2O} \rightarrow \mathrm{ZrO_2} + 2\,\mathrm{H_2}\ ;\ \Delta\mathrm{H} = -585\,\mathrm{kcal/mol} \tag{2.15}$$

This in itself is not reason enough to disqualify zirconium as a cladding material. All metals oxidize in water to some extent. The important property of this reaction is its tendency to rapidly accelerate at high temperatures. An estimation of the oxidation rate of zirconium is given in equation 2.16 [71, p.11].

$$\text{Oxidation Rate } [\mathrm{g/cm^2\text{-}s}] = 13.9 \cdot P^{1/6} \cdot \exp\left(\frac{-1.47\,\mathrm{eV}}{k_B T}\right) \tag{2.16}$$

In the above equation, P is the pressure in atmospheres, k_B is the Boltzmann Constant in eV/K, and T is the temperature in Kelvin. As seen in figure 2.8, this leads to a rapid increase in oxidation rate above roughly 1000°C. This rapid oxidation is undesirable for three reasons. First, oxidation of zirconium eats away at the cladding material, potentially allowing the direct interaction of fuel and coolant. Secondly, the oxidation reaction produces hydrogen gas, which (in accident scenarios, such as those present at Fukushima) can lead to explosions within the primary system or containment. Finally, the heat generated by oxidation can cause a runaway reaction, where oxidation increases cladding temperature, which increases the oxidation rate. This will eventually lead to melting the cladding and or the fuel. Run-away corrosion is kept in check through the generation of a passivating oxide layer on the surface of the cladding [73, p.53]. A surface oxide layer slows the diffusion of oxygen and hydrogen atoms required for oxidation to proceed [73, p.50]. If the layer becomes

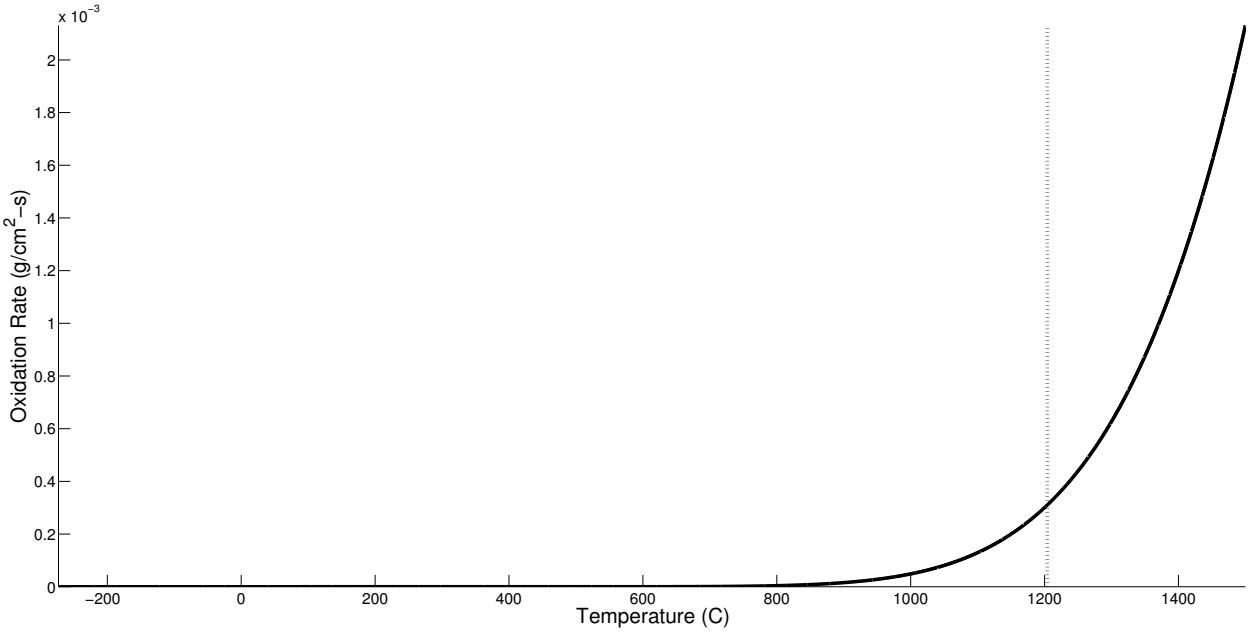

Figure 2.8. The oxidation rate of zirconium follows an exponential curve based on equation 2.16. The NRC specifies a peak cladding temperature limit of 2200°F in 10 CFR 50.46, here represented by the vertical line at 1204°C [72, p.690].

fractured or porous, the rate of oxidation can once again increase [73, p.55].

Generally, steady-state zircaloy outer temperature is kept below 349°C to prevent excessive corrosion [64, p.11]. The Phillips correlation used for Nusselt number (discussed in section 3.2.2) is generally an underestimation of heat transfer, so the temperature rise predicted by equation 3.13 will be up to 25% high [74, p.1348].[42] Therefore, a more generous limit of 375°C will be used for the maximum outer cladding temperature.[43] Additionally, zircaloy loses its strength above 400°C [64, p.10]. Therefore, the average cladding temperature will be kept below 350°C.

The last necessary step is to estimate the cladding thickness required for the fuel. Commercial reactors typically use between 0.4 mm and 0.8 mm of cladding [75, p.1]. However, commercial fuel pins and naval reactor fuel face different challenges. First, commercial fuel pellets are allowed to crack, allowing fission product gases to fill a pellet-cladding gap within the pin. Therefore, if the cladding were to rupture these gases would be released into the coolant. Plate fuels do not have this gap for structural reasons, and generally hold fission products within the fuel matrix [76]. Therefore, even if the cladding were corroded through

[42]Equation 3.13 calculates the Nusselt number of the flow. This can be used to calculate the heat transfer coefficient in equation 3.7, which can calculate the temperature difference between the bulk fluid and outer cladding temperature using equation 3.3.

[43]The new maximum temperature of 375°C was calculated by determining the highest cladding temperature which can be reduced to 349°C by increasing the heat transfer coefficient by 25%.

Table 2.5. Zircaloy Limits

Measurement	Criteria
Maximum Outer Cladding Temperature	375°C
Maximum Average Cladding Temperature	350°C
Cladding Thickness	0.4mm

or ruptured, fission products would not be entirely released into the coolant. Second, naval fuel materials are made of more durable materials than uranium oxide, and so have a corrosion resistance that provides safety even in the absence of cladding. In the Ippolito study, for example, naval fuel is estimated to have 0.385 mm of cladding [44, p.78]. This thesis will use a cladding thickness of 0.4 mm on either side of the fuel.[44] A summary of reactor constraints created by the use of zircaloy cladding is provided in table 2.5. The material composition of Zircaloy-4 used in this thesis is shown in table 2.9.

2.4 Structural Materials

To increase accuracy, the simulation boundary of this project will be the outside of the reactor pressure vessel. This means that the thickness of a core baffle, core barrel, and reactor pressure vessel must be estimated. Additionally, specific steels must be identified for each of these components.[45] For sizing requirements and materials choices, the MIT BEAVRS Benchmark will be heavily referenced.[46]

The reactor pressure vessel of a PWR is designed to contain the high-pressure coolant of the reactor, as well as all of the fuel and other core components. In a typical PWR, the pressure vessel has an inner radius of 230 cm and an outer radius of 251.9 cm [77, p.110]. Submarine reactor pressure vessels have an estimated outer radius of 83.5 cm [22, p.78]. However, they would not need the same 22 cm thickness for an equivalent strength. The maximum tangential stress on a thin[47] cylinder can be estimated by equation 2.17 [78,

[44]This makes naval fuel have a cladding thickness equal to the lower boundary of commercial PWR cladding. However, commercial burnup is much lower than that of naval reactors. Naval reactor cladding may have to be thicker due to increased swelling or corrosion. This uncertainty will be addressed in section 7.3.9.

[45]This is one area of design that will not be exhaustively explored here. This thesis will attempt to indentify a steel that could work for each purpose, not to fully determine the optimal choice.

[46]The Benchmark for Evaluation And Validation of Reactor Simulations (BEAVRS) is a full-core light water reactor benchmark developed by the MIT Computational Reactor Physics Group [77]. It incorporates data from two full burnup cycles to provide a realistic model for simulation testing.

[47]Equation 2.17 also relies on an assumption that t/R is less than 0.1 [78, p.22]. This will be verified in all calculations.

p.21].[48]

$$R = r_i + \frac{t}{2} \tag{2.17a}$$

$$R = r_o - \frac{t}{2} \tag{2.17b}$$

$$\sigma_{t,max} \approx \frac{p_i R}{t} \tag{2.17c}$$

In the above relations, r_i is the inner radius of a cylinder, r_o is the outer radius of a cylinder, t is the thickness of the cylinder, p_i is the interior pressure on the cylinder, and $\sigma_{t,max}$ is the maximum tangential stress applied to the cylinder wall. If it is assumed that the maximum stress requirement of a naval reactor is similar to that of a commercial reactor, then this results in the ratio shown in equation 2.18.[49]

$$\begin{aligned} \frac{R_{\text{Commercial}}}{t_{\text{Commercial}}} &= \frac{R_{\text{Naval}}}{t_{\text{Naval}}} \\ &= \frac{r_{o,\text{Naval}} - t_{\text{Naval}}/2}{t_{\text{Naval}}} \end{aligned} \tag{2.18}$$

This ratio results in a pressure vessel thickness of 7.6 cm for the naval reactor simulation, with an interior and exterior radii of 75.9 cm and 83.5 cm respectively.[50]

The core barrel provides structural support to the core and reactor internals, while keeping the interior upwards flow of water separate from the water flowing in the downcomer outside of it. In a commercial PWR, the core barrel is 5.7 cm thick [77, p.107-108]. This value will be adopted for the naval reactor model.

The core baffle is a series of vertical plates that provides support to the core as well as directing coolant flow through the core. In a typical PWR, it is about 2.2 cm thick [77, p.106]. A typical core baffle looks like figure 2.9(a). However, this design is just thick enough to act as a poison to thermal neutrons, while not being thick enough to significantly reflect fast neutrons back into the core [79, p.41]. A thicker baffle can reflect fast neutrons back into the core. Additionally, the traditional baffle design allows roughly 5% of the coolant flow to bypass the core entirely [77, p.78]. By filling in the bypass space with steel, all of the coolant will be forced into the core. This results in a baffle similar to figure 2.9(b).

It is possible that naval reactors could use different types of steel than commercial re-

[48]For this thesis, the pressure vessel will be assumed to have the same strength if they have the same maximum tangential stress. In this simulation, accuracy of this measurement is not incredibly important, as the final thickness of the pressure vessel is placed a quarter of a meter away from the core. Relatively few neutrons will travel this far, and even fewer will be reflected all the way back into the fuel.

[49]The pressure of a commercial reactor and the assumed naval reactor are both 15.51 MPa [77, p.3].

[50]These measurements also satisfy the t/R $\leq$ 0.1 requirement.

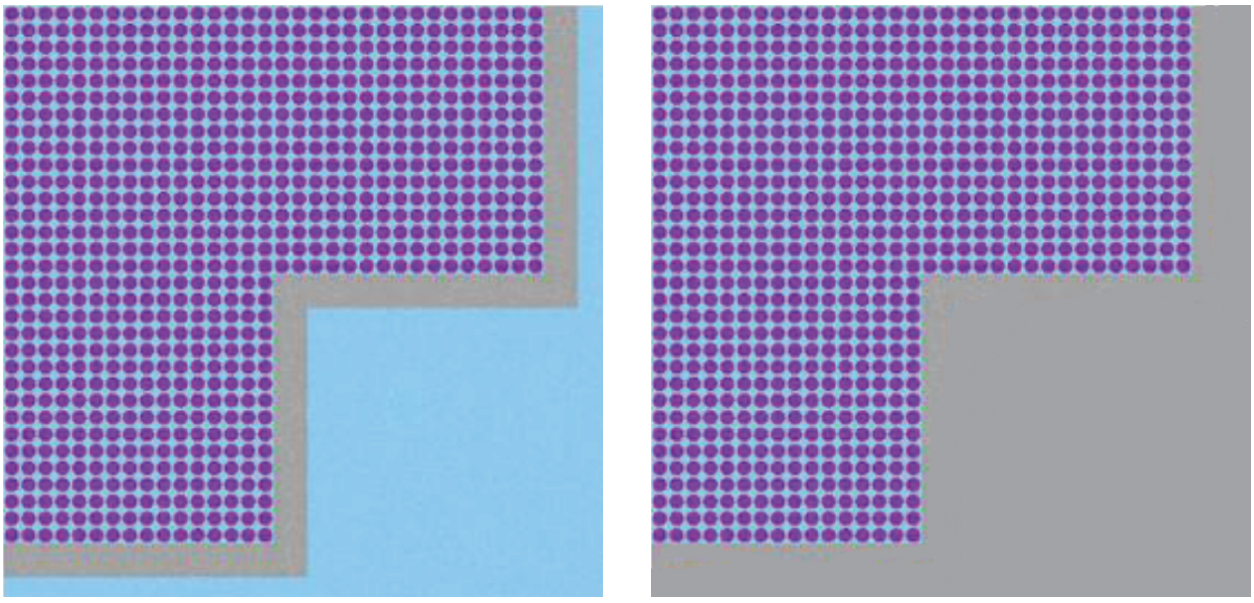

(a) Traditional Core Baffle

(b) Improved Core Baffle

Figure 2.9. Above are depictions of two kinds of core baffle. In the first, the baffle provides structural support for the core and separates coolant flow into core and bypass regions. In the second, the core bypass region is eliminated, forcing coolant into the core, and the thicker steel serves as a fast-neutron reflector.

actors. Defense projects typically operate under much more lax funding constraints than profitable enterprises, and a priority on performance over economics could drive naval reactors to use expensive alloys for major components. Without knowing more about the specifics of naval reactors, the pressure vessel will be simulated as carbon steel, and the barrel and baffle will be 304 stainless steel [77, p.25].[51] The elemental composition of these materials is shown in table 2.9.

2.5 HEU Fuel

The HEU fuel selection starts from an open-source estimation of a Russian icebreaker reactor, modified to allow for a much higher burnup. This will allow for the HEU fuel to meet the reactivity requirement demanded by a lifetime submarine reactor. In the end, the HEU case will provide a proof of concept of the modeling techniques used in this thesis, as well as illustrate the ease with which HEU cores can meet lifetime reactivity requirements.

[51] Both carbon steel and 304 stainless steel have proven capable of use for fourty year reactor lifetimes in commercial reactors. While the exact fluence they receive in commercial reactors may be different from use in naval reactors, the materials should be capable of attaining a sufficient lifetime. The BEAVRS Benchmark also provides a list of material compositions of carbon and 304 stainless steel.

2.5.1 Open-Source Naval Reactor Estimates

The design of U.S. naval reactor fuel remains classified and there have not been many open-source estimates [45, p.12-8]. However, the Norwegian Radiation Protection Authority was able to gain detailed information on the fuel used in the *Sevmorput*, a Russian nuclear-powered icebreaker [20, p.100]. The fuel was determined to be a metal alloy, containing 48.2% uranium and 51.8% zirconium by weight [20, p.100]. While this does not necessarily reflect the fuel used by the US Navy, there should be similarities. The icebreaker uses HEU in the fuel, and the core is 135 MW_{th}, close to the estimations of US submarine reactors shown in table 2.1 [80, p.34]. The reactor core is 1 m tall with a 1.2 m diameter, close to estimates of submarine core sizes discussed in section 2.1.4.

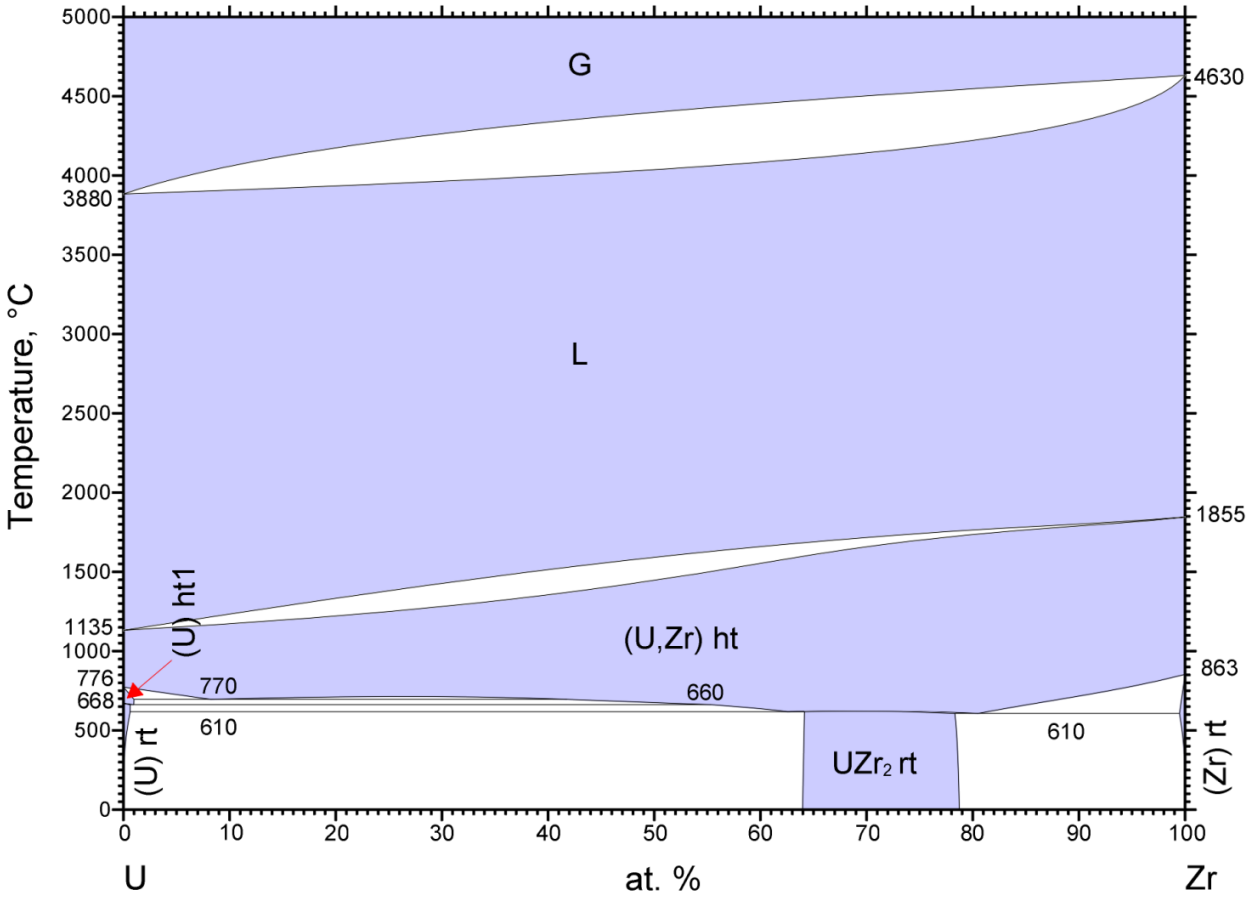

Figure 2.10. This figure shows the uranium-zirconium binary phase diagram, taken from [81]. Weight percentages of 48.2% and 51.8% correspond to atomic percentages of 26.3% and 73.7% for uranium and zirconium respectively. This would give the proposed alloy a melting temperature of about 1750°C.

However, there are significant differences between the icebreaker fuel and theories about US naval reactors. The icebreaker's estimated operating period is 417 full power days,

compared to roughly 1,500 full power days estimated in equation 2.6 [80, p.34].[52] Finally, the icebreaker fuel pins are annular with a hollow core. This design is unlikely to meet the US Navy's strict requirement for battleshock conditions of up to 50gs of force [22, p.14].

This thesis will use the chemical composition of the Norwegian model of HEU fuel as a starting point. US and Russian fuel development likely faced similar challenges in extending submarine life, and the well documented history of espionage during the Cold War could have led to parallels in the two programs. In the end, the Norwegian estimate will not provide a perfectly accurate reflection of US naval fuel, but it should provide a fuel with many similar characteristics.

While the literature gives a good estimate of the weight percentages of uranium and zirconium in the alloy, as well as the resultant uranium density (4.5 U-g/cm^3), it does not give an estimate of the alloy density of the fuel. This can be estimated using equation 2.19.

$$\frac{1}{\rho_{alloy}} = \frac{w_U}{\rho_U} + \frac{w_{Zr}}{\rho_{Zr}} \tag{2.19}$$

In the above equation, ρ_{alloy}, ρ_U, and ρ_{Zr} are the densities of the alloy, uranium, and zirconium w_U and w_{Zr} are the weight fractions of uranium and zirconium. This results in an alloy density of 9.55 g/cm^3. The Norwegian study also did not provide the volume fraction of uranium and zirconium in the alloy fuel. This can be calculated through equation 2.20.

$$v_i = \frac{w_i}{\rho_i} \cdot \rho_{alloy} \tag{2.20}$$

where v_i, w_i, and ρ_i represent the volume percent, weight percent, and density of each element. This equation gives the volume percentages of uranium and zirconium as 24.1% and 75.9% respectively.

2.5.2 Alteration of the Open-Source Model

The problem with the Norwegian U-Zr alloy is that it cannot reach the burnup required of a lifetime core. Even if half of the core is packed with fuel (leaving the reactor more than significantly undermoderated), burnups in excess of 250 MWd/kg are required to meet the energy demand estimated in equation 2.6. The Russian icebreakers using this fuel generally do not exceed 75 MWd/kg, despite refueling while k_{eff} is still roughly 1.2 [80, p.44,47]. This suggests that the fuel is limited by the physical effects of burnup rather than a loss of criticality. This is a common problem of metal alloy fuels that have to operate in the high

[52] This comparison comes out to roughly 56,000 MWd for the icebreaker while attack submarines require 230,000 MWd.

temperatures of a nuclear reactor [44, p.38].

However, it is possible to make a slight change to the Norwegian estimate and enable a high burnup. The significant problems at high burnup faced by metal alloy fuels can be avoided by using a dispersion fuel.[53] By switching out the uranium for uranium oxide the possible burnup of the reactor can be significantly extended. Figure 2.11 shows an estimate of dispersion fuel burnup limits as a function of uranium oxide volume fraction. For this thesis, the weight fraction of uranium from the Norwegian study will be held constant. Oxygen will then use a weight fraction equal to 32/(235+32),[54] or 12%, of the value for uranium.[55] Zirconium will then make up the balance of the HEU fuel.[56] The material density, uranium density, and constituent volume fractions are recalculated using the new weight density of uranium, oxygen, and zirconium.

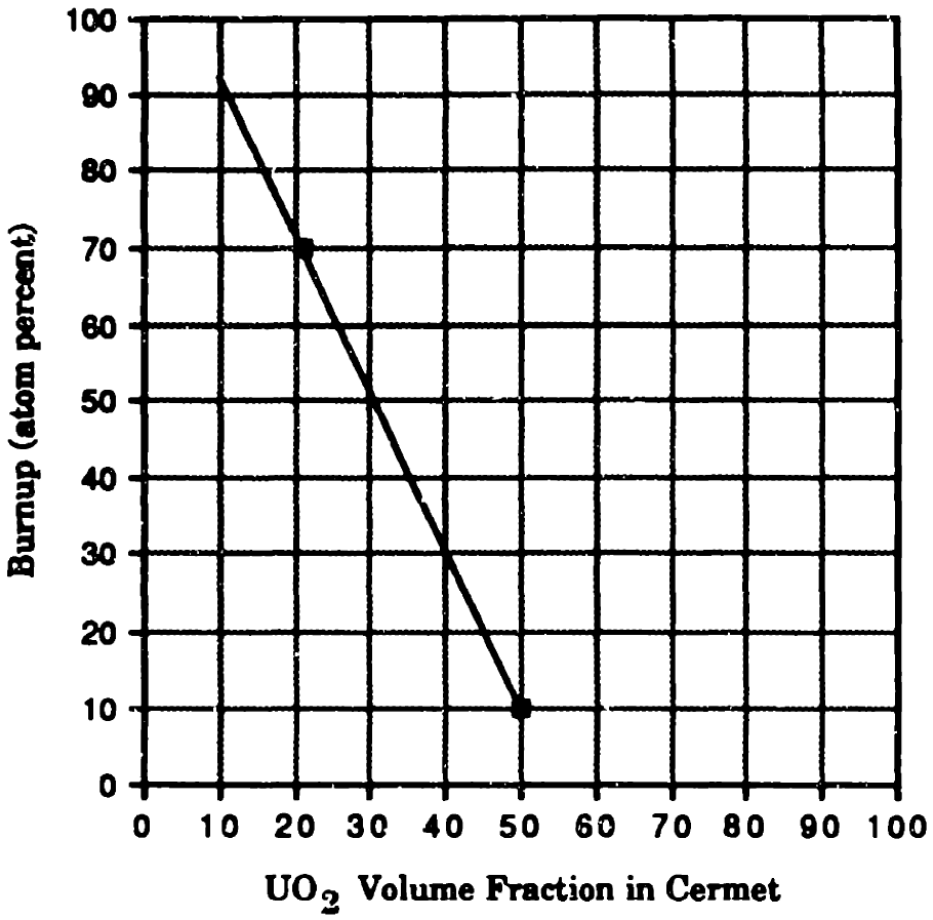

Figure 2.11. Dispersion burnup limits taken from [44, p.68]

[53]Details about dispersion fuels are discussed in section 2.6.

[54]The weight fraction of oxygen in UO_2.

[55]Because uranium makes up 48.2% of the fuel, oxygen takes up 6.56% of the weight.

[56]The uranium oxide - zirconium dispersion fuel will be referred to as UO_2-Zr for the rest of this thesis.

Table 2.6. Uranium Enrichment

Isotope	Weight Percent[1]
93% Enriched	
^{234}U	0.739%
^{235}U	93.0%
^{238}U	6.27%
20% Enriched	
^{234}U	0.540%
^{235}U	20.0%
^{238}U	79.5%
Natural Uranium	
^{234}U	$\approx 0\%$
^{235}U	0.711%
^{238}U	99.3%

The first step of this process is to determine the molecular weight of the uranium used in HEU. For uranium enriched to a 93% (the enrichment of current Virginia class submarines [7, p.ii]) the relative weights of uranium isotopes are shown in table 2.6. Using these values and the isotopic masses given in [77, p.138], the required weight of oxygen in the fuel can be calculated. The final result of these calculations gives the fuel breakdown shown in table 2.9.[57]

The UO_2-Zr fuel has a lower uranium density than the icebreaker fuel (4.04 g/cm^3 compared to 4.5 g/cm^3).[58] However, because the uranium oxide volume fraction is low, a burnup of about 30% atomic can be achieved.[59] The exact fractions used in these calculations are shown in table 2.7. This fuel will be used in chapter 4 to simulate a modern, HEU naval reactor.

The dispersion fuel has many benefits. First, the melting point of both zirconium and uranium oxide are high. The melting point of zirconium is about 1,800°C and the melting point of uranium oxide is about 2800°C. As long as the uranium oxide particles are kept small, the low thermal conductivity of the ceramic will not have much of an effect, and the high thermal conductivity of zirconium metal will dominate, keeping temperatures low.[60]

[57]The substitution of uranium oxide (density of 10.97 g/cm^3) for uranium (density of 19.1 g/cm^3) also requires a recalculation of the dispersion fuel total density using equation 2.19.

[58]While the UO_2-Zr fuel has the same weight fraction of uranium, the fact that it is composed of uranium oxide and zirconium as opposed to uranium and zirconium leads to the lower density.

[59]Using equation 2.20, it can be shown that the new fuel has a UO_2 volume fraction of 41.8%. Figure 2.11 can then be used to approximate a burnup limit of 30% atomic, or about 300 MWd/kg.

[60]The thermal conductivity of the dispersion fuel as a whole is 12 W/m-K [82, p.142].

Table 2.7. UO_2 Dispersion Fuel

Compound	Weight Percent	Volume Percent
Zr Metal	45.2%	58.2%
UO_2[1]	54.8%	41.8%

[1] Due to the enrichment level, shown in table 2.6, the molar mass of uranium here is 235.22 g/mol, and the resultant molar mass of UO_2 is 267.22.

This makes the fuel an adequate choice to simulate a naval reactor.[61]

2.6 LEU Fuel

The LEU fuel selection process is more unconstrained than the HEU selection. The LEU fuel requires a fuel with a much higher uranium density, significantly lowering the required burnup. Early studies showed that LEU fuels have difficulty keeping k_{eff} over one past 100 MWd/kg. Therefore, it is important to get as much uranium into the core as possible, to maximize the amount of energy extracted at the lower burnup limit. This thesis will consider LEU fuels studied by the Reduced Enrichment for Research and Test Reactors (RERTR) program.

2.6.1 High Density Fuels

The RERTR program has developed a variety of advanced LEU fuels that could be considered for use in naval reactors. These fuels can be broken into two types: dispersion fuels, which have been used in research reactors for decades, and monolithic fuels, which are at a much earlier stage of development but offer higher uranium densities.

Dispersion Fuels

Dispersion fuels are two-phase mixtures of a uranium-bearing dispersant in a metal matrix [44, p.41]. The uranium dispersant can be a ceramic (such as UO_2 or U_3Si) or metal alloy (such as UAl_2 or UN). In research reactors, the metal matrix is generally aluminum due to its low cost and good thermal properties. In his 1991 study, Ippolito used a UO_2 dispersion fuel in zircaloy to improve neutronic performance [44, p.66].[62] The main focus of the RERTR

[61] It is also the same fuel used by Ippolito to simulate naval reactors [44, p.65].

[62] Ippolito and others sometimes refer to these fuels as "cermet," short for ceramic-metal, fuels.

program has been in developing new dispersive compounds that have a higher local uranium density to increase overall uranium loading. This can be seen in figure 2.12.

FUEL CHARACTERISTICS

Fuel Alloy	Matrix Material	Rho_d Alloy Density (g/cm^3)	W_d^u	W_d^u*Rho_d Alloy U-Density (g/cm^3)
Al		2.7	-	-
Al_2O_3		3.94	-	-
UAl_4	Al	5.7	0.653	3.72
UAl_3	Al	6.8	0.746	5.07
UAl_2	Al	8.14	0.815	6.63
UAl_x[a]	Al	6.42	0.717	4.60
UO_2	Al	10.96	0.882	9.67
U_3O_8	Al	8.30	0.848	7.04
U_4O_9	Al	11.19	0.869	9.72
Russian Oxide[b]	Al	9.50	0.869	8.26
USi	Al	10.96	0.895	9.81
Compd U_3Si_2	Al	12.20	0.927	11.31
U_3Si	Al	15.30	0.960	14.69
U-10Mo	Al	17.02	0.90	15.32
U-9Mo	Al	17.20	0.91	15.65
U-8Mo	Al	17.36	0.92	15.97
U-7Mo	Al	17.55	0.93	16.32
U-6Mo	Al	17.72	0.94	16.66
U-4Mo	Al	18.09	0.96	17.37
Compd U_2Mo	Al	16.60		13.81
U-6Mo-1Pt	Al	17.74		16.50
U-6Mo-0.6Ru	Al	17.64		16.48
U-6Mo-0.1Si	Al	17.59		16.52
U-10Mo-0.05Sn	Al	17.01		15.30
U-9Nb-3Zr	Al	16.08		14.15
U-6Nb-4Zr	Al	16.41		14.77
U-5Nb-3Zr	Al	16.86		15.51
U-2Mo-1Nb-1Zr	Al	17.94		17.22
U_6Fe	Al	17.40	0.962	16.74
UN	Al	14.30	0.944	13.50
U	-	19.05	1.00	19.05

Rho_d = Density of Dispersed Phase
W_d^u = Weight Fraction of Uranium in Dispersed Phase
W_d^u*Rho_d = Density of Uranium in Dispersed Phase
(a) Assumed to consist of 69 wt% UAl_3 and 31 wt-% UAl_4 after fabrication.
(b) Russian oxide powder is commonly referred to as UO_2, but is actually U_4O_9. Actual density of this oxide powder is 9 - 10 g/cm^3. We use a density of 9.5 g/cm^3.

Figure 2.12. Dispersion fuels developed over the course of the RERTR program. The densities contained in the table are densities of the dispersed phase alone. To determine the density of uranium in the fuel meat as a whole it is necessary to determine the volume fractions for the fuel and metal. The figure is taken from [83].

Dispersion fuels have three distinct advantages to a solid fuel.[63] First, fission fragment damage is usually localized around individual fuel particles. When designed correctly, this allows dispersion fuels to reach extremely high burnups (70% atom fraction) safely [44, p.67]. Second, in the event of the fuel material becoming exposed to the coolant, only the particles on the surface of the matrix will be affected. Finally, the metal matrix materials generally has very high thermal conductivity. This lowers the fuel operating temperature.

Judging from the results of the Ippolito study, it is unlikely that an LEU dispersion fuel, no matter how uranium-dense the dispersant is, would be able to meet the energy requirements of a full size attack submarine while maintaining reactivity.[64] To test this, the UO_2-Zr fuel described in section 2.5 was burned using LEU. In this simulation, k_{inf} fell below one within 150 MWd/kg of burnup. This fuel already uses close to the maximum possible volume fraction of uranium oxide, so increasing the uranium loading to increase lifetime is impossible. Dispersion fuels do not have an adequate uranium density to use LEU.[65]

Monolithic Fuels

Monolithic fuels are uranium alloys without a matrix. This greatly increases the uranium density by eliminating the matrix material entirely. The RERTR program discovered that some reactors could not switch to high-density dispersion fuel, regardless of the dispersant because of insufficient uranium density [84, p.1]. This led to the development of monolithic uranium-alloy fuels, bringing total uranium density close to its maximum theoretical value.[66]

With dispersion fuels eliminated, one of the monolithic fuels under development must be selected. The best of these options is an alloy of uranium mixed with 10% by weight of molybdenum.[67] While uranium metal undergoes a series of phase changes as it is heated from room temperature to roughly 600°C, the addition of a small amount of molybdenum during manufacturing is able to stabilize the metal in its gamma phase, independent of temperature changes [85, p.170]. This allows the alloy to work well in the high temperatures of nuclear reactors without geometrical change or severe swelling.

The effects of burnup on monolithic fuels are still being researched. However, early tests have indicated that under the right conditions, fuel swelling resulting from fission gas

[63] These advantages are only captured when the matrix metal dominates the volume percentage of the fuel.

[64] The Ippolito study analyzed a *Rubis* class French submarine with a 50 MW_{th} reactor on a seven to ten year refueling schedule [44, p.28]. US attack submarines are rated for a longer life and roughly triple the reactor power [44, p.146].

[65] This is assuming that the goal is still for a life of the ship core. If a single refueling were acceptable, a dispersion fuel could be an attractive option due to their high achievable burnup.

[66] The maximum theoretical uranium density being that of solid uranium. For reasons discussed in many places, elemental uranium makes a poor nuclear fuel [44, p.34].

[67] The uranium molybdenum alloy fuel will be referred to as U-10Mo for the rest of this thesis.

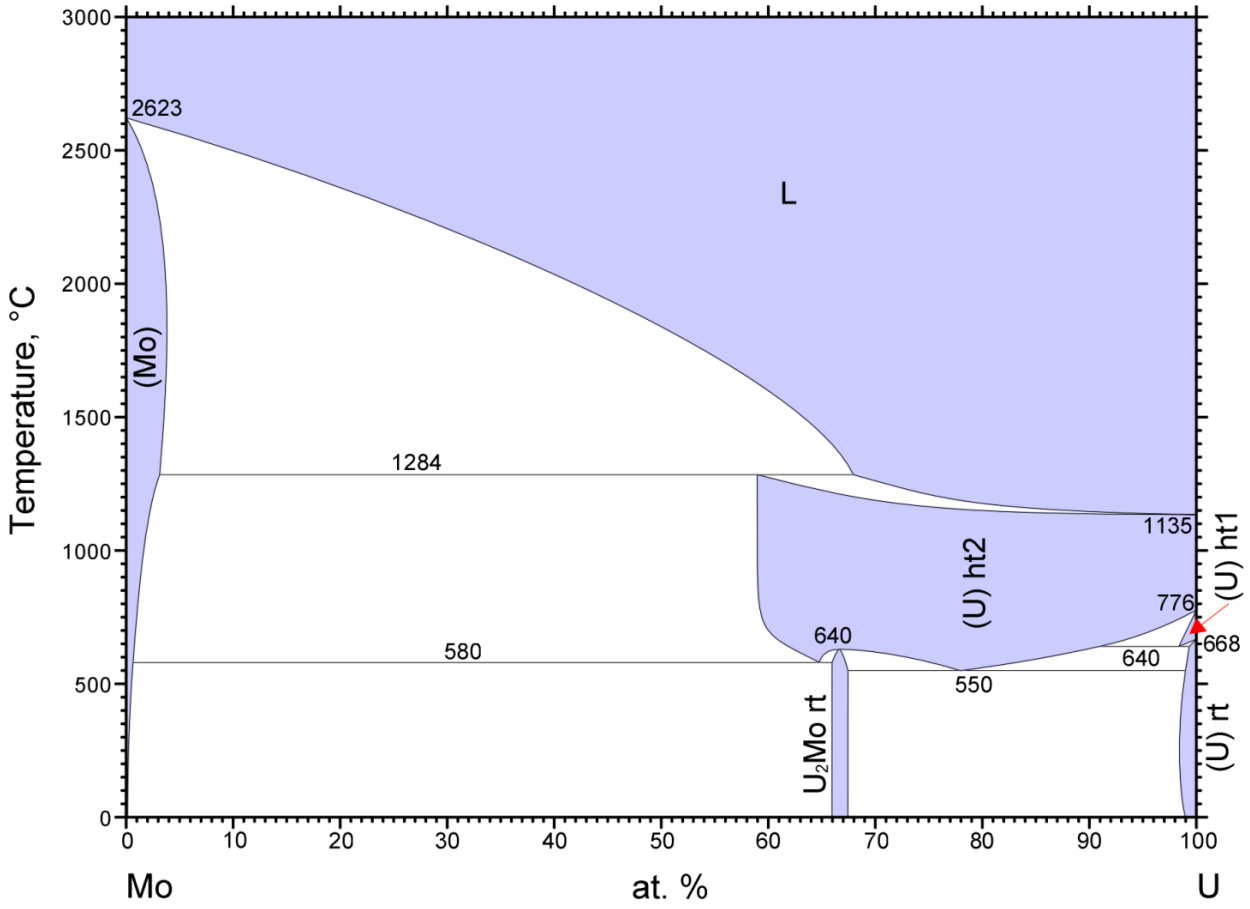

Figure 2.13. This figure shows the uranium-molybdenum binary phase diagram, taken from [81]. Weight percentages of 90.0% and 10.0% correspond to atomic percentages of 78.4% and 21.6% for uranium and molybdenum respectively. This would give the proposed alloy a melting temperature of about 1150°C.

accumulation in monolithic plates can mirror the patterns of dispersion fuels as shown in figure 2.14 [84, p.7]. Current research of U-10Mo is focused on thin foils (roughly 0.5mm), but the thickness of the foils continues to increase as manufacturing processes improve [86, p.1]. Research has also shown that 10% weight of molybdenum is the lowest amount that ensures gamma phase stabilization, and prevents local depletion of molybdenum that may result in phase dissolution. Increasing the weight of molybdenum further would result in unnecessarily lowering uranium density.

To accurately represent the Doppler broadening and melting margin of the monolithic fuel, it is necessary to estimate its temperature and therefore its thermal conductivity. Table 2.8 shows a summary of experimental estimates of the thermal conductivity of U-10Mo.

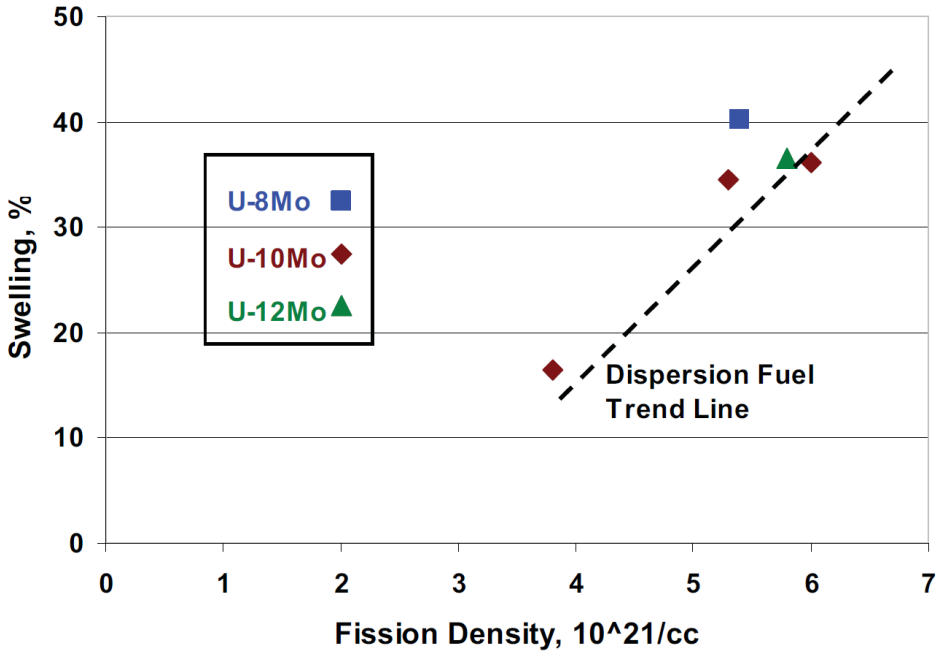

Figure 2.14. This figure shows the trend of fuel swelling in monolithic fuels, and compares it to what is normally seen in dispersion type fuels. With high ($\approx$ 8-12% by weight) concentrations of molybdenum, metal alloy fuel can undergo similar burnup to dispersion fuel. 1×10^{21} fission/cm^3 is about 25 MWd/kg for the U-10Mo fuel and about 95 MWd/kg for the UO_2-Zr fuel according to equation 2.12. This figure is taken from [84, p.7].

From these measurements, the following correlation was developed [87, p.7].[68]

$$k_{\text{U-10Mo}} = (10.2 \pm 0.688) + \left(3.51 \times 10^{-2} \pm 1.61 \times 10^{-3}\right) \cdot T \tag{2.21}$$

For the temperature ranges used in this thesis, this gives a thermal conductivity of 25 W/m-K.

Finally, it is necessary to estimate the maximum burnup of U-10Mo. The fuel has not yet been qualified for use in any reactor, so further experimentation and qualification is required before U-10Mo could be used in a naval reactor. However, experimentation has pushed the fuel to 150 MWd/kg in some experiments, and even 200 MWd/kg in a few others [84, p.5][88, p.3]. Therefore, for this thesis, a hopefully conservative limit of 100 MWd/kg will be applied. It will be up to experiments to verify if this burnup is actually attainable.

Uranium molybdenum monolithic fuel plates represent a "best case" for the use of LEU fuel in naval reactors in term of reactivity and required burnup.[69] Therefore, if this fuel is

[68] In this equation, the temperature (T) is in Kelvin and the value for thermal conductivity (k) is in W/m-K

[69] The U-10Mo fuel has the highest possible uranium density of any fuel being studied. Therefore, its use also would require the lowest burnup of any material used, as it would have the largest weight of uranium

Table 2.8. U-10Mo Thermal Conductivity[1]

Temperature (°C)	Thermal Conductivity (W/m-K)				
	Burkes	Klein	McGeary	Touloukian	Average
20		12.1	9.7	12.1	11.3 ± 1.4
100		14.2	11.7	13.8	13.2 ± 1.3
200	20.0	17.2	14.0	17.3	17.1 ± 2.4
300	23.9	20.1	17.2	20.1	20.3 ± 2.7
400	27.1	23.0	21.6	23.3	23.7 ± 2.3
500	31.2	26.4	25.7	27.2	27.6 ± 2.5
600	35.5	30.1		30.1	31.9 ± 3.1
700	36.9	33.9			35.4 ± 2.1
800	37.4	37.7			37.5 ± 0.2

[1] Table adapted from Table 4 in [87, p.6].

unable to meet requirements, it is unlikely that a submarine can be fueled with LEU without requiring a larger core or at least one refueling during the life of the submarine. The final composition of the LEU fuel is shown in table 2.9. In chapter 5 this fuel will be used to determine the reactivity lifetime of a naval reactor fueled by LEU.

for the same space.

Table 2.9. Materials Summary

UO_2-Zr (HEU Fuel)		8.38 g/cm^3 4.04 U-g/cm^3
	^{16}O	6.56%[4]
	Zr	45.2%
	^{234}U	0.356%
	^{235}U	44.8%
	^{238}U	3.02%
U-10Mo (LEU Fuel)		17.0 g/cm^3 15.3 U-g/cm^3
	Mo	10.0%
	^{234}U	0.486%
	^{235}U	18.0%
	^{238}U	71.5%
Zircaloy-4 (Cladding)		6.50 g/cm^3
	^{16}O	0.125%[4]
	Cr	0.100%
	Fe	0.210%
	Zr	98.1%
	Sn	1.45%
Carbon Steel (Reactor Vessel)		7.80 g/cm^3
	C	0.250%
	Si	0.275%
	P	0.0250%
	Mn	1.32%
	Fe	97.1%
	Ni	0.550%
	Mo	0.525%
Stainless Steel-304 (Core Baffle / Barrel)		8.03 g/cm^3
	Si	0.600%
	Cr	19.0%
	Mn	2.00%
	Fe	68.4%
	Ni	10.0%

[1] All percentages are weight percentages.
[2] U-g/cm^3 refers to the uranium density within the fuel.
[3] The specific isotopes of uranium are calculated using standard enrichment equations. All other isotopes are assumed to be present in their natural abundances, as seen in [77, p.140].
[4] Serpent does not support the input of "natural oxygen." Therefore, oxygen is put into Serpent as ^{16}O.

Chapter 3

Core Design Process

This chapter outlines the method used to design a core, and details the background physics required in each step. The subsequent simulation results chapters (Chapters 4 and 5) will mirror the structure of this one, allowing a more clear presentation of results without describing the physics and methodology.

This thesis uses six broad steps to develop a full core burnup simulation for a pressurized light-water reactor. The first is to determine the temperature profile of the fuel and moderator, ensuring that safety margins are met. The second is to optimize the moderator-to-fuel ratio using an infinite lattice simulation. The third is to calculate the coolant pressure drop across the height of the core, and use that to estimate the pressure drop across the primary loop.[1] The fourth is to determine the number of neutrons required at each burnup step to calculate accurately the power shape and k_{eff}. The fifth is to estimate burnable poison loading to flatten the power distribution and help with temperature margins. Finally, the poisoned, fresh core is burned to estimate its life.

Each of these steps are described in individual sections of this chapter. Included in each section are a brief review of the theoretical background and implementation requirements of the step. The results of these steps for HEU and LEU cases are described in Chapters 4 and 5.

The core design process is not as sequential as the chapter presents. There are interrelated dependencies between many of the steps. For example: a key parameter in determining the temperature is setting the power density of the fuel. However, the power density has a large dependence on the total fuel volume, set by the size and number of fuel plates. This, in turn, is dependent on the moderator to fuel ratio. Finally, the moderator to fuel ratio is affected by the temperature of the fuel due to Doppler broadening. The process is ultimately an iterative optimization process. Some of these interdependencies will be discussed in the first

[1] This step is not so much a design requirement as a check to ensure that the reactor is realistic.

section of the chapter.

3.1 Iteration Requirements

This section describes some of the interdependencies between the thermal-hydraulic and neutronic calculations. These relationships complicate the reactor design process, as the steps described later in this chapter cannot be followed in a purely sequential manner.

Power Density and Temperature

The relation between power density and fuel temperature is straightforward. There is a linear correlation between an increase in power density and a corresponding increase in the maximum fuel temperature.[2] What is more insidious is the fact that due to the parabolic distribution of temperature across the thickness of the plate, increases in maximum temperature have a disproportionate effect on the average temperature of the fuel. This, in turn, affects the next step in the cycle.

Temperature and Optimal Moderation Ratio

A change in the average temperature of the fuel changes the Doppler broadening of the fuel's neutron cross sections. As the neutronic characteristics of the fuel change, the optimal moderator-to-fuel ratio also changes. This effect is small if the average fuel temperature has been accurately estimated, limiting the number of iterations.

Optimal Moderation Ratio and Fuel Volume

A changing moderator-to-fuel requires a different plate to plate pitch for the reactor's fuel elements. For small deviations, this effect will only require the changing of a few parameters. However, if the pitch changes significantly enough then the number of fuel assemblies in the reactor must be recalculated. By changing the number of fuel assemblies, the total volume of fuel is likely to grow or shrink considerably.[3]

[2]Actually, equation 3.6 shows that the linear relationship is between an increase in power density and a corresponding increase in the ΔT across the fuel. This is a subtle difference in actual calculation that isn't terribly important to understanding the overall trend.

[3]It bears mentioning that in addition to changing the power density, a significant difference in fuel volume would affect the required burnup of the fuel. This will have an effect on what "final value" of reactivity will be analyzed in section 3.3.3. This simply becomes one more piece of feedback in the iteration process to be analyzed.

Fuel Volume and Power Density

With a change in the total volume, the power density of the core would have to change. The total power of the core is set to a hard value of 150 MW_{th}, so any large change in fuel volume will obviously have a corresponding effect on power density. Changing power density influences fuel temperature, the first dependency listed in this section.

3.2 Thermal Analysis

One of the steps in modeling is estimating the average and peak fuel temperatures. Fuel temperature is a safety concern due to the possibility of fuel melt, and also has an appreciable influence on the neutronic characteristics of the reactor. A high fuel temperature broadens the absorption cross sections of fuel isotopes. This is of greater importance in an LEU reactor, as the resonances of ^{238}U captures a large fraction of thermalizing neutrons [58, p.49].

3.2.1 Plate Geometry

For this thesis, the z direction (height, also referred to as the axial direction), of the plate will be considered in the traditional vertical direction, opposite that of gravity and along the central axis of the cylindrical core. The x direction (width, also referred to as thickness) will then be the thinner of the two remaining directions, while the y direction (length) will be the longer side of the horizontal cross section. These axes apply specifically to each individual plate, not to the core as a whole.[4] These definitions, along with the final shape of the temperature profile, are shown in figure 3.1.

3.2.2 Horizontal Temperature Variation

The heat equation governs the relationship between heat transfer and temperature. In its most general form, all thermodynamic properties of the material may vary as functions of both position and time. In most applications, these properties can be assumed uniform across materials without large temperature gradients, and constant in time. With this assumption, the heat equation can be stated as equation 3.1.

$$\rho\, c_p \frac{\partial T}{\partial t} = \kappa\, \nabla^2 T + q''' \tag{3.1}$$

[4]When referring to the (roughly) cylindrical core as a whole, the x and y directions will be replaced by r, referred to as the "radial" direction.

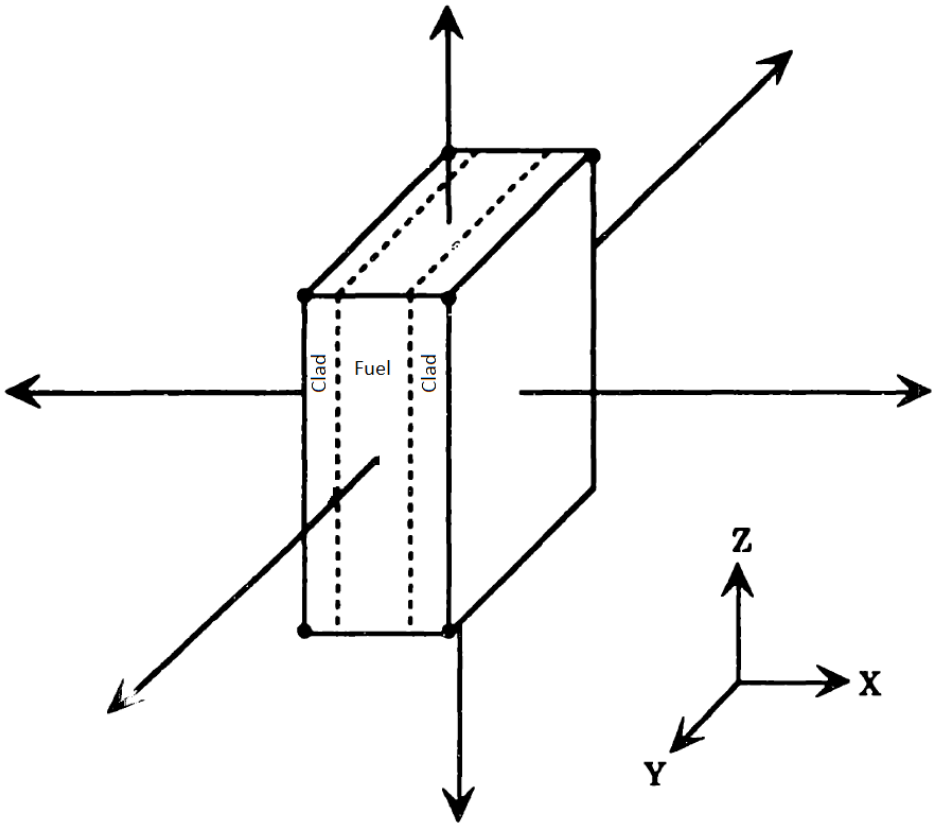

Figure 3.1. This image shows the x, y, and z coordinate system referred to in this thesis.

For all materials in this thesis, density (ρ), specific heat, (c_p) and thermal conductivity(κ) will be assumed to remain uniform and constant in materials, despite local temperature gradients and transient behavior. Additionally, both temperature (T) and volumetric heat generation (q''') will be assumed to be invariant in the y direction.[5] Heat generation will also be assumed to be uniform in the x direction, as the plates should remain thin enough that neutron self-shielding effects on heat generation can be ignored.[6]

Both the x and z temperature distributions will need to be derived to determine the steady-state average fuel temperature. In the x direction, the method of thermal resistors was used to solve for the temperature profiles in the cladding and fluid. However, due to internal heat generation, the heat equation must be used to solve for the temperature in the fuel meat. The analytic solution of the temperature profile in the x direction will then

[5]Heat transfer will be greatly dominated by movement in the x direction due to the much larger temperature gradients. The individual fuel plates will be roughly five times as long as they are wide. This immediately means that the gradient across the narrow direction will be a larger value.

[6]When real reactor designs are being considered, this factor will become important, as a much higher degree of accuracy about the reactor's performance will be required. For this thesis, that degree of accuracy is judged unnecessary, as the errors in neutron flux, and thus heat generation, from ignoring self-shielding will be smaller than the errors simplified fuel design.

be coupled with the z dependent heat generation curve and fluid temperature variation to create a 2D temperature profile.

Thermal Resistors

In describing the transfer of heat from the interior of the fuel plate to the coolant, it is more straightforward to start at the outside of the plate.[7] Additionally, the thermal resistor terms in the coolant and cladding can be better described in terms of q'' (the heat flux) rather than q'''. The latter is more useful in the interior of the fuel plate. Equation 3.2 shows the relation between these two values. For a discussion of the thermal resistors method of heat transfer (also referred to as thermal circuits) see [34, p.384] or most heat transfer textbooks.

$$q'' = q'''t \tag{3.2}$$

In equation 3.2, q'' is the heat flux (W/m^2), q''' is the heat generation rate (W/m^3), and t is half the thickness of the fuel plate.

The transfer of heat from the outer cladding to the coolant is governed by the steady state Newton's Law of Cooling:

$$q'' = h\left(T_{\text{co}} - T_{\text{bulk}}\right) \tag{3.3}$$

In equation 3.3 h is the heat transfer coefficient, T_{co} is the outer cladding temperature, and T_{bulk} is the bulk coolant temperature.[8] The heat flux at the plate face as a function of z can be approximated by neglecting heat loss through the narrow sides and assuming all internally generated heat is transferred through the two wide faces. Provided cooling is symmetrical on both faces, the flux per face is the volumetric heat generation integrated over the plate half thickness. Recall that the volumetric heat generation is assumed to be constant over the plate thickness. The bulk fluid temperature as a function of z is derived in section 3.2.3. Finally, the heat transfer coefficient can be calculated using an empirical approximation for the Nusselt number, discussed in section 3.2.2. With all of the terms in equation 3.3 defined, the temperature at the outer edge of the cladding can be calculated.

The temperature difference across the cladding is a much simpler calculation. Because there is negligible heat generation within the cladding, the heat equation results in a linear

[7] When finding the analytic solution for the temperature profile, the starting point of the problem is irrelevant. However, because a numeric solution is required in the end, it is easier to start solutions at Dirichlet boundary conditions (such as the known temperature of the coolant) rather than Neumann boundary conditions (such as the zero derivative of temperature at the fuel centerline).

[8] The bulk coolant temperature is the temperature of the coolant away from the heated face of the fuel plate. The heat transfer coefficient is used to calculate the difference in temperature between the main part of the coolant and the face of the fuel.

temperature profile across the cladding.[9] Fourier's law can then be used to calculate the temperature difference across the cladding:

$$-\kappa \nabla T = -\kappa \frac{dT}{dx} = -\kappa_c \frac{T_{\text{ci}} - T_{\text{co}}}{\Delta x} = q'' \tag{3.4}$$

In equation 3.4, κ_c is the thermal conductivity of the cladding (W/m-K), T_{ci} is the temperature at the inner edge of the cladding, T_{co} is the temperature at the outer edge of the cladding, Δx is the cladding thickness, and q'' is the heat flux, as in equation 3.3. The outer cladding temperature was calculated in the equation 3.3. The cladding thickness is a design parameter, discussed in section 2.3. The thermal conductivity of the cladding is 21.5 W/m-K [89]. Equation 3.4 can then be rearranged to solve for the cladding inner temperature.

In a commercial fuel pin, the cladding and fuel are separated by a gas gap that provides a large thermal resistance. Plate fuels do not have a fuel cladding gap, and the solid cladding-fuel contact facilitates a large heat flux [76]. Although the fuel-clad interface does create a small contact thermal resistance, the isostatic pressing and friction bonding processes used to attach cladding minimize contact resistance to such an extent that it becomes negligible [86, p.9]. By ignoring the contact resistance between fuel and cladding, the outer fuel and inner cladding temperature become equal. The symbol T_{fo} then refers to the temperature at the outer edge of the fuel, and is equal to the temperature at the inner edge of the cladding (T_{ci}).

$$T_{\text{ci}} = T_{\text{fo}}$$

The thermal resistors of equations 3.3 and 3.4 can be combined to solve for the temperature at the outer edge of the fuel solely in terms of the bulk fluid temperature and various physical and geometrical properties. The result of this manipulation is shown in equation 3.5.

$$T_{\text{fo}} = T_{\text{bulk}} + q'' \left(\frac{1}{h} + \frac{\Delta x}{\kappa_c} \right) \tag{3.5}$$

Heat Equation in the Fuel

The heat equation must be used to solve for the steady state temperature distribution within the fuel.[10] The problem is greatly simplified by assuming that there is negligible heat

[9] In reality, there is a small amount of heat generation in the cladding due to neutron slowing down and gamma heating. However, both of these are small compared to the heat generated in the fuel. It will be neglected for temperature estimations, but Serpent will account for it to calculate the total heat generation of the reactor.

[10] Some textbooks, such as [34] continue to use the thermal resistor method when addressing the temperature within the fuel. While the method can technically be used to calculate the maximum fuel temperature, it requires a previously calculated solution to the heat equation, and provides no information about the

conduction in the z and y directions. This assumption is justified because the temperature gradient in the x direction (towards the cladding) will be much higher than any other due to the small distance, driving heat in that direction. Heat generation will be assumed to be uniform in the x direction.[11] With these assumptions, equation 3.6 can be arranged to solve for the temperature distribution in the x direction.

$$\kappa_f \nabla^2 T = q'''$$

$$\kappa_f \frac{d^2T}{dx^2} = -q'''$$

$$T_f(x) = T_{\text{fo}} + \frac{q'''}{2\,\kappa_f}\left(t^2 - x^2\right) \tag{3.6}$$

In the above equation, $T_f(x)$ is the temperature of the fuel as a function of x, T_{fo} is the temperature at the outer edge of the fuel, q''' is the volumetric heat generation rate within the fuel, κ_f is the thermal conductivity of the fuel, and t is the half-width of the fuel plate. Applying two boundary conditions, (1) the outer fuel temperature solved from the thermal circuit earlier in equation 3.5; (2) due to symmetry, there is no heat transfer across the centerline of the fuel plate, therefore the temperature gradient goes to 0 at the center, the heat equation can be solved for a temperature profile in the x direction (equation 3.6).

Nusselt Number and Heat Transfer Coefficient

The Nusselt number, defined in equation 3.7, is a dimensionless number representing the ratio of convective to conductive heat transfer [90, p.401]. It is commonly used in heat transfer coefficient correlations. The Reynolds number, defined in equation 3.8, is a dimensionless number representing the ratio of inertial to viscous forces [90, p.390]. It is commonly used in both convective heat transfer correlations as well as in many fluid flow calculations. It will be used later in estimations of the pressure drop across the core. Both values require the calculation of an equivalent diameter (sometimes referred to as a hydraulic diameter) of the fluid flow, as shown in equation 3.9.

$$\text{Nu} = \frac{hD_e}{\kappa} \tag{3.7}$$

temperature profile shape across the fuel. Additionally, solutions to this are usually so specific to certain scenarios that they can easily be misapplied. It is simpler and more accurate to proceed from the heat equation directly.

[11] This is really a combination of two assumptions. First, self-shielding within the fuel is ignored as negligible. Secondly, it is assumed that the fuel plates are thin enough that the core-wide radial power distribution is constant over the plate.

$$\mathrm{Re} = \frac{\dot{m} D_e}{\mu A} \tag{3.8}$$

$$D_e = \frac{4A}{P_w} \tag{3.9}$$

In the above equations, h is the heat transfer coefficient, D_e is the equivalent diameter, and $\dot{m}$ is the mass flow rate in the unit cell. Nu and Re are the Nusselt and Reynolds numbers. For the equivalent diameter, the area (A) is the total flow area in the unit cell, while P_w is the wetted perimeter of the fuel plate. Finally, both the Nusselt number and Reynolds numbers require the use of many physical properties of the coolant. All of these will be estimated at 15 MPa and 300°C. The specific properties used are the thermal conductivity and dynamic viscosity, represented by κ and μ respectively.

The Nusselt number of a flow is normally calculated using an empirical correlation based on the characteristics of the flow. The most common correlation used is the Dittus-Boelter correlation, shown in equation 3.10, due to its wide range of application and tendency to underestimate the heat transfer coefficient, leading to higher levels of precaution taken with temperature margins.

$$\mathrm{Nu} = 0.023 \mathrm{Re}^{4/5} \mathrm{Pr}^{0.4} \tag{3.10}$$

$$\mathrm{Pr} = \frac{c_p \mu}{\kappa} \tag{3.11}$$

The variable Pr is the Prandtl number of the fluid, a dimensionless property representing the ratio of momentum diffusivity to thermal diffusivity of the fluid [90, p.407]. Unlike the Nusselt and Reynolds numbers, it is calculated only using properties of the fluid, and is independent of the flow geometry, as shown in equation 3.11.[12] However, the Dittus-Boelter correlation is only valid for fully developed flow.[13] Due to the short height of the reactor, the effects of developing flow will be important. Figure 3.2 shows the difference in Nusselt number between the Dittus-Boelter correlation, and two other correlations that account for entrance-region effects, the Short-Tube correlation (equation 3.12) and the Phillips correlation (equation 3.13) [91, p.7][74, p.1348].

$$\mathrm{Nu} = \left(1 + \frac{1}{(z/D_e)^{2/3}}\right) \cdot \mathrm{Nu}_{\text{Dittus-Boelter}} \tag{3.12}$$

$$\mathrm{Nu} = 0.012 \left[1 + (D_e/z)^{2/3}\right] \left[\mathrm{Re}^{0.87} - 280\right] \mathrm{Pr}^{0.4} \tag{3.13}$$

[12] In equation 3.11, c_p, μ, and κ are the isobaric specific heat (or heat capacity), dynamic viscosity, and thermal conductivity of the fluid respectively.

[13] For a discussion of developing and fully developed flow, please see section 3.4.2.

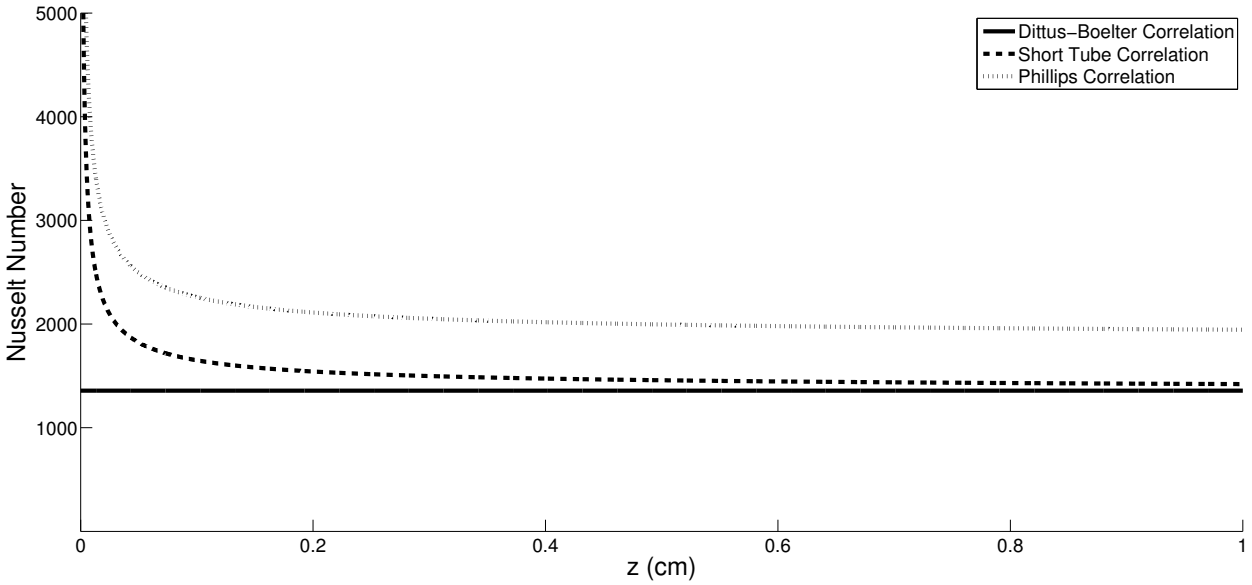

Figure 3.2. Three Nusselt number correlations are compared here. The first is the Dittus-Boelter correlation, shown in equation 3.10. The second is the Short-Tube correlation, shown in equation 3.12. The third is the Phillips correlation, shown in equation 3.13. The latter two clearly show the difference in heat transfer coefficient during the entrance region before leveling out to a single value once the flow is fully developed along the axis.

For this thesis, the Phillips correlation will be used. The Short-Tube correlation is a less rigorous correlation, and still relies on results from Dittus-Boelter, while the Phillips correlation incorporates results of experiments [74, p.1348]. Furthermore, there is disagreement between sources on the value of the numerator and exponent in the z/D_e fraction of the Short-Tube correlation. While the Phillips correlation provides a developed flow Nusselt number roughly 50% larger than that of Dittus-Boelter, this has been attributed to the poor accuracy of the Dittus-Boelter correlation [90, p.525].[14]

3.2.3 Vertical Temperature Variation

The temperature variation in x will be combined with a z dependence to create a 2D profile of the fuel temperature. This will allow for a more accurate estimation of the average and peak fuel temperatures.

[14]The inaccuracy of Dittus-Boelter is due to the large range of application of the correlation. This makes it a poor estimation of any one particular case, but useful when comparing large ranges of cases.

Power Distribution

The heat generation will be cosine-shaped in the z direction because of the neutron flux buckling along the axis of a right cylinder [34, p.88].[15] The following equation is defined so that z=0 is at the vertical center of the core, while $z = -H/2$ is the bottom of the core, and H is the overall height of the core.

$$q'''(z) \approx q'''_{\max} \, cos\left(\frac{\pi z}{H_e}\right) \tag{3.14}$$

$$H_e = H + 4D \tag{3.15}$$

In equation 3.14, $q'''(z)$ is the volumetric heat generation rate as a function of z, $q'''_{\max}$ is the maximum value of the volumetric heat generation rate, H_e is the neutron diffusion theory extrapolated height of the core, and D is the diffusion coefficient. The extrapolation height must be used because the diffusion equation alone causes an incorrect estimation of criticality by forcing the neutron flux to zero at the edges. The diffusion length attempts to correct for this factor, setting the flux to zero at a distance of $2D$ from the edge. Heat generation is proportional to the neutron flux, so it will have the same shape (the cosine factor in equation 3.14). However, there is no heat generation outside of the fuel.[16] So while the physical limits of z are based on the height of the reactor, the cosine function zeros will be at the extrapolated height.

In the simplest approximation, the extrapolated height is equal to the physical height plus four times the Fick's Law diffusion coefficient [92, p.145]. [17] While equation 3.14 describes the shape of the profile, it is necessary to know the peak volumetric heat generation $q'''_{\max}$ to solve for the amplitude. This can be estimated by using the temperature profile and the fact that the total power of the core is the integrated heat over the total volume of fuel.

$$q'''_{\text{avg}} = \frac{\int_{-H/2}^{H/2} q'''_{\max} \, cos\left(\frac{\pi z}{H_e}\right) \, \mathrm{d}z}{\int_{-H/2}^{H/2} \mathrm{d}z.}$$

[15] This assumption is based on the solution to the neutron diffusion equation. For a more detailed description, see Chapter 5 of [58].

[16] Again, this ignores the heat generation due to gamma heating and neutron slowing down.

[17] The simplest approximation of the extrapolation distance is that it extends for two times the diffusion coefficient in every direction from the reactor [92, p.145]. This approximation can be improved by solving the Milne problem, which results in the extrapolation distance increasing to 2.1312 times a modified diffusion coefficient [58, p.154]. However, this slightly improved accuracy is irrelevant, the diffusion coefficient has to be approximated as that of a thermal reactor initially anyway. For more details on the one group diffusion equation, see Chapter 5 of [58].

$$q'''_{\max} = \frac{\pi H}{2H_e \, sin\left(\frac{\pi H}{2 H_e}\right)} q'''_{\text{avg}}$$

$$q'''(z) = \frac{\pi H}{2H_e \, sin\left(\frac{\pi H}{2 H_e}\right)} q'''_{\text{avg}} \, cos\left(\frac{\pi z}{H_e}\right) \tag{3.16}$$

Coolant Temperature

The final step in determining the axial temperature variation in the fuel is to model the distribution of the coolant temperature. This is straightforward, as the bulk coolant in a PWR remains as a single-phase liquid along the entire channel (neglecting the sub-cooled boiling along the plates). The starting point for this calculation is the 1D Conservation of Energy Equation.

$$\rho \frac{\partial h}{\partial t} = -\frac{\dot{m}}{A}\frac{\partial h}{\partial z} + \frac{q'' P_h}{A} + \frac{\partial P}{\partial t} + \frac{\dot{m}}{A\rho}\left(\frac{\partial P}{\partial z} + \frac{\tau_w P_w}{A}\right) \tag{3.17}$$

The time dependent terms can be ignored, as can the pressure gradient terms.[18] Finally, the heat flux term is more usefully expressed in terms of the volumetric generation rate for this derivation. All that remains after this simplification is equation 3.18.

$$\dot{m}\frac{dh}{dz} = t\ell q'''(z) \tag{3.18}$$

In the above equation, h is the enthalpy of the coolant (J/kg), $\dot{m}$ is the mass flow rate (kg/s), $q'''(z)$ is the volumetric heat generation rate as a function of z (W/m^3), and t and ℓ are the half thickness and length of the fuel plate. At this point, the equation can be integrated from the inlet temperature and enthalpy to any point in the vertical channel. In the implementation for this thesis, the program "X Steam" (a steam table lookup program) was used in Matlab to convert temperatures to enthalpy values and vice versa.[19] The two commands to be utilized are `XSTEAM('h_pT',p,T)` which returns an enthalpy from a pressure and temperature and `XSTEAM('T_ph ',p,h)` which returns a temperature from a pressure and enthalpy [93, p.3]. With these two commands included, the derivation of the coolant enthalpy and temperature results in equations 3.19 and 3.20.

$$h(z) = \frac{t\ell}{\dot{m}} \int_{-H/2}^{z} q'''(z') \, \mathrm{d}z' + \text{XSTEAM}(\text{`h\_pT'},\text{p},\text{T}_{in}) \tag{3.19}$$

[18] The pressure gradient terms are negligible compared to the massive enthalpy changes due to heat transfer. The time dependancies drop out simply because this is a steady state calculation.

[19] In both cases, the pressure of the reactor (15.51 MPa) was used as the second state variable.

$$T_{\text{bulk}}(z) = \text{XSTEAM('T\_ph',p,h(z))} \tag{3.20}$$

Equation 3.19 is a simple definite integral that adds the energy generated in the fuel plate to the enthalpy of the coolant at the channel entrance. Equation 3.20 then converts the enthalpy as a function of z into a temperature profile for use with equation 3.5.

With equations in section 3.2, the temperature profile of the fuel is fully defined. By solving these equations simultaneously, a 2D (in the x and z directions) profile of the fuel temperature can be generated and used to solve for the average fuel temperature.

3.3 Moderator to Fuel Ratio

The first step in designing the geometry of the reactor's core is to choose the plate-to-plate pitch.[20] This geometrical factor governs the moderator to fuel ratio, which in turn affects the neutron spectrum, plutonium production, and peak power. It is imperative that this choice be made with the optimization of fuel life in mind.[21] This was done by iterating through a series of simulations using many different fuel pitches. A pitch was selected based on core-life requirements.

3.3.1 Pitch and Moderator-to-Fuel Ratio

When exact results are required, discussions of moderator-to-fuel ratio will involve calculations based on the relative atomic densities of the fuel and moderator. However, in this thesis, such exact calculations are not required for the desired accuracy. Instead, pitch will be used as a stand-in for the moderator-to-fuel ratio. As the pitch between fuel plates is increased, the moderator-to-fuel ratio also increases. Therefore, the trends of k_{eff} plotted against pitch and moderator-to-fuel ratio should be the same.

3.3.2 Safety Significance

The power coefficient of reactivity is a measurement of a reactor's criticality feedback based on changes in power level. The Nuclear Regulatory Commission requires that civil reactors maintain a negative power coefficient, so that increases in power lead to decreases in reactivity and vice versa, creating a stable equilibrium point for reactor operation.[22] It is generally

[20] This is assuming that the plate thickness has already been chosen, as was done in section 2.1.9.

[21] The moderator to fuel ratio can also be changed by altering the width of the fuel plate. However, the width of the HEU and LEU fuel plates was set in sections 2.1.9 due to other considerations.

[22] Stable here referring to the reactor's tendency to resist small power fluctuations.

composed of three first-order effects: a fuel-temperature coefficient of reactivity, a moderator-temperature coefficient of reactivity, and a void coefficient of reactivity. Of these, the latter two are governed by the moderator-to-fuel ratio (and thus the pitch) of the reactor.[23]

For the purposes of this thesis, it is not necessary to calculate the magnitude of the moderator temperature and void coefficients of reactivity. Instead, both will simply be confirmed to have negative values. The simplest method of doing this is to ensure that the reactor is under moderated instead of over moderated. In an over moderated reactor, a decrease in moderator to fuel ratio causes an increase in k_{eff}. In an under moderated reactor, a decrease in moderator to fuel ratio causes a decrease in k_{eff}. An under moderated reactor is desirable due to the feedback mechanism between power and coolant density. As power in the reactor increases, the coolant gets warmer, and therefore less dense. This causes a decrease in k_{eff}, and therefore a decrease in power. Likewise, an decrease in power will lead to an increase in moderation, pushing power back up.

Figure 3.3 shows an example of the difference between over and undermoderation. In this thesis, similar results (using pitch as a stand-in for moderator to fuel ratio) will be generated to ensure the reactor is under moderated.[24] These results were not calculated using the burnable poison loading of the final runs. More detailed research should recalculate these curves using burnable poisons.

3.3.3 Optimization Process

The moderator to fuel ratio will be optimized with three basic targets in mind. First, the moderator to fuel ratio should be chosen in a manner that maximizes the reactivity of the core, extending its lifetime. Second, the ratio should be kept low to fit the largest amount of fuel in the core, lowering the required fuel burnup.[25] Finally, the safety effect of fuel to moderator ratio must be taken into consideration, and it should be ensured that moderator temperature and void coefficients of reactivity will be negative.

A series of simulations will be run to determine the ideal moderator to fuel ratio. Each will consist of a single fuel assembly made up of five fuel plates, their cladding, and the surrounding and filling water. An infinite boundary condition is taken for the z and y directions will be used so that power density is uniform across the assembly. This serves

[23]The fuel temperature coefficient of reactivity will always be negative due to the parasitic effect of Doppler broadening.

[24]This can be estimated so simply because naval reactors are almost exclusively PWRs. Using water as both a coolant and a moderator ensures that increases in power lead to decreases in moderator density, especially when it begins to boil. Boiling water reactors require much more in-depth analysis due to the high void coefficients ($\approx 15\%$) at the top of the core.

[25]The more space that is used for moderator, the less fuel can be packed into the space. This forces the per-mass burnup of the fuel to increase.

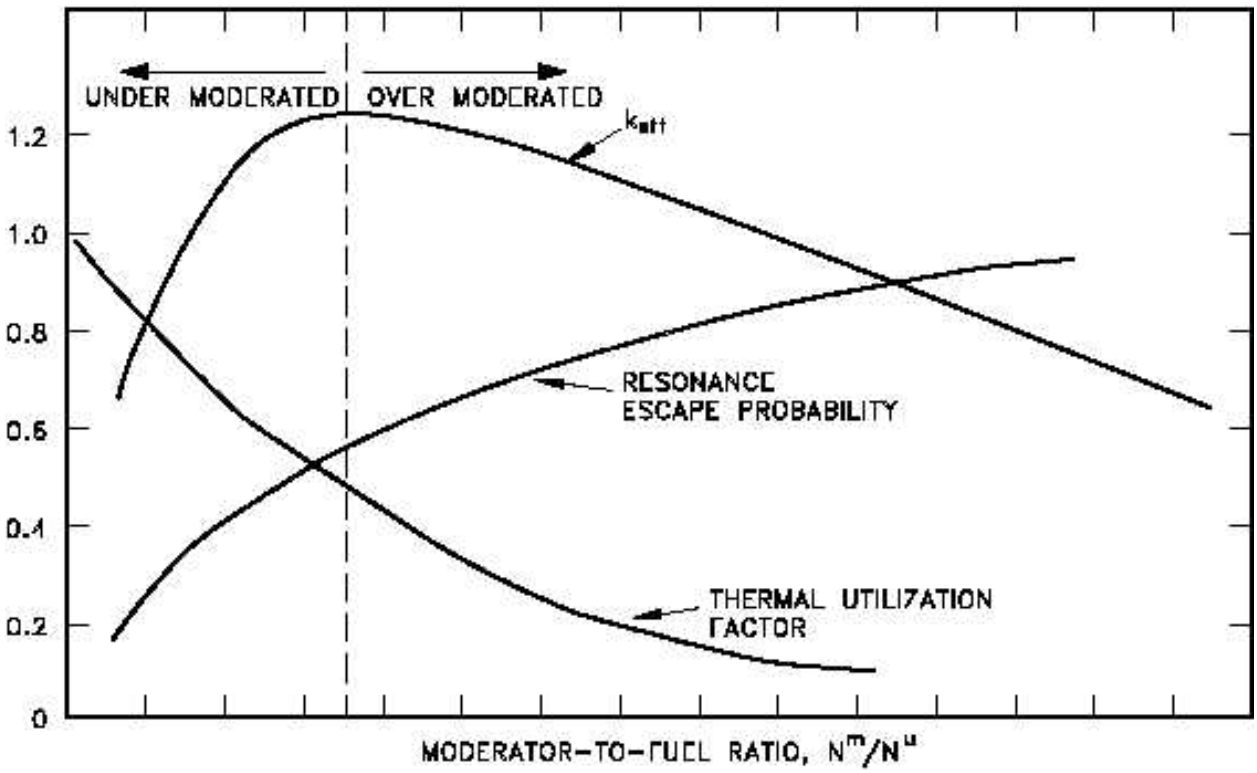

Figure 3.3. In the under moderated region, k_{eff} increases with an increase in the amount of moderator. Once the maximum k_{eff} is passed, additional moderation begins to lower reactivity. It is important for reactor safety that the core be under moderated at all times as a control mechanism [94, p.25].

several purposes. First, it allows the simulation to run faster. A flat power distribution allows for the fission source to converge in a very short amount of time. Second, it helps to isolate the effect of pitch on k_{eff}.[26]

It is important to note that the optimal moderator to fuel ratio will shift over the life of the reactor.[27] The end of simulation burnup is chosen by estimating the amount of uranium that would be loaded into a full core, and determining the target burnup required to meet the lifetime energy requirement. This allows for an analysis based on both the initial and final conditions of the reactor. For ease of analysis, results are presented as graphs of k_{eff} versus pitch. The k_{eff} curve will shift to the left as the fuel is burned, meaning that less

[26]This approach neglects end effects of the fuel for two reasons. First, the increased accuracy obtained from dealing with end effects is overwhelmed by the large-scale accuracy issues due to assumptions of naval reactor performance and specifics. Secondly, as will be explained in Chapters 4 and 5, the final selection of pitch is more constrained by the core geometry than neutronic effects.

[27]As the fuel burns, multiple changes happen. First, the amount of fissile material in the core changes as ^{235}U undergoes fission and ^{238}U captures neutrons to become ^{239}Pu. Secondly (more in the case of the LEU reactor) this may also cause a spectral shift in the reactor, as ^{239}Pu builds up in a greater amount and has significant contributions to fission. Finally, the buildup of long-lived fission products can cause changes in the geometry of the fuel on the micro and macro scale.

moderation is required [95, p.29].[28]

Generally, when designing a power reactor, the governing design parameter is maximization of burnup. Therefore, once curves such as figure 3.3 are generated, a pitch close to the left side of the maximum will be chosen. However, naval reactors must design to preserve space as well as reactivity. Therefore, k_{eff} might not need to be maximized for the life of the reactor. Instead, the pitch can be optimized to provide as much reactivity as is necessary while taking up a minimum amount of space for each individual fuel element.

This, of course, assumes that the reactor is burnup limited at end of life. It is also possible that the reactor will be reactivity limited. In that case, the pitch will have to be chosen to maximize the amount of energy that can be extracted from the core, in this case, measured as a maximum burnup set by the reactivity limit discussed in section 2.1.5.

3.3.4 Preparation for Full Core

In the initial exploration of moderator-to-fuel ratio, the simulation used fuel plates that were infinitely long and tall. This helped to isolate the effect of pitch and eased the computational demands of the problem. Once the ideal pitch is identified in this infinite lattice, it is necessary to identify the pitch that has the same moderator-to-fuel ratio using finite length plates. This comparison is illustrated in figure 3.4.

The conversion between an infinite and finite plate is highly dependent on the final length of the fuel plate. For this project, a fuel assembly was chosen to be five plates of the same orientation packed together. Additionally, in order to ease the computational aspects of the project, fuel assemblies are designed to be perfectly square. Therefore, the plate length is just short of five times the pitch. This makes the problem fully defined, and allows the finite length plate pitch to be calculated from that of the infinite plate, as seen in equation 3.23.

The geometrical conversion is computationally simple, if algebraically involved. It starts with equation 3.21, a simple comparison of the ratio of areas of water to fuel.[29] The areas are the cross-sectional areas for planes perpendicular to the z-axis.

$$\left(\frac{A_{\text{fuel}}}{A_{\text{moderator}}}\right)_{\text{infinite}} = \left(\frac{A_{\text{fuel}}}{A_{\text{moderator}}}\right)_{\text{finite}} \tag{3.21}$$

[28] As time goes on, more uranium nuclei undergo fission, resulting in fewer fuel atoms. The k_{eff} versus pitch curve will then shift left as fewer water molecules are required to maintain the same moderator to fuel ratio.

[29] In this scenario, an area ratio is acting as a stand-in for the atomic ratio between the fuel and moderator. This works because the fuel and moderator will both be held at a uniform temperature and pressure for the simulation. Therefore, while the area ratio will have a numerically different optimal value, the values will correspond to each other by a density ratio.

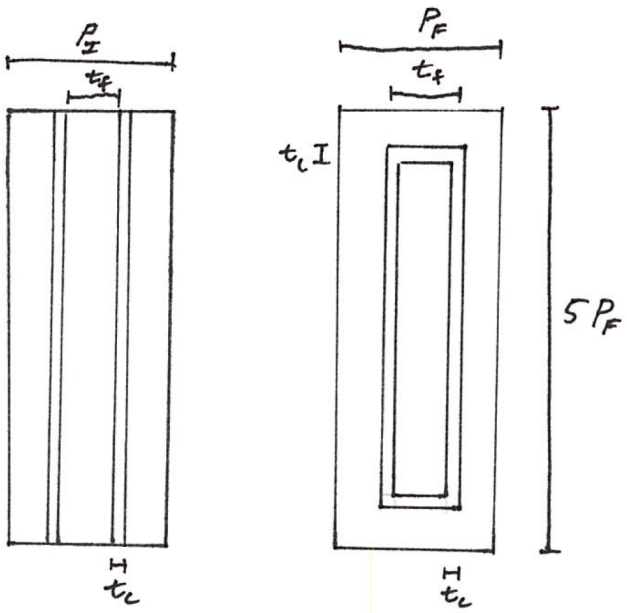

Figure 3.4. The two figures show the difference between an infinite and a finite plate. On the left, the furthest outline represents the cell of a single fuel plate and the water surrounding it: P_I is the pitch between infinitely long fuel plates. t_f is the fuel thickness and t_c is the cladding thickness. On the right is the finite length fuel plate. P_f is the pitch between the finite length fuel plates. The length of the cell is $5P_f$, as there are five fuel plates in each of the square fuel assemblies. Equation 3.23 shows the relationship between these variables.

$$\frac{t_f}{P_I - t_f - 2t_c} = \frac{t_f\,(4P_f + t_f)}{P_f \cdot 5P_f - (t_f + 2t_c)\,(4P_f + t_f + 2t_c)} \tag{3.22}$$

$$P_f = \frac{2P_I + \sqrt{4P_I^2 + 10t_f t_c + 5t_f P_I + 20t_c^2}}{5} \tag{3.23}$$

The caption to figure 3.4 describes the variables in the above equations. After cross multiplying, applying the quadratic formula, and rejecting the non-physical negative solution, equation 3.23 gives the conversion from an infinite length plate pitch to the equivalent finite pitch model.[30] Once the pitch is chosen, the pressure drop must be estimated before simulating a full core.

3.4 Pressure Drop

The final check before moving to a full core is an estimation of the pressure drop across the primary loop. This is to ensure that the pumping power required to run the reactor is not too high. The relationship between pumping power and pressure drop is governed by

[30]Equation 3.23 also assumes that the end effects of neutron flux and power will be negligible.

equation 3.24.

$$\text{Pump Power} = \frac{\dot{m}\Delta P}{\eta\rho} \tag{3.24}$$

In the above equation, $\dot{m}$ is the mass flow rate of the coolant in the core, ΔP is the total pressure drop across the primary loop, η is the isentropic efficiency of the pump, and ρ is the average density of the coolant. The mass flow rate is governed by the inlet and outlet temperatures and maximum power of the core. The isentropic efficiency is a set value determined by the pump. The density of water is a property based on the temperature and pressure of the fluid. The only factor that is controlled by design is the pressure drop across the primary loop. There are four main contributors to the pressure differential across the loop: gravity, friction, form losses, and acceleration terms. The actual pressure drop and pump power of naval reactors is classified, so estimates will be based off of commercial plant performance.[31] In a typical commercial PWR the summed power of the reactor coolant pumps is about 17.5 MW, or just under 2% of output power and roughly 0.6% of thermal power.[32] Arguable, a naval reactor might have more pumping power to rapidly accelerate coolant in an emergency situation.

This section will also assume that the limiting case of pump power will be full reactor power operation. This assumption is based on the various equations for pressure loss. Most of the terms (friction, form, and acceleration) are proportional to the mass flow rate squared. During any kind of accident condition, the required mass flow rate through the core will drop to about 7% of its value at full power requirement.[33] Due to the cubic relation between mass flow rate and pressure drop, pump power can be expected to drop significantly.[34] Full power operation will be assumed as the limiting case for pump requirements. However, it is likely that higher power pumps than necessary are installed in submarines in order to enable the crud-bursts discussed in section 2.1.8 or to provide excess coolant in an accident scenario. The rest of this section will detail the process of approximating the pressure loss in the core to estimate required pump power.

[31]Pumps for the US *Los Angeles*, *Ohio*, *Seawolf*, and *Virginia* class submarines, as well as many surface ships, are provided by the Curtiss Wright Flow Control Company [96]. Details of their products are only provided to naval procurement personnel.

[32]The pressure differential across the pumps is about 90 psi, or 620 kpa [97, p.4-15]. The total mass flow rate is about 17,476 kg/s [34, p.971]. The density of water at 15 MPa and 300°C is about 725 kg/m^3, and pump efficiency is roughly 0.85 [34, p.44]. This results in a power of 17.58 MW. A typical commercial plant is roughly 1000 MW$_e$ and 3000 MW$_{th}$.

[33]The first response to many accident scenarios is to respond to scram the reactor, allowing the submarine's diesel engines and batteries to temporarily provide power [98, p.7]. The scram reduces core power to 6.6% of full power within the first second [34, p.104]. The relationship between mass flow rate and core power in equation 2.5 shows that required mass flow rate will similarly drop.

[34]Most pressure drop terms vary with the mass flow rate squared, and pump power varies by the mass flow rate times the pressure differential, shown in equation 3.24. This gives an approximate cubic relation.

3.4.1 Pressure Differential Goal

About 80% of the pressure drop in the primary loop happens in the non-reactor part of the system in a commercial PWR.[35] This implies that the pump power is primarily dependent on the balance of the primary loop, not the core. Without knowing the type, length, and geometry of piping involved, as well as the details of the steam generator, it becomes impractical to estimate the pressure drop of the primary loop. As a rough estimation, the pressure drop across the core will be calculated and multiplied by a factor of five to estimate the total loop loss. It is difficult to estimate whether this will provide an over or underestimation of pressure loss. In theory, the compact submarine reactor compartment will have a smaller distance of piping to induce friction and form losses as a large commercial plant. However, contorting the piping through the small compartment may require more joints and turns, and the smaller flow volume may use smaller diameter pipes.[36] The goal for the pressure calculation will be that the pump power remain under 1% of reactor thermal power.[37]

3.4.2 Pressure Loss Theory and Equations

The four main components of pressure drop across the core are gravity, friction, acceleration, and form losses.[38]

$$\Delta P = \Delta P_{\text{gravity}} + \Delta P_{\text{friction}} + \Delta P_{\text{acceleration}} + \Delta P_{\text{form}} \tag{3.25}$$

Each term in equation 3.25 will be calculated separately then summed to determine the total pressure loss across the core. Many of the terms will require estimations of the coolant's physical properties. For these, the coolant will be assumed to be regular water at 15 MPa and 300°C, the target mean in-core properties of the coolant during operation. The gravity term is the simplest, and the relation is shown in equation 3.26 where ρ is the coolant density, g is the standard acceleration due to gravity, and H is the height of the core.

$$\Delta P_{\text{gravity}} = \rho g H \tag{3.26}$$

[35]The pressure drop across the reactor core is about 140 kPa [34, p.530]. The total pressure loss is about 620 kPa [97, p.4-15].

[36]Any joint or turn in a pipe induces a form loss. Additionally, while the slower overall flow rate will decrease friction loss, this could be countered by the smaller diameter piping required.

[37]The more ideal comparison would be to calculate the pump's share of electrical power generated by the core. However, while both the thermal and electrical powers of naval reactors are classified, it is possible to find sources estimating the thermal power of naval reactors [20, p.91][45, p.12-5].

[38]In this discussion, ΔP is defined as the pressure loss. Therefore, a positive value represents a drop in pressure that must be counteracted by the reactor coolant pump eventually. While this may seem counter-intuitive, it works out because it is guaranteed that the total pressure loss will be a positive value, so this saves having to make almost every term a negative value.

Because the coolant is flowing upwards through the core, the gravity term will always be a positive pressure loss. [39]

The friction term is calculated for a single fuel plate then applied to the full core by assuming the core is everywhere similar. Frictional pressure loss is given by equation 3.27.[40]

$$\Delta P_{\text{friction}} = f_D \frac{H}{D_e} \frac{1}{2\rho} \left(\frac{\dot{m}}{A} \right)^2 \tag{3.27}$$

The terms for calculating the frictional pressure drop are the friction factor (f_D), equivalent diameter of the unit cell (D_e), mass flow rate in a single unit cell ($\dot{m}$), and flow area of a unit cell (A).[41] The first step in determining the frictional pressure drop is to determine the mass flow rate around a single fuel plate.

$$\dot{m} = \frac{\dot{M}_{\text{core}}}{\text{number of fuel plates}} \tag{3.28}$$

The next step is to determine the equivalent diameter (also referred to as a hydraulic diameter) of the fuel plate. This is the geometrical factor given in equation 3.9 earlier. The next step is to determine whether the flow is fully developed.[42] For turbulent flow, the boundary layer develops very quickly, and the flow can be considered fully developed after a distance of 25–40 times the equivalent diameter [34, p.484].[43] In this thesis, it was determined that the flow was not fully developed until a significant fraction of the way through the core.

The Darcy friction factor is commonly calculated using the Colebrook equation, some-

[39] In the case of natural circulation, the gravity pressure term can give a net driving pressure for the primary loop. Natural circulation is discussed in section 3.4.3.

[40] In equation 3.27 the friction factor f_D uses the subscript D to indicate a Darcy friction factor as opposed to the Fanning friction factor, which is smaller by a factor of 4. This is purely a matter of convention. Further references to the friction factor will simply use f but always be of the Darcy type.

[41] The equivalent diameter is defined in equation 3.9.

[42] As fluid enters a channel, the velocity profile is generally uniform. As the flow moves down the channel, a boundary layer of slower velocity builds near the channel wall. "Fully-developed" flow refers to flow that has attained a stable flow profile [99, p.283]. Figure 3.5 illustrates the difference between developing and fully developed flow. For a more detailed description of flow development, see [99] or most fluid mechanics textbooks. It should also be noted that a similar phenomenon occurs with a thermal, temperature-based, boundary layer.

[43] It is theoretically possible that laminar flow could be present in the reactor, however this is extremely unlikely. Almost all PWRs operate in the turbulent regime due to the high mass flow rates being pushed through narrow channels in the core. Turbulent flow greatly amplifies the heat transfer out of the fuel rod or plate and into the bulk coolant, a desirable condition for which the thermal-hydraulic designer will seek to achieve. Therefore, it will be assumed (but later verified) that the reactor has turbulent flow.

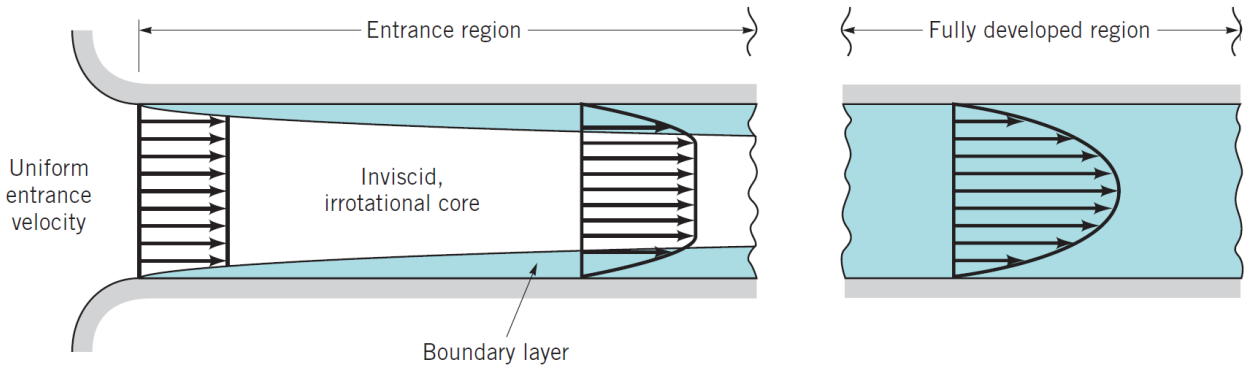

Figure 3.5. In the entrance region, the flow velocity profile is constantly changing as the boundary layer develops. The fully developed region is defined as the region where the flow velocity profile has become stable. This figure is taken from Figure 6.14(b) in [99, p.282].

times known as the Colebrook-White equation, shown in equation 3.29 [34, p.481].[44]

$$\frac{1}{\sqrt{f}} = -2\log_{10}\left(\frac{\lambda/D_e}{3.7}\frac{2.51}{\mathrm{Re}\sqrt{f}}\right) \tag{3.29}$$

In the Colebrook equation, λ is the surface roughness (in this case of the fuel cladding), D_e is the equivalent diameter, Re is the Reynolds number.[45] This requires calculation of the Reynolds number of the flow, as shown in equation 3.8 earlier. With the Reynolds number determined, the friction factor is fully defined, and the pressure loss due to friction can be calculated. Friction will always be a positive contributor to pressure loss.

The acceleration terms of pressure loss apply at the inlet and outlet of the core, and are caused by the squeezing of water from a large inlet plenum into the narrow fuel channels, and vice versa at the top of the core. If it is assumed that these plena are much larger than the fuel channels, then the pressure change due to acceleration is shown in equation 3.30.[46] This equation solves for the acceleration from a large inlet plenum to a small channel, and from a small channel to a large exit plenum. This is appropriate, as the individual coolant channels are a few centimeters wide, while the plena are the diameter of the full core. This simplification is also used in the calculation of the pressure drop in commercial reactors [34,

[44]For complete accuracy, an additional term should be added to the friction factor to account for the heating of the liquid by the wall [34, p.481]. However, these changes usually result in about a 1% increase in friction factor [34, p.483]. Due to the Colebrook equation's tendency to overestimate the friction factor by up to 17%, this accuracy is deemed unnecessary [100, p.6]. This conservatism will also be used to account for the difference in friction factor in the entrance region compared to the developed flow.

[45]The surface roughness of Zircaloy-4 is roughly 4μm [101, p.833].

[46]In equation 3.30, the i and e subscripts on ρ refer to the inlet and exit points of the reactor, showing that ρ must be calculated at these specific locations as opposed to an average value.

p.531].

$$\begin{aligned}\Delta P_{\text{acceleration}} &= \Delta P_{\text{acceleration, inlet}} + \Delta P_{\text{acceleration, exit}} \\ &= \frac{1}{2\rho_i}\left(\frac{\dot{m}}{A}\right)^2 - \frac{1}{2\rho_e}\left(\frac{\dot{m}}{A}\right)^2 \end{aligned} \tag{3.30}$$

In the above equation, the A refers to the cross sectional area of the flow within the channel. Unlike with the gravity and friction terms, the acceleration pressure changes require that local densities be used to preserve the difference between the acceleration entering and leaving the core.

Finally, the form losses across the core must be calculated. This is the most difficult of the terms to estimate for a naval reactor. In a commercial reactor, the largest contributors to form loss are the entrance and exit, spacers, fittings, and any turbulence enhancing mixers attached to the fuel grid [34, p.531]. While the entrance and exit form losses are easily calculable, any description of spacers, mixers, or fittings used in naval reactors would be classified [45, p.12-9]. Therefore, only the entrance and exit form losses will be calculated. In a commercial reactor, other form losses account for about 35% of the pressure losses [34, p.531]. Therefore, the final calculated pressure loss will likely be low, but the uncertainty introduced is small compared to the unknown ΔP in the primary loop. The entrance and exit form losses take the form of equation 3.31.

$$\begin{aligned}\Delta P_{\text{form}} &= \Delta P_{\text{form, inlet}} + \Delta P_{\text{form, exit}} \\ &= \frac{K_i}{2\rho_i}\left(\frac{\dot{m}}{A}\right)^2 + \frac{K_e}{2\rho_e}\left(\frac{\dot{m}}{A}\right)^2 \end{aligned} \tag{3.31}$$

In this form, K_i and K_e are 0.5 and 1.0 respectively [34, p.495]. As in the acceleration term, the form loss requires that the local density of the coolant be used for the two terms. With this, all of the pressure loss terms are fully defined, and can be summed as in equation 3.25.

3.4.3 Natural Circulation

The weight of fluid mass will always be a positive contributor to pressure loss in the reactor. However, buoyancy of warming fluid provides a driving pressure in the primary loop, resulting in natural circulation. In any natural circulation loop, the net pressure loss is given by equation 3.32, where the h and c subscripts refer to the hot and cold limits of the loop. If an average value of ρ for the reactor were used, the whole natural circulation calculation would

be thrown out due to oversimplifiying assumptions.

$$\Delta P_{\text{natural circulation}} = gH\left(\rho_h - \rho_c\right) \tag{3.32}$$

Just based on knowledge of the density behavior of water, natural circulation will always (when the steam generator is placed above the reactor) provide a negative pressure loss, which serves as a driving pressure for the coolant. Some submarines have used this phenomenon to run emergency shutdown cooling without pumps, and the Ohio class can run at a significant portion of full power without pumps [59, p.10]. However, this effect cannot be used to operate a submarine at full power. The HEU and LEU core would both need a height differential of about 200 meters to overcome the full power pressure drop.This is impractical, even with the Ohio class's generous 13m outer diameter.

The other option to increase natural circulation is to maximize the density differential between the hot and cold legs. Using 280°C and 320°C provides a difference of 84.8 kg/m^3 (between 763.57 and 678.76 kg/m^3 respectively). This temperature differential of 40°C is already applying significant thermal stresses to the reactor however. Example inlet and outlet temperatures are 279.4°C and 324.7°C for an AP1000, 289.4°C and 330.9°C for a Westinghouse 3-Loop plant, and 279.9°C and 321°C for a Westinghouse 4-Loop Uprated plant [47, p.22]. It seems that 40°C is the sweet spot for temperature difference to prevent long term damage to the core.[47] To go further beyond this would move outside of current design practices.

None of this changes the fact that gravity will inevitably be a driving pressure in the primary loop. However, it validates that there is a limit on what can be accomplished through natural circulation in submarines. Between the limits on submarine diameter and density differential, it is impractical to consider a naval reactor that could operate at full power without pumps. Ultimately, the contribution of natural circulation will be ignored. This will make the estimation of overall pressure drop more conservative, as natural circulation would provide a driving pressure in the primary loop.

3.4.4 Conclusions

Once the pressure drop across the core is fully calculated, it can be multiplied by a factor of five (as discussed earlier), and applied to equation 3.24 to determine the pumping power required for the reactor. Again, this is simply meant to be an estimation of the power

[47] Additionally, a 40°C temperature differential may be an overestimation of naval reactors. Each of the commercial reactors is roughly 3 m in height. For the same temperature differential, a 1 m naval reactor would have three times the temperature gradient. It is likely that naval reactors operate with a smaller temperature difference than commercial reactors.

required as a sanity check on the core design. The most likely way for the check to fail is because of excess friction loss. If the fuel-element pitch is too small, then the frictional losses will increase dramatically, as water is forced through a very narrow channel. Therefore, if the pressure drop is too large, the plates will have to be moved farther apart, even if this means sacrificing reactivity due to the increase in moderator to fuel ratio. If this pushes the core into an over-moderated state at any point in the fuel cycle, then a more fundamental reexamination of the design will be necessary.

3.5 Monte Carlo and Convergence

Monte Carlo calculations with multiple cycles of simulated neutrons are used to estimate k_{eff} and update the fission source distribution. After each iteration, the updated fission distribution is taken as the starting point for the next cycle. In principle, the process continues until k_{eff} and the fission-source have each converged such that they show no significant change between sequential runs. At this point, tallies are started, and the iteration process continues until results with a small enough statistical uncertainty have been obtained [102, p.1]. This process requires an initial guess of the fission source distribution. To ensure that the final result is uncontaminated by the initial guess, all cycles before fission source convergence are discarded.[48] This dividing line separates neutron cycles into two types: "inactive" cycles, where the fission source is being converged, and "active" cycles where tallies are running [102, p.1].

This process presents two complications. The first is that the computational time of the simulation is greatly increased, as inactive cycles require just as many neutrons (and thus computer time) as the active ones. The second is that a convergence criteria has to be established to determine when the simulation can move from inactive to active cycles. Many codes establish a criteria based on convergence of k_{eff} alone. This is not sufficient, as k_{eff} can appear converged even when the underlying fission-source distribution has not [102, p.2].

An improved metric is to use the Shannon entropy, defined in equation 3.33 [103, p.390]. [104, p.69].

$$H_{src} = -K \sum_{i=1}^{n} p_i \log\left(p_i\right) \tag{3.33}$$

In the definition of Shannon entropy, p_i is the fraction of fissions that happened in the grid location i, and K is an arbitrary normalization constant. In a Monte Carlo calculation, the

[48] Due to the random nature of Monte Carlo simulations, the fission source distribution will never perfectly converge. However, there will be a point where further changes in the distribution are due to statistical noise rather than increased accuracy.

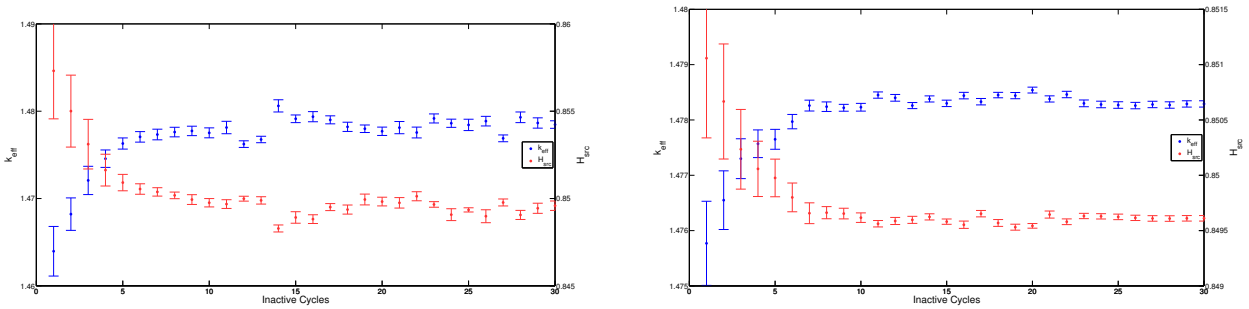

(a) 10,000 Neutrons per Cycle (b) 1,000,000 Neutrons per Cycle

Figure 3.6. Increasing the number of neutrons per cycle overcomes random noise in both k_{eff} and the Shannon entropy, improving precision. Increasing the number of cycles discarded improves accuracy.

geometry is divided into a grid, and fissions are tallied in each grid cell. Once the cycle is complete, the fraction of total fissions in each grid cell is determined and used to calculate the Shannon entropy. Serpent chooses a value for K to normalize the Shannon entropy with a maximum value of 1 and a minimum value of 0.[49] By using both k_{eff} and Shannon entropy as tests for convergence, the accuracy of the simulation can be improved.

In the graphs for variability of k_{eff} and Shannon entropy, two trends can be detected, shown in figure 3.6. The first is that as the number of cycles increases, both k_{eff} and the Shannon entropy asymptotically approach a converged value.[50] The number of inactive cycles has to be chosen to ensure that no tallies are begun before both of these values have converged. The second trend is in the random variability (noise) along the curves. As the number of neutrons in each cycle is increased, the noise in the curve decreases. Reference [102] contains a more in depth discussion of Shannon entropy and its use in testing fission source convergence.

The HEU and LEU cases were run with independent convergence tests to verify that each was using a sufficient number of neutrons and cycles to ensure accurate results.

[49]Once normalized to a maximum value of one, a Shannon entropy value of 0 reflects the situation where the probability of all events except for one are zero, and the last event has a probability of one. A Shannon entropy value of one reflects the situation where all events are equally likely [103, p.390]. In terms of a k_{eff} calculation, zero represents all fissions taking place in a single grid location, while one represents a uniform fission distribution.

[50]In reality, due to statistical noise, a single value will never be attained. However, convergence tests allow for identification of when further changes in fission source and k_{eff} are due to noise and not increasing accuracy.

3.6 Burnable Poisons

One of the largest complications encountered in moving from a simulation of infinite fuel plates to a finite core is power peaking—the concentration of reactivity towards the center of the core because of neutron leakage at the periphery. The peak power differs substantially from the average power and that at the periphery of the core. Despite this, the locations where the maximum power is generated must still not exceed limits set for fuel blistering and thermal crisis. Power peaking also has a hysteresis effect on the reactivity and power distribution in the core at the end of its life. It is a natural phenomenon that cannot be eliminated, but can be mitigated through the use of burnable poisons. This section will describe a process through which power peaking can be reduced and controlled to (ideally) prolong the effective life of the core.

3.6.1 Power Profile and Peaking

The general calculation of the temperature profile in a fuel plate is covered earlier in section 3.2. While this is an effective check of whether fuel centerline temperatures will approach their melting point, the core-wide power distribution must also be accounted for.[51] The solution to the one group diffusion equation in a right cylinder is a bessel function distribution of power in the radial direction [34, p.88].[52] This would provide a relative peaking factor of about 1.6.[53] Large peaking factors are important to account for when determining the margin to melting.

3.6.2 Burnable Poison Theory

One way to even the flux distribution is through the use of burnable poisons. A poison is any material with an absorption cross section that is large compared to the fission cross-section of ^{235}U. They are referred to as "burnable" because, unlike fission products or control rods, they are designed to be significantly depleted over the life of the reactor. Poisons are pre-loaded into the core in order to reduce local reactivity in peak power areas, thereby flattening the power distribution. Through the creative application of a variety of poisons

[51] The power peaking factor for the core will lead to a higher temperature than the core average power would estimate.

[52] Earlier discussions of temperature and power distributions focused on the shape across a fuel plate. At this point, the discussion is about the power shape across the entire core. For the initial estimation, the core is treated as a homogeneous cylinder reactor. This provides the bessel function solution to the one group diffusion equation.

[53] Early experimentation showed that the actual peaking factor was closer to 1.5 when the baffle, core barrel, and downcomer were included in the simulation. All of these components act as reflectors for neutrons that would otherwise escape from the reactor.

in planned configurations, the power profile of the reactor can be flattened for the entire life of the reactor, even as the spatial distribution of fissile materials changes. Designing a good poison loading is a very complex process that involves many different isotopes in many different concentrations. To optimize a core requires experience, planning, and a considerable amount of simulation. As such, only a simplified treatment is performed in this thesis.

Adding materials with large absorption cross sections to the reactor has a significant effect on global reactivity as well [94, p.30].[54] In this simulation, this effect will have to be balanced against the benefits of flattening the power distribution of the core. Early in the fuel cycle, this effect will be very beneficial, as initial tests show that the beginning of life k_{eff} of the core could be as high as 1.3. This gives a large margin of reactivity to work with when loading the core with burnable poisons used for power shaping.

3.6.3 Commercial Methods

There are a variety of methods in which burnable poisons are added to commercial reactors. The first is burnable poison pins. These pins come in a variety of designs, including solid-poison pins, glass-core annular pins, or water-filled annular pins [106, p.2]. These poison rods can be moved or replaced during refueling, allowing for reactor engineers to have considerable control over core. The second method is to fabricate the burnable poison as an integral part of the fuel [106, p.2]. This can be done either by spraying poisons on the outside of the fuel pellets before they are clad, or mixing a poison-oxide with uranium-oxide during pellet fabrication.

The most common burnable poisons for this purpose are boron, gadolinium, and erbium [69, p.1163]. Gadolinium and erbium are especially useful, as they can form oxides (Gd_2O_3 and Er_2O_3 specifically) that can be easily mixed into uranium oxide during fuel fabrication [107, p.73]. Boron is usually used in separate burnable poison pins or sprayed in thin layers on the outside of the fuel due to its extremely large cross section [106, p.2].[55]

[54] The use of burnable poisons is separate from the chemical shim process in which boric acid (a neutorn poison) is dissolved in the coolant in order to globally reduce reactivity [58, p.554]. The boric acid concentration starts out high during core loading, and is steadily lowered over the life of the reactor. Once the reactor can no longer go critical at 0 ppm boron, it is time to refuel. There is a limit to the maximum amount of boric acid that can be added to the coolant. If too much is added, the coolant becomes a net poison instead of a moderator, leaving the reactor with a negative void coefficient [105, p.13]. For this reason, boric acid concentration is usually capped around 1000 ppm at the beginning of the fuel cycle.

[55] The large thermal absorbtion cross section of boron gives it a huge self-shielding effect. This means that fuel pins with mixed boron would have an even larger than usual thermal flux depression in the interior of the pin. In addition to its use as a burnable poison, boron is also used in two other ways. The chemical shim process of boric acid loading is discussed earlier. Additionally, boron is commonly used in control rods.

3.6.4 Simulation Application

To simulate poison loading in a naval reactor accurately is impractical. Instead, this thesis will focus on creating the effects of a good burnable poison loading without addressing the actual procedure or process for doing so. A team of naval reactor engineers will be able to design a better result using actual methods.[56] Therefore, in this study, only a single burnable poison will be used. Additionally, only the power shape at beginning of cycle will be optimized to lower the power peaking factor. Finally, the poison will be implemented using a simple mechanism.

Gadolinium Effects

This thesis will attempt to balance power peaking and reactivity effects only using gadolinium as a burnable poison. Gadolinium is widely used in commercial reactors due to the ease with which it can be mixed into the fuel during the fabrication process. There are two parameters that gadolinium controls in the lifetime reactivity curve. The number of fuel pins that include gadolinium oxide controls the magnitude of the reactivity reduction [108, p.24]. This can be seen in figure 3.7(a), where increasing the number poisoned pins pulls down k_{eff} further and further. Additionally, the weight concentration of gadolinium can be varied in order to prolong the time that reactivity is held down [108, p.24]. This can be seen in figure 3.7(b), where increasing the gadolinium concentration extends the effect further and further out in burnup.

Burnable Poison Lifetime

While an effort will be made to ensure that the effects of the burnable poison do not significantly diminish after a few steps in the burnup cycle, flattening the power distribution over the entire cycle is a daunting task. Firstly, the fuel composition at high burnup is subject to chaotic effects, where slight modifications in initial design create large deviations in power shape, fission product concentrations, and fuel history at the end of the cycle. Secondly, it is much more computationally intensive to optimize the power shape at high burnup, as all previous burnup steps must be rerun in order to accurately calculate k_{eff}. This requires the simulation of hundreds of millions or billions of neutrons to refine the power shape. Therefore, the power shape will only be optimized in the initial time step, and a good faith effort

[56] Additionally, much of the information about how this process is actually done is highly controlled. Naval Reactors acknowledges the existence of poison elements in its reactors, but has kept classified the exact details [45, p.12-8]. Similar information for commercial reactors is proprietary. In the end, the accuracy requirement of this work can be met using a simple estimation.

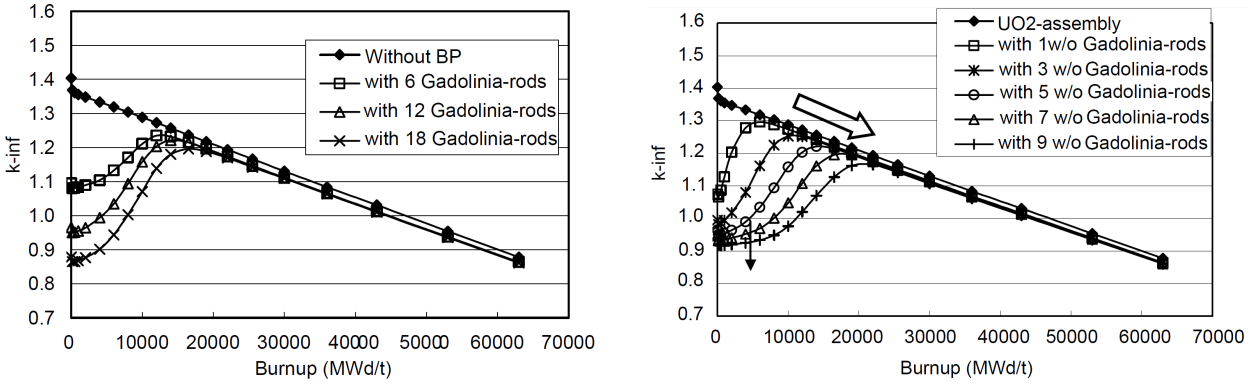

(a) Number of Poisoned Rods

(b) Weight Percentage of Poison

Figure 3.7. These figures show the effects that gadolinium poisoning has on reactivity in a nuclear reactor. Figure (a) shows how as the number of poisoned rods increases, the amount of reactivity pulled down initially increases. However, this has a small effect on the speed at which the reactivity effect goes away. Figure (b) shows how the reactivity pull-down effect lasts longer as the weight percentage of gadolinium increases. This is due partially due to neutron self-shielding, and partially due to the fact that there is simply more gadolinium to burn away. Both of these graphs are reprinted from [108, p.24]

will be made to ensure that it does not deviate significantly over the course of the burnup cycle.[57]

Poison Loading Method

Gadolinium will be loaded into the core in a non-physical manner. In both the HEU and LEU core, the atomic density of the fuel will simply be increased by adding gadolinium atoms in varying amounts throughout the core. Again, this is not meant to simulate a manner in which the reactor can actually be poisoned and balanced.[58] Instead, it is simply simulates the end result of a poisoned core.

3.7 Full Core Serpent Simulation

Once the initial core loading of burnable poisons is completed, the next step is to begin the burnup simulation of the reactor. This is the longest process of the thesis, and gives the results for final analysis. However, there are a number of things that must be checked and verified before the simulation can begin.

[57] This step is entirely a subjective process. However, it can be seen in many sources that the major effects of gadolinium poisoning on reactivity have usually gone away by 15-20 MWd/kg [108, p.6][105, p.40]. This will be used as a guiding principle.

[58] In fact, this method is impossible in monolithic fuels [76].

3.7.1 Maximum Required Burnup

In the end, the driving requirement for the reactor is the amount of total energy delivered, as discussed in section 2.1.3. By taking the total energy and dividing by the total fuel loading, the required burnup of the core can be easily calculated. This number has to be checked against the physical limits of the fuel to ensure it is below void and fission-product swelling limits before the neutronic simulation can begin.

3.7.2 Burnup Steps

One of the more technical decisions required to initialize the simulation is the choice of burnup steps. Steps should be large enough to minimize the calculation requirements, but small enough to track the changing solution to the Bateman equations during depletion. The early steps, while fission-product concentrations are changing rapidly, are of particular importance. The Serpent Manual suggests an initial step of 0.1 MWd/kg, followed by increments of 0.5 MWd/kg until 15 MWd/kg, and then steps of 5 MWd/kg to the end of the simulation [104, p.121].[59] The consequence is that computational time is heavily front-loaded in the simulation and the marginal cost of extending simulations 10 or 20 MWd/kg beyond the required point is low. This means that it is very simple not only to determine if the required life of the reactor can be met, but to burn to the actual limit of reactor life.

3.7.3 Results Analysis and Requirements

Serpent provides the reactivity of the reactor over the course of its life. This should be the determining factor in whether a naval reactor can use LEU to get the same kind of lifetime as when it uses HEU. It also provides the power peaking and power distributions of the reactor over time. Serpent can also provide minor factors such as the fast-to-thermal flux ratio (which can be used to estimate damage to non-fuel core materials), neutron leakage probability, fuel activity, and end-of-life fuel composition.

[59] The small initial steps allow the simulation to reach equilibrium concentrations of fission products while capturing the early behavior of the core reaching equilibrium.

Chapter 4

Highly Enriched Uranium Core

This chapter presents the results of the HEU core simulation using the UO_2 fuel. Additionally, it discusses unexpected results of general interest. The first six sections follow the outline of chapter 3: the core's temperature profile and thermal properties, moderator-to-fuel ratio selection, coolant pressure drop estimate, monte-carlo parameters, burnable-poison loading, and full burnup results. Section 4.7 discusses fabrication requirements for the HEU fuel. Section 4.8 discusses the reactor's flux spectrum and associated consequences. Finally, section 4.9 discusses the consequences of substituting LEU in the fuel designed for use with HEU, explaining why the Navy's 1995 evaluation proved to be so negative. Table 4.1 and figure 4.1 show a short summary of the final geometry of the HEU core.

The final HEU core design did not meet the margins set in chapter 2 at all points in the burnup cycle, as shown in table 4.2. Once the gadolinium burnable poison was sufficiently depleted, the radial peaking factor in the core began to rise, resulting in the violation of several thermal margins. This was expected, as gadolinium alone is not sufficient to control reactivity and power profiles over the full life of a reactor. A more detailed core design, which satisfies all thermal margins at all points of core life, would require more detailed design, and is outside the scope of this thesis. The focus of this thesis is to satisfy reactivity limits to determine core lifetime, and to have realistic thermal-hydraulic parameters at the beginning of core life which, with a more detailed design, could be preserved for the full burnup cycle.

4.1 Fuel Temperature and Thermal Margins

The first step of the simulation was determining the average fuel temperature of the reactor. The results of this analysis are shown in table 4.2.[1] The HEU core was found to have an

[1]Table 4.2 breaks the thermal results into three sections. In the first section, the temperature is reported using the average power density of the core. In the second section, the power peaking factor at beginning of

Table 4.1. HEU Core Geometry

Fuel Plate Length	4.49 cm
Fuel Plate Width	0.25 cm
Fuel Plate Height	100 cm
Cladding Width	0.04 cm
Fuel Assembly Length / Width	5.3 cm
Core Radius[1]	55 cm
Core Height	100 cm
Uranium Weight	678 kg[2]
Required Burnup	333 MWd/kg

[1] The core radius is equivalent to the inner radius of the core barrel or outer radius of the core shroud.

[2] This makes the total weight of ^{235}U equal to 630 kg, roughly equal to the 0.5 MT estimate in literature [10, p.78][20, p.92].

average fuel temperature of 393°C, with a peak average centerline temperature of 470°C 2.4 cm above the center of the core. With the beginning of cycle assembly peaking factor accounted for, the maximum temperature of the fuel rises to 487°C. With the largest power peaking factor over the life of the reactor accounted for, the maximum temperature of the fuel is 558°C. All of these are within the margins set in section 2.1. However, the cladding and MDNBR limits were violated by the end-of-life power peaking factor.

4.1.1 Fuel Melting and Blistering Margin

The HEU core easily meets the 300°C margin to fuel melting. Section 2.5.2 set the conservative measurement of the melting point of the fuel at 1800°C, the melting point of the zirconium matrix of the fuel. In order to come within 300°C of this measurement, an assembly power peaking factor of 6.5 would be required. This helps to show that fuel melting is the easiest margin to meet when using thin fuel plates. In thicker fuel plates, fuel melting would be a much more important margin for consideration. Figure 4.2(b) shows the fuel centerline temperature in the average fuel plate as a function of z. This plot does not account for power peaking factors. The graph shows that the fuel is closest to melting at the center of the plate, implicating that the use of an axial burnable poison loading pattern could help in obtaining even more margin.

core life is multiplied by the average power density, and temperatures are recalculated. In the third section, the maximum peaking factor from the depletion cycle is used.

Table 4.2. HEU Core Thermal Properties

Power Density[1]	0.221 kW/g-U
Power Density[2]	0.891 kW/cm^3
Average Cladding Temperature	344°C
Maximum Outer Cladding Temperature	353°C
Outer Fuel Temperature	383°C
Average Fuel Temperature	393°C
Maximum Fuel Temperature	470°C
MDNBR	1.84
Recalculation using Beginning of Cycle Peaking Factor[3]	
Corewide Power Peaking Factor	1.09769
Average Cladding Temperature	349°C
Maximum Outer Cladding Temperature	359°C
Outer Fuel Temperature	393°C
Average Fuel Temperature	403°C
Maximum Fuel Temperature	487°C
Coolant Exit Temperature	312°C
MDNBR	1.63
Recalculation using Maximum Peaking Factor[4]	
Corewide Power Peaking Factor	1.48825
Average Cladding Temperature	370°C (350°C limit)
Maximum Outer Cladding Temperature	383°C (375°C limit)
Outer Fuel Temperature	429°C (425°C limit)
Average Fuel Temperature	443°C
Maximum Fuel Temperature	558°C
Coolant Exit Temperature	319°C
MDNBR	1.06 (1.3 limit)

[1] The power density in kW per gram of uranium is used as the normalization factor for Serpent simulations.

[2] The power density in kW per cm^3 is used in the temperature calculations described in section 3.2.

[3] The beginning of cycle power peaking factor. This value was calculated using Serpent, and is discussed in section 4.5.2.

[4] The largest power peaking factor over the life of the reactor. This value was calculated using Serpent, and is discussed in section 4.6.2.

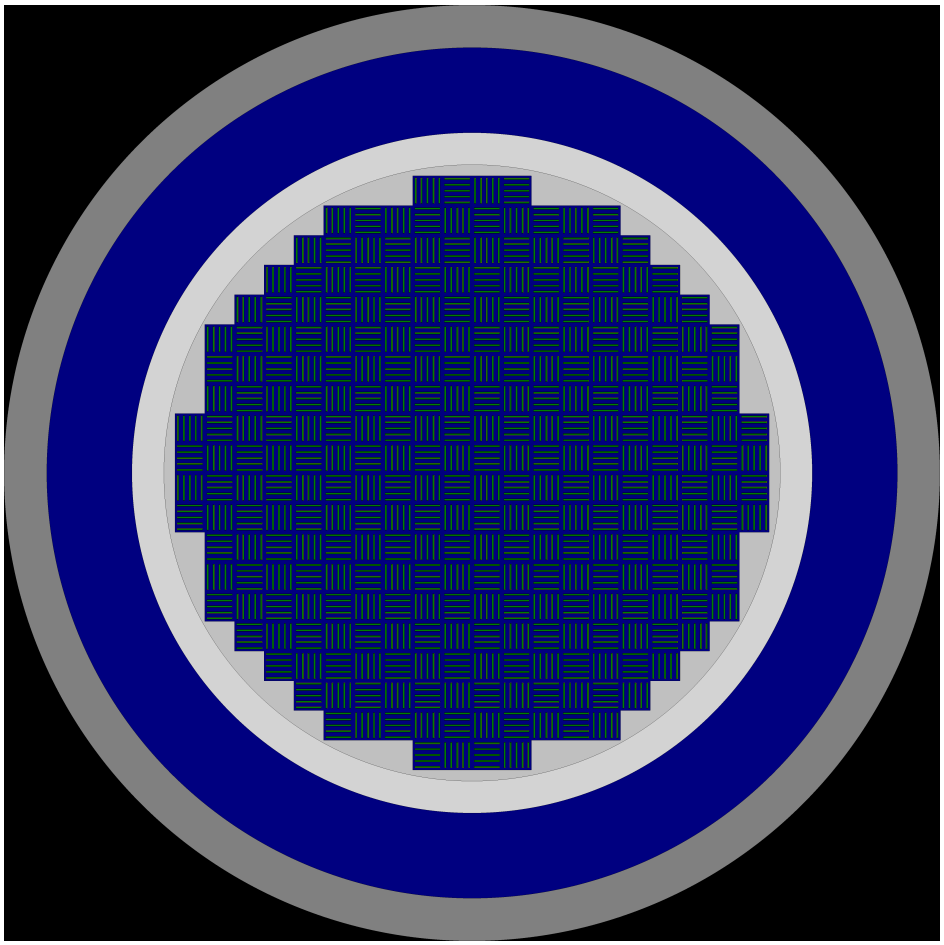

Figure 4.1. This is the final version of the HEU fueled reactor. The detailed measurements of the geometry are shown in table 4.1.

The fuel-blistering margin was met at the beginning of the core's life. However, once the gadolinium poison burned out and the peaking factor increased, the fuel blistering margin (set in section 2.1.7) was violated. The outer fuel temperature increased to 429°C, 4°C over the 425°C limit. This shows that a slight improvement to the burnable poison loading, decreasing the peaking factor at the end of the core's life, would cause the fuel-blistering margin to be met.

4.1.2 DNB Margin

As shown in table 4.2, the HEU core meets the DNB acceptance criterion laid out in section 2.1.8 at the beginning of the fuel cycle, and up until the gadolinium poison burns out. The average fuel assembly had an MDNBR of 1.84 and the peak power assembly at beginning of core life had an MDNBR of 1.63. However, once the gadolinium burned out, MDNBR dropped to 1.06, in a clear violation of the 1.3 safety limit. There were three easily

controlled parameters that assisted with controlling departure from nucleate boiling. The first was the fuel thickness. As the fuel plates became narrower, the heat flux through each plate decreased. This helped lower the heat flux (q''), as shown in figure 4.2(d), leading to a higher MDNBR. The second controllable parameter is the coolant entrance and exit temperatures. By decreasing these values, the mass flow rate of the core increases, leading to a higher MDNBR. Finally, MDNBR is significantly affected by the power peaking factor in the core. By altering the distribution of burnable poisons throughout the core the peaking factor can be lowered, increasing the MDNBR. It is possible that different burnable poisons that burn out over different timescales could be loaded into the core in order to keep the power profile flatter over the life of the core, thereby eliminating the DNB violation late in the core life.[2]

4.1.3 Cladding Margins

Section 2.3 set two requirements for cladding temperature in the reactor: first, that the average temperature of the cladding be kept below 350°C, second, that the peak outer cladding temperature be lower than 375°C. The HEU core has an average cladding temperature of 344°C, and a maximum outer cladding temperature of 353°C. If a single fuel assembly operates at 110% of average power for the life of the reactor (the beginning of cycle assembly peaking coefficient), its average fuel temperature is 349°C while its outer cladding temperature would be 359°C. These measurements meet the acceptability criteria set out in section 2.3. The outer cladding temperature of the average assembly is shown in figure 4.2(c). However, gadolinium burnout also caused this margin to be violated.

There are a few ways that extra margin could be achieved. One is through a decreased cladding thickness. This would lower the total temperature increase across the cladding, decreasing the average temperature. Research would be needed to determine minimum cladding thickness to resist corrosion. The second way to achieve extra margin would be to increase the heat transfer between the cladding and the coolant. One way to do this is through increasing the heat transfer coefficient by increasing turbulence. This is commonly done in commercial reactors through the use of mixing vanes [109, p.1]. Another way is by increasing the area of the plate through the use of fins, which increase the total amount of surface area available for convection but reduces moderation [90, p.155]. Both of these methods come at the cost of an increased pressure drop over the core [34, p.487]. Reducing the core-wide power peaking factor would also help to meet margins, and is needed regardless.

[2]Control rod movements could also be used for detailed power shaping.

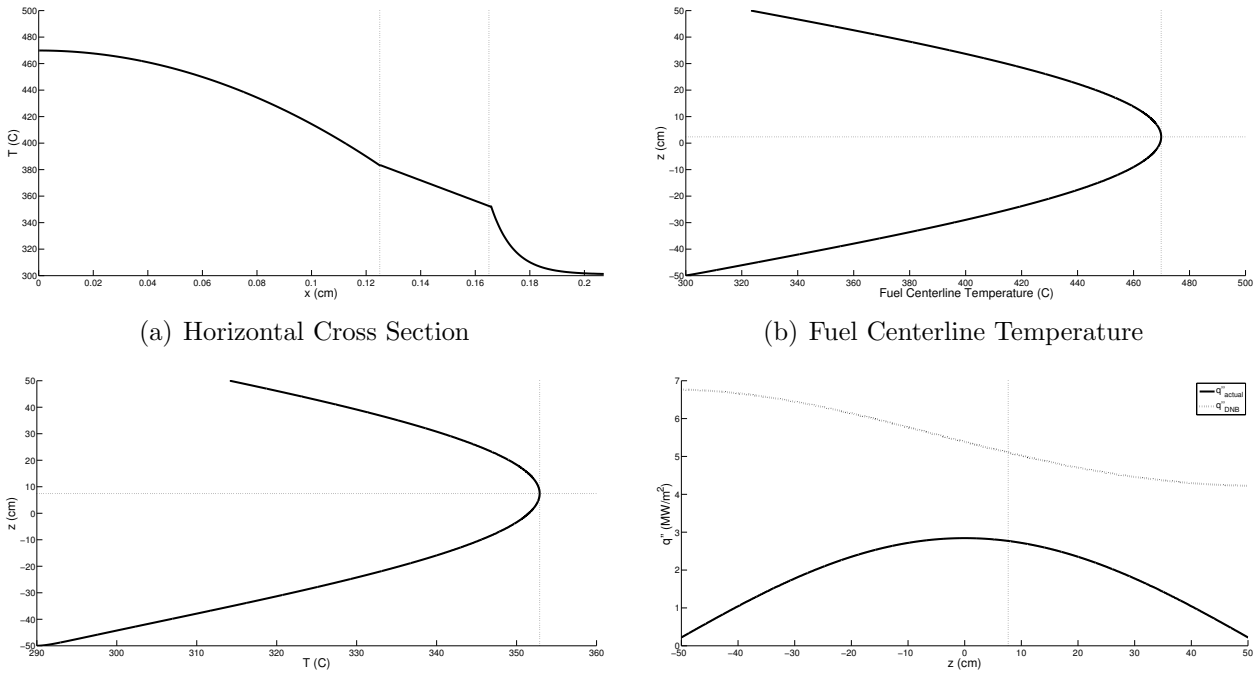

(a) Horizontal Cross Section

(b) Fuel Centerline Temperature

(c) Outer Cladding Temperature

(d) DNB Margin

Figure 4.2. Subfigure (a) shows the temperature of the fuel plate as a function of x at the vertical position of the maximum centerline temperature. The vertical lines mark the boundaries of the fuel and cladding respectively. Subfigure (b) shows the fuel centerline temperature as a function of z with the maximum temperature marked. Subfigure (c) shows the outer cladding temperature as a function of z with the maximum temperature marked. Subfigure (d) shows the heat flux and departure from nucleate boiling heat flux as a function of z. The fuel power density is that of the average fuel assembly, and not of that of either beginning or end of life peak assembly.

4.2 Moderator-to-Fuel Ratio

With the fuel temperature determined, the next step is to determine the moderator-to-fuel ratio by setting the plate-to-plate pitch. The core will use fuel assemblies of five plates. The fuel assemblies must be overall square in order to use the lattice commands built into Serpent. These lattice commands are important, as without them it is not possible to easily calculate power peaking factors [104, p.93]. In order to ensure long fuel plates and thus negligible heat transfer in the y direction, there must be a "large" number of plates in each assembly.[3] For example, a single plate assembly with a pitch of one centimeter would result in a fuel plate with a fuel length of a quarter centimeter, in effect becoming a rectangular pin. However, an assembly of ten plates with the same pitch would have a (roughly) 9.5 cm

[3]The x, y, and z directions are defined in figure 3.1.

fuel length.[4] However, these extremely long fuel plates would provide a scattering direction for neutrons in which they are unlikely to reenter the fuel. For example, imagine a neutron that scatters "up" the long side of the plate in figure 4.3. This would decrease the number of neutrons that cause fission, lowering k_{inf}. An assembly of five plates was found to balance these competing effects. Additionally, as mentioned in section 3.3.4, the lattice simulations will use infinitely tall and long plates. Once a pitch has been selected, a finite-plate pitch that maintains the same ratio of moderator to fuel cross-sectional area will be calculated. Figure 4.3 shows what these infinite plate assemblies look like.

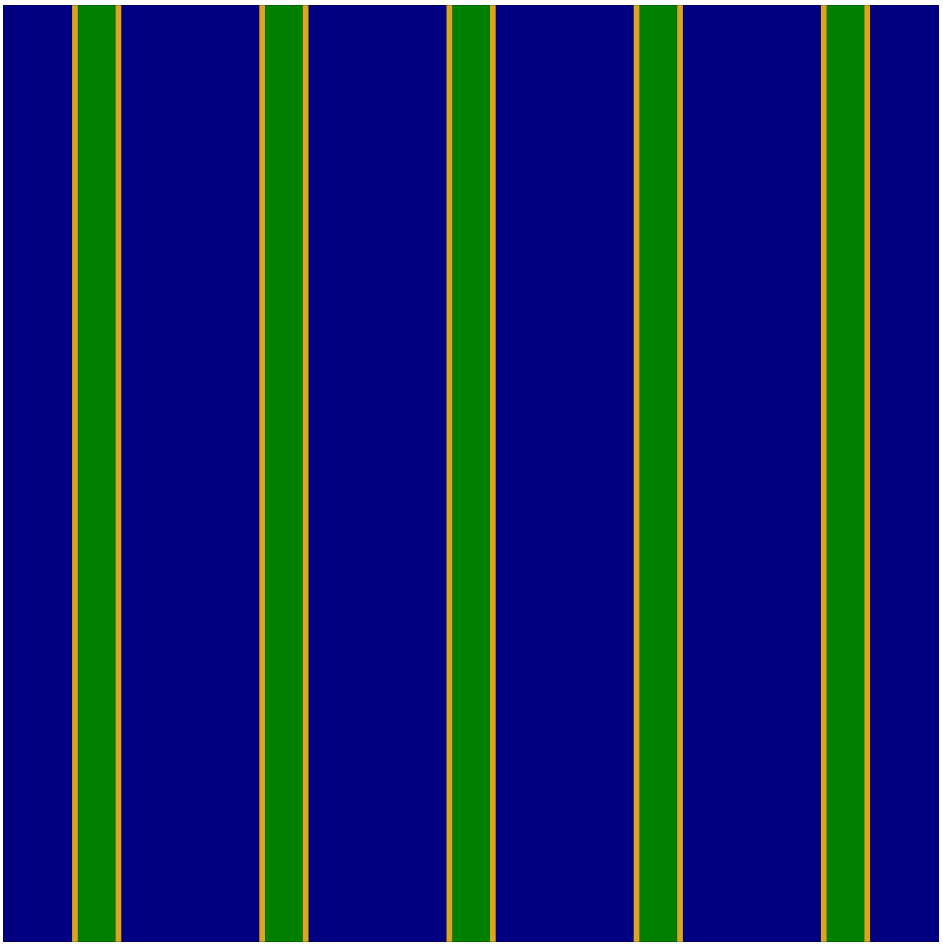

Figure 4.3. This figure shows the fuel assembly shape used in figure 4.4. Each fuel plate is a quarter centimeter thick, with a cladding thickness of 0.04 cm. The pitch will be varied to determine an optimal moderator-to-fuel ratio.

The results of the infinite plate simulations are shown in figure 4.4. Each fuel assembly was burned to 350 MWd/kg, slightly past the fuel burnup limit discussed in section 2.5.2.

[4]These calculations assume that the same channel width along the long sides of the plate are desirable along the short sides. More intricate core designs could use different parameters.

The results show a few interesting trends. First, increased moderation slows the decrease in k_{eff} with fuel burnup. While k_{inf} of the one-centimeter pitch assembly dropped by about 0.35 over 350 MWd/kg of burnup, k_{inf} of the 2.5 cm pitch assembly only dropped by 0.27. Secondly, the HEU fuel is clearly physically burnup limited as opposed to reactivity limited. Even the heavily undermoderated assembly with a pitch of 0.5 cm (representing a full channel width of about 0.15 cm) has a k_{inf} of about 1.3 at 350 MWd/kg of burnup. These results confirm one of the primary advantages of HEU fuel: that the reactor can operate for a long time provided the fuel is capable of containing the fission products.

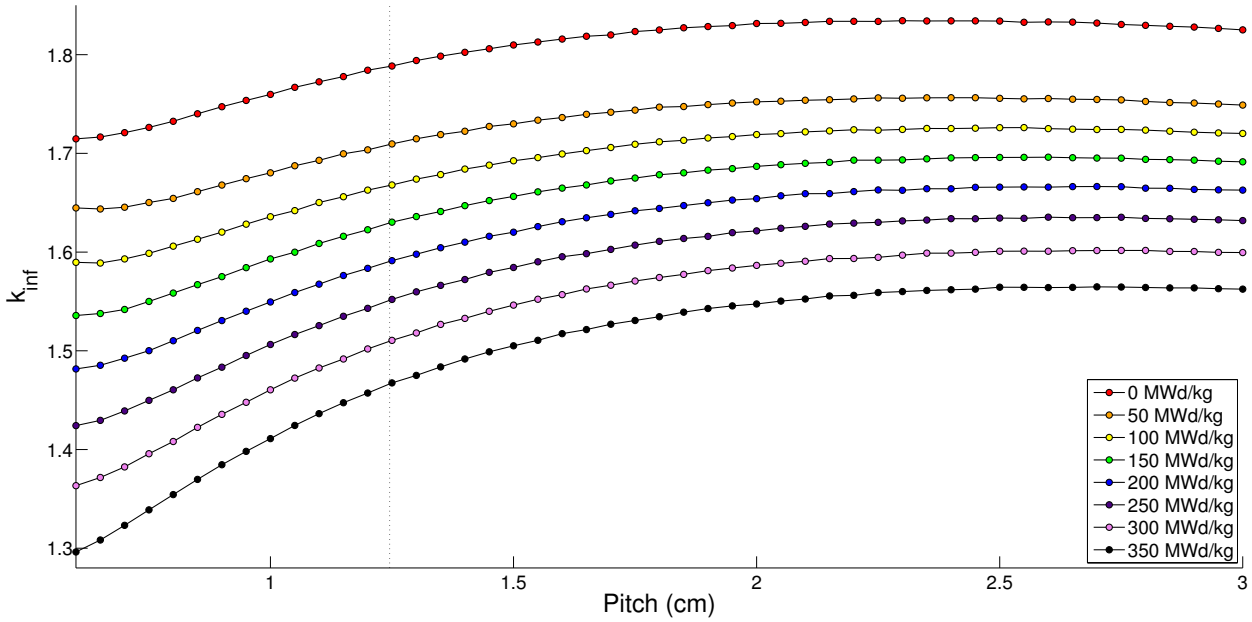

Figure 4.4. This figure shows the effect of pitch on k_{inf} throughout the burnup of the HEU dispersion fuel. Pitch is used as a stand-in for the moderator-to-fuel-ratio. Each simulation is a five plate fuel assembly, as shown in figure 4.3, and simulates 20,000 neutrons for each of 50 active cycles with 50 inactive preceding cycles. Each measurement is accompanied by an average error of 0.00022, or 2.2 pcm, with a maximum error of 0.00044, or 4.4 pcm. The line at 1.245 cm represents the final pitch chosen for use in the full reactor model.

One of the primary advantages of the HEU core is its amount of excess reactivity. This means that the choice of a plate-to-plate pitch doesn't depend strongly on the reactivity. The choice of pitch can instead focus on lowering the required burnup of the fuel, thermal, safety, and battleshock requirements. For example, the use of a two-centimeter pitch would restrict the core to about ten assemblies across the centerline of the reactor, while using a one centimeter pitch would allow for 20 assemblies across the reactor.[5] The pitch was

[5]The diameter of the core is 1.1 m. A two centimeters pitch would make the five plate assemblies about ten centimeters across, leaving room for 10 assemblies across the core. The same calculation for a one centimeter pitch allows 20 assemblies.

chosen to be small enough so that 20 assemblies could fit across the core. This resulted in choosing a pitch of 1.245 cm with the infinite plates, which corresponds to a pitch of 1.06 cm using finite length fuel plates.[6] With a pitch of 1.06 cm, the fuel assemblies become 5.3 cm square. The square fuel assemblies are arranged in a pattern similar to the assembly pattern of commercial reactors. An example of this pattern is shown in figure 4.1. The assemblies alternate their orientation to prevent neutrons having a preferential direction out of the core and to maintain rotational symmetry within the core.

4.3 Primary Loop Pressure Drop

Using the mass flow rate through the core from equation 2.5, the process laid out in section 3.4.2, and the pitch determined in the previous section, the pressure drop throughout the primary system can be calculated. Table 4.3 details the specific results of these calculations. The most important takeaway from the results is that, even under fairly conservative estimates, the required pumping power is still low compared to the power of the reactor. The estimated power required is 184 kW, roughly 0.12% of the reactor's thermal power.[7] This is low enough to validate that the proposed core has a realistic design with respect to pressure drop.

In general, these results indicate that primary coolant pumps do not impose an overly large load on the electrical system of the submarine. As long as the electrical generation process maintains an efficiency of at least 20%, the pumps do not require more than 1% of electrical power. These results depend on a few assumptions about the pressure loss outside of the reactor. A more thorough pressure drop analysis would require an estimation of the particulars of the primary system piping.

4.4 Shannon Entropy / Neutrons per Cycle

With the majority of the physical parameters determined, the next step was to build a full core and begin estimating the "run parameters" for Serpent. In particular, this means the number of neutrons per cycle, the number of active cycles, and the number of inactive cycles. A series of simulations were run using one-hundred thousand, one million, and two million neutrons per cycle to determine the accuracy gains and computational time of each neutron population. Figure 4.5 shows the results of these simulations.

[6]The resultant fuel plates are therefore 0.25 cm wide, 4.49 cm long, and 100 cm tall, and preserve the reactivity of the infinite plates.

[7]This is well under the 1% requirement set in section 3.4.1.

Table 4.3. HEU Core Pressure Drop

$\Delta P_{\text{gravity}}$	7.13 kPa
$\Delta P_{\text{friction}}$	3.25 kPa
$\Delta P_{\text{acceleration}}$	-0.195 kPa[1]
ΔP_{form}	6.83 kPa
ΔP_{Core}	17.0 kPa
ΔP_{Total}[2]	85.1 kPa
$\dot{M}$[3]	1,370 kg/s
Pump Power[4]	184 kW

[1] According to equation 3.30, the pressure loss of entering the core is overcome by the pressure gain as the coolant exits the core. This is due to the density difference between the coolant at the top and bottom of the core.

[2] The total pressure drop is equal to five times the pressure drop over the core of the reactor, as discussed in section 3.4.1.

[3] $\dot{M}$ is the total mass flow rate through the entire core. However, the individual pressure drop components are calculated using the mass flow rate around a single fuel plate (0.914 kg/s).

[4] The pump power relationship is given in equation 3.24. The isentropic efficiency used is 0.85, as given in [34, p.44].

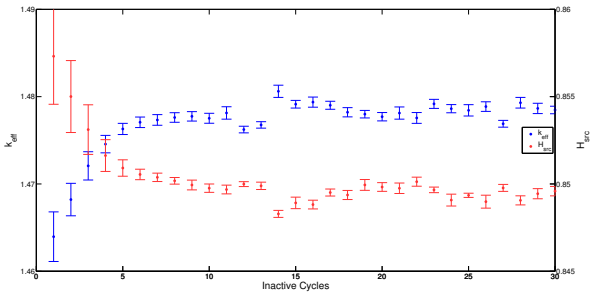

(a) 100 Thousand Neutrons, 10 Active Cycles

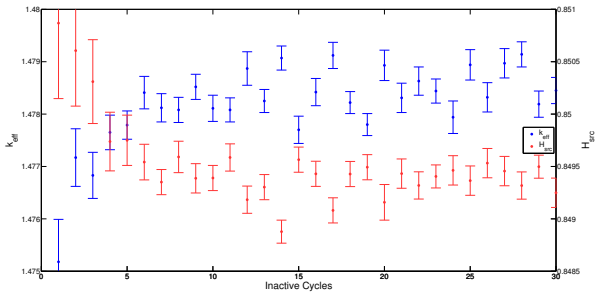

(b) 100 Thousand Neutrons, 50 Active Cycles

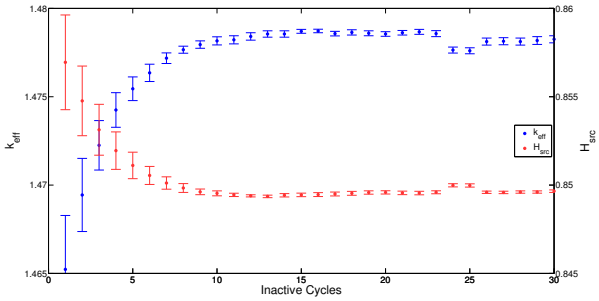

(c) One Million Neutrons, 10 Active Cycles

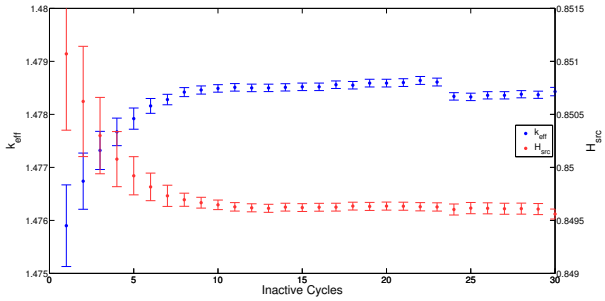

(d) One Million Neutrons, 50 Active Cycles

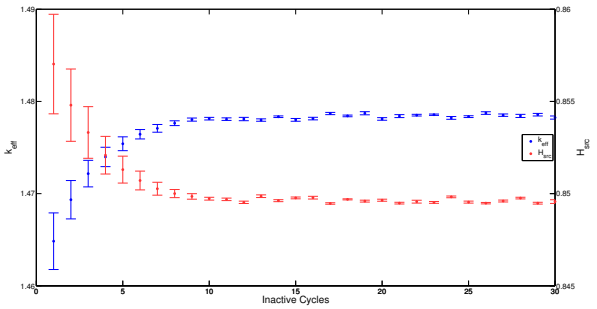

(e) Two Million Neutrons, 10 Active Cycles

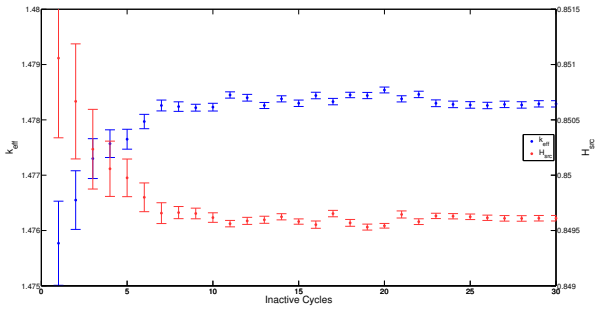

(f) Two Million Neutrons, 50 Active Cycles

Figure 4.5. Subfigures (a) and (b) use one-hundred thousand neutrons per cycle. Subfigures (c) and (d) use one million neutrons per cycle. Subfigures (e) and (f) use two million neutrons per cycle. The subfigures on the left use 10 active cycles of neutrons, while those on the right use 50 active cycles. These plots show three trends. First, increasing the number of inactive cycles causes the measurements to converge. Second, increasing the number of neutrons per cycle decreases the size of errors. Finally, having too many active cycles can cause the error to increase, as the fission source continues to update after each cycle.

While programs such as OpenMC will report the value of k_{eff} and Shannon entropy after each inactive cycle, Serpent does not have this capability [110]. Therefore, each point on the graphs represents an independent simulation, run with a certain number of inactive and active cycles. The random nature of Monte Carlo codes causes the separate simulations to converge differently, causing the final "level-off" of the curves in figure 4.5 to be less steady. One of the artifacts of this run behavior is the jumps in certain measurements of k_{eff} and

Shannon entropy. This can be clearly seen in figure 4.5(c). However, the overall trend of convergence can still be identified.

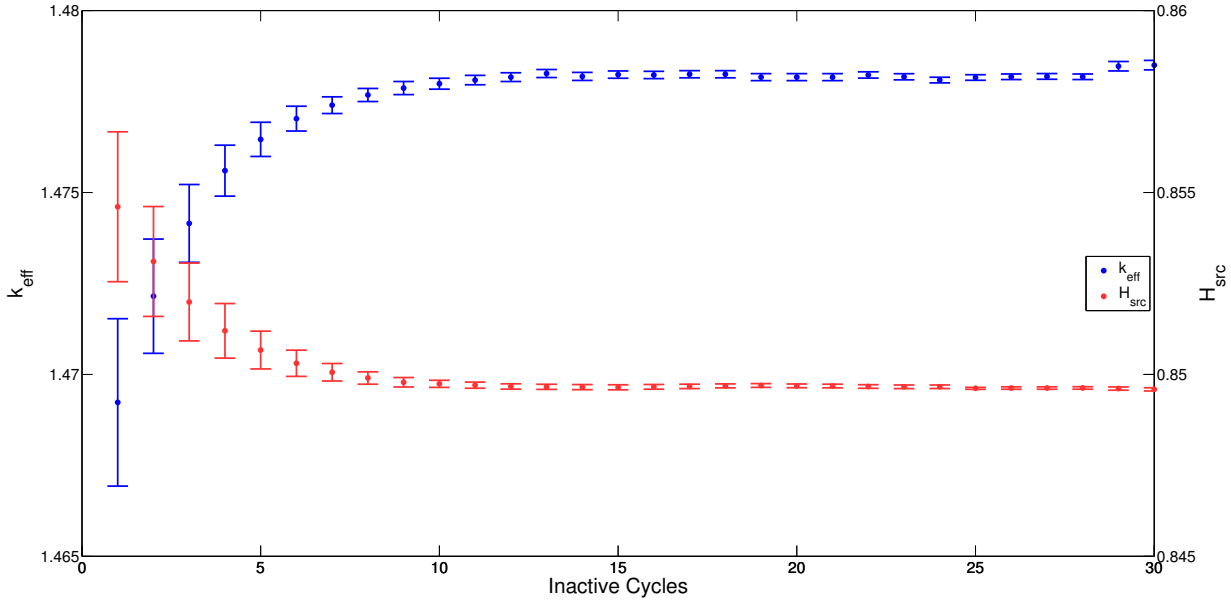

Figure 4.6. Above is the convergence pattern for the neutron population parameters used for the HEU core. There are two million neutrons per cycle, and 15 active cycles.

This thesis uses two million neutrons per cycle, 15 active cycles, and 15 inactive cycles for full core burnup simulations. The two million neutrons per cycle was chosen in order to increase the accuracy of the simulation past that provided by the smaller batch sizes. This allows for the reporting of k_{eff} within 10 pcm. The 15 active cycles limit will be used as a compromise between the precision provided by the large number of cycles and the computational speed of using fewer total cycles. The 15 inactive cycles was chosen, in all cases, as it appears to be a value at which k_{eff} and Shannon entropy have become relatively stabilized from the initial uniform power profile. Figure 4.6 shows the convergence pattern for this selection.

4.5 Burnable Poison Loading

The burnable poison loading is the most complicated and time-consuming step in the core design. In practice, it could continue until the reactor has a flat power distribution at all points in its life cycle. For this thesis, the power distribution will be shaped until a power peaking factor of 1.1 is obtained at the beginning of the core's life. This requires a series of tests to modify the amount of gadolinium in each section of the core until a final distribution is obtained. The unpoisoned HEU core has a power peaking factor of around 1.6 in the

Table 4.4. HEU Power Distribution, No Burnable Poisons[1]

0.522	0.486								
0.706	0.681	0.629	0.575	0.488					
0.872	0.854	0.807	0.744	0.666	0.544				
1.039	1.016	0.964	0.897	0.804	0.703	0.560			
1.196	1.168	1.115	1.039	0.940	0.828	0.703	0.543		
1.334	1.300	1.245	1.168	1.062	0.939	0.810	0.665	0.486	
1.440	1.410	1.355	1.275	1.166	1.037	0.895	0.746	0.571	
1.528	1.501	1.444	1.358	1.248	1.117	0.965	0.809	0.636	
1.585	1.561	1.498	1.413	1.302	1.167	1.014	0.854	0.681	0.487
1.616	1.594	1.528	1.441	1.328	1.190	1.040	0.875	0.708	0.519

[1] This table shows the power peaking factor of each assembly. Each value is an average of the position indicated and it's three rotationally symmetric partners in the core.

center of the core, as shown in table 4.4 and figure 4.7.

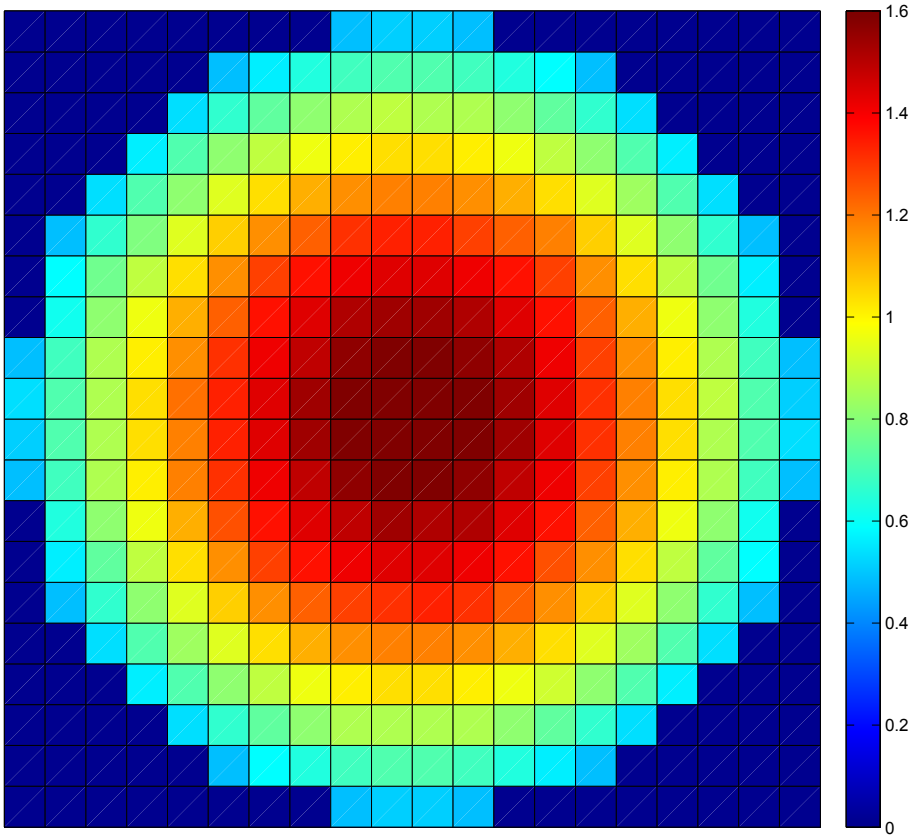

Figure 4.7. Above shows the power distribution of the HEU core at the first burnup step of the simulation without gadolinium.

4.5.1 Poison Zones

In order to balance the power distribution, the reactor will be split into a series of different zones. Fuel assemblies in these zones will be loaded with different amounts of gadolinium to shape the flux distribution. In theory, the best way to poison the core is to load each assembly individually, allowing for the power distribution to be finely tuned. For this thesis, the core will be broken into zones, each with a different amount of gadolinium.

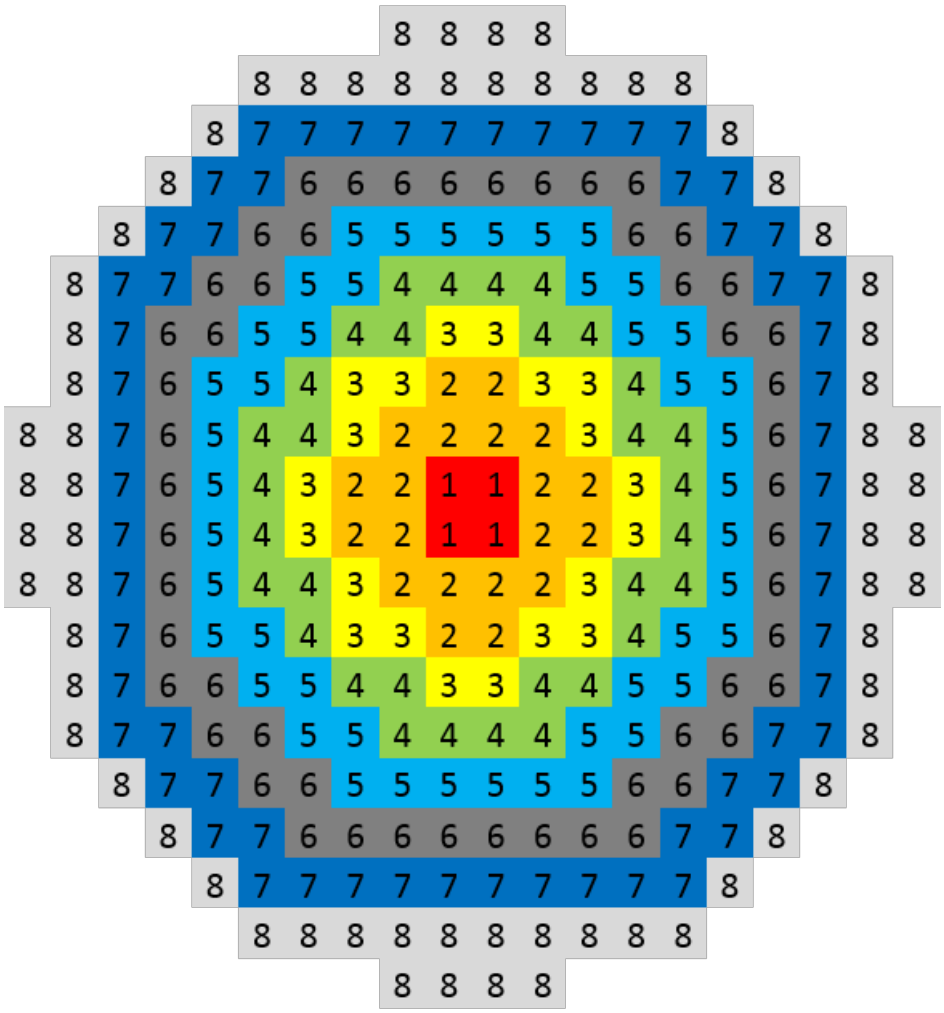

Figure 4.8. This figure shows the 8 different poison zones of the HEU core. Zone one has the highest density of gadolinium, while zone eight has the lowest.

Based upon the initial power distribution, the core was broken into eight zones, as shown in figure 4.8. Initially, the zones were loaded with an atomic density of gadolinium matching the original power profile. The distribution was then refined to lower the power peaking factor while keeping k_{eff} above unity. In order to do the poison loading correctly, the weight percentages used to describe the fuel in table 2.9 had to be converted into atomic densities.

Table 4.5. HEU Fuel Atomic Densities

Element	Weight Percent	Atomic Density[1]
^{16}O	6.56%	2.07×10^{-2} (barn-cm)$^{-1}$
Zr	45.2%	2.50×10^{-2} (barn-cm)$^{-1}$
^{234}U	0.356%	7.67×10^{-5} (barn-cm)$^{-1}$
^{235}U	44.8%	9.62×10^{-3} (barn-cm)$^{-1}$
^{238}U	3.02%	6.41×10^{-4} (barn-cm)$^{-1}$

[1] Atomic densities are given in (barn-cm)$^{-1}$, the unit used by Serpent.
[2] Atomic densities are calculated using equation 4.1, the weight fractions from table 2.9, and isotope and elemental molar masses from [77, p.138,142].

This was done using equation 4.1.

$$N_i = \frac{w_i \cdot \rho \cdot N_{Av}}{A_i} \tag{4.1}$$

In the above equation, N_{Av} is Avogadro's Number (6.02×10^{23} mol^{-1}), ρ is the compound density, and N_i, w_i, and A_i are the isotope or element number density, weight fraction, and molar mass respectively. The results for HEU fuel are shown in table 4.5.

4.5.2 Final Gadolinium Loading and BoL Power Distribution

It was discovered during the initial gadolinium-loading tests that there is a limit on how much gadolinium can be put into the core before the power peaking factor plummets in the interior of the core. When the gadolinium density approaches 1×10^{-2} (barn-cm)$^{-1}$ in the center of the core, the power peaking factor drops below 0.01, while the outer edge assemblies increase as high as 100.[8] The final loading used a maximum gadolinium density of about 1×10^{-3} (barn-cm)$^{-1}$.

After testing, the final gadolinium loadings in table 4.6 were chosen for the HEU core. The loading pattern began shaped roughly like a bessel function. As testing continued, the gadolinium density was pushed further up in the center of the core and pulled down on the outside of the core from this initial distribution. This resulted in the power distribution shown in figure 4.9. This distribution has a maximum value of 1.0977. The low power peaking

[8]The method of initial gadolinium loading was to set a maximum weight in the center of the core, and then have the gadolinium density decrease as a Bessel function moving away from the center of the core. When the maximum value approached 1×10^{-2} (barn-cm)$^{-1}$, the effects of gadolinium poisoning increased dramatically.

Table 4.6. HEU Gadolinium Loading

	Gadolinium Atomic Density
Zone 1	1.0248×10^{-3} (barn-cm)$^{-1}$
Zone 2	9.9010×10^{-4} (barn-cm)$^{-1}$
Zone 3	9.0934×10^{-4} (barn-cm)$^{-1}$
Zone 4	8.1865×10^{-4} (barn-cm)$^{-1}$
Zone 5	7.1179×10^{-4} (barn-cm)$^{-1}$
Zone 6	5.7229×10^{-4} (barn-cm)$^{-1}$
Zone 7	4.1207×10^{-4} (barn-cm)$^{-1}$
Zone 8	1.4688×10^{-4} (barn-cm)$^{-1}$

factor allows for additional margin on fuel melting, DNB, and cladding temperature. The core was then run to a burnup of 350 MWd/kg to determine the lifetime of the reactor.

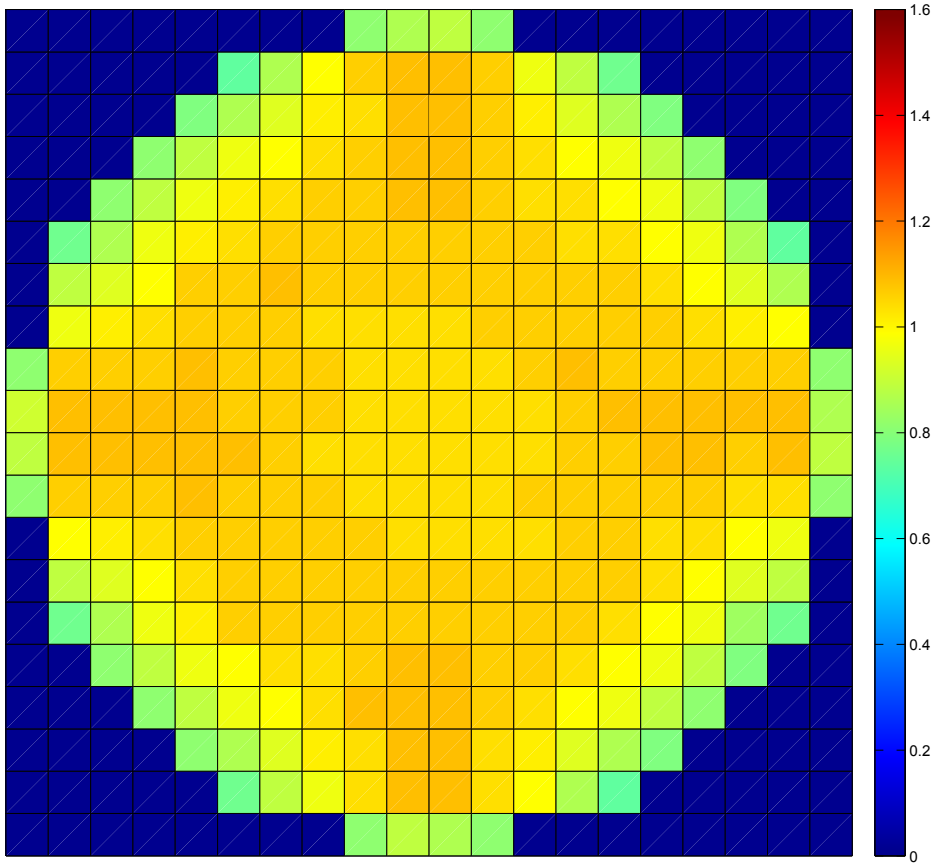

Figure 4.9. Above shows the power distribution of the poisoned HEU core at the first burnup step of the simulation.

4.6 Full Core Run and Results

From the energy requirement in equation 2.6, the core is required to reach 333 MWd/kg. This is about 11% past the allowable limit on physical burnup described in section 2.5.2. However, the HEU core was modeled mainly to understand the effect of burnup on reactivity in an environment dominated by ^{235}U. A more accurate simulation of an HEU core would decrease the volume fraction of UO_2 in order to increase the allowable burnup.[9] k_{eff} as a function of burnup for the HEU core, both with and without gadolinium, is shown in figure 4.10.

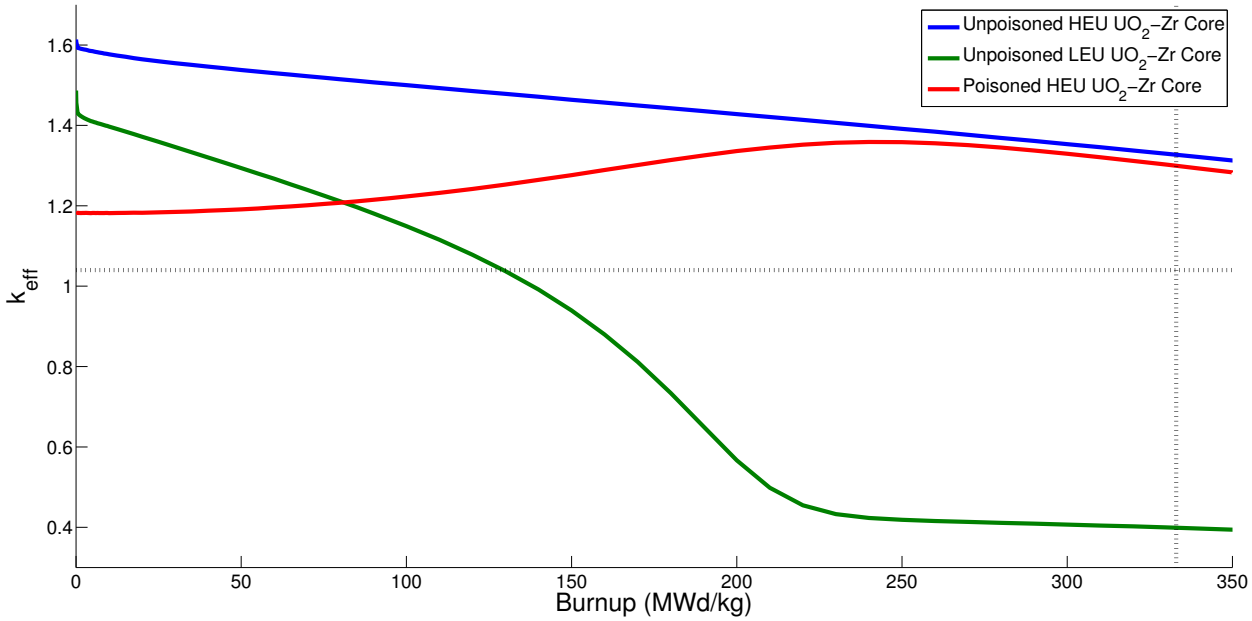

Figure 4.10. This figure shows k_{eff} vs burnup for three cases. The first is the unpoisoned HEU core. The second shows k_{eff} for the unpoisoned core loaded with 20% enriched uranium instead of 93% enriched uranium, but using the HEU fuel design. Finally, the third line is the poisoned HEU core. The horizontal line is the 1.04 reactivity limit, while the vertical line is the required burnup of 333 MWd/kg.

4.6.1 Excess Reactivity

As shown in the figure, the HEU core has a significant amount of excess reactivity at all points of its life. This would need to be controlled in order to operate the reactor. This would be done through the use of a combination of burnable poisons and control rods. The

[9]Specifically, a volume fraction of 30% UO_2 would allow for a maximum burnup of 500 MWd/kg (50% atomic). This fuel, used in the same geometry as the current HEU core, would require 463 MWd/kg to reach a full submarine lifetime. Judging from the linear pattern of k_{eff} shown by the current HEU core, this would be achievable.

gadolinium used in this thesis is insufficient for the remainder of excess reactivity to be controlled with control rods, and so likely would require the use of soluble boron or thicker plates.[10] However, this does show that even with burnable poisons, the HEU core is not reactivity limited. If the burnup could be extended, it appears that another 350 MWd/kg could be extracted from the core before k_{eff} drops below unity.[11]

4.6.2 Power Distribution

The power distribution at the beginning of the core's life is very flat. However, once the gadolinium burns away (roughly two thirds of the way through the core's life), the power distribution becomes peaked in the center. Figure 4.11 shows the power distribution at the most uneven stage in the core's lifetime. At this point, several of the thermal margins are violated.[12] A future model should improve time-dependent flattening of the power distribution over the life of the reactor, allowing the thermal margins to be met at all times.

4.7 Fuel Fabrication

There are two aspects of fuel fabrication that are specified when creating a dispersion fuel. The first is the grain size. This can affect reactivity, as larger grains tend to provide more self shielding, leading to a reactivity drop in the core. The second is the volume fraction of UO_2 within the fuel. While the volume fraction was set in section 2.5 under the assumption of homogenous composition, there is a problem with large volume fractions that arises because of grain particle size.

4.7.1 UO_2 Grain Size

The design of the HEU dispersion fuel focused on selecting a volume fraction of fuel, and did not specify the grain size of the ceramic dispersant. It is desirable for the ceramic particles to be small for a few reasons. First, small particles will have lower interior temperatures, as there will be less total heat generated within a particle that must be conducted to the outside of the particle. Second, smaller particles will exhibit smaller amounts of self-shielding, which improving reactivity.

[10] A k_{eff} value of 1.24 is the maximum allowed to be controlled using rods in commercial reactors [44, p.26]. Thicker fuel plates would increase the effect of gadolinium self-shielding in the fuel.

[11] This continues the roughly linear decrease in reactivity of the unpoisoned core in figure 4.10.

[12] Specifically the margins on cladding average and outer temperature, as well as the margin to DNB. These results are shown in table 4.2.

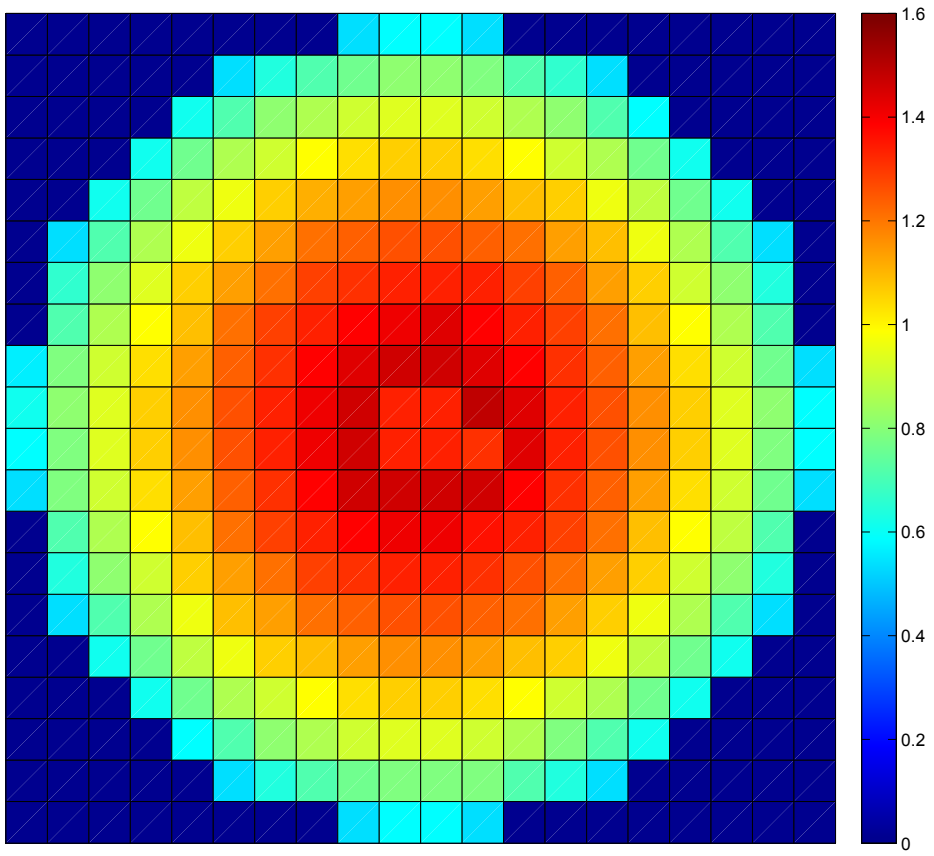

Figure 4.11. Above shows the power distribution of the poisoned HEU core 280 MWd/kg into the burnup cycle. At this point, the power peaking factor reaches 1.488, the highest of any point in the cycle.

In order to calculate the effect of particle size, a series of simulations were run that explicitly modeled the fuel as particles of UO_2 in a zirconium matrix, as shown in figure 4.12.[13] The size of the particles was varied from a nanometer up to a fraction of a centimeter. The value of k_{inf} was then plotted as a function of dispersant particle size. The average error in k_{inf} was 4.8 pcm, with a maximum value of 5.7 pcm. These values were then compared with the value of k_{inf} using a homogeneous mixture of uranium, oxygen, and zirconium. The results of these simulations are shown in figure 4.13.

There are two important conclusions from these results. The first is that treating the uranium oxide as a dispersant as opposed to a homogeneous mixture induces a drop in reactivity. This is predicted due to the effects of self-shielding. This reactivity drop is probably greater than that shown in figure 4.13 because the low thermal conductivity of

[13]Each simulation preserved the volume fraction of uranium oxide used in the homogeneous fuel (41.8%). Each simulation used 500,000 neutrons per cycle with 50 active cycles and 25 inactive cycles. The fuel plates modeled were infinitely long and tall with a pitch equal to that used in the full core simulation.

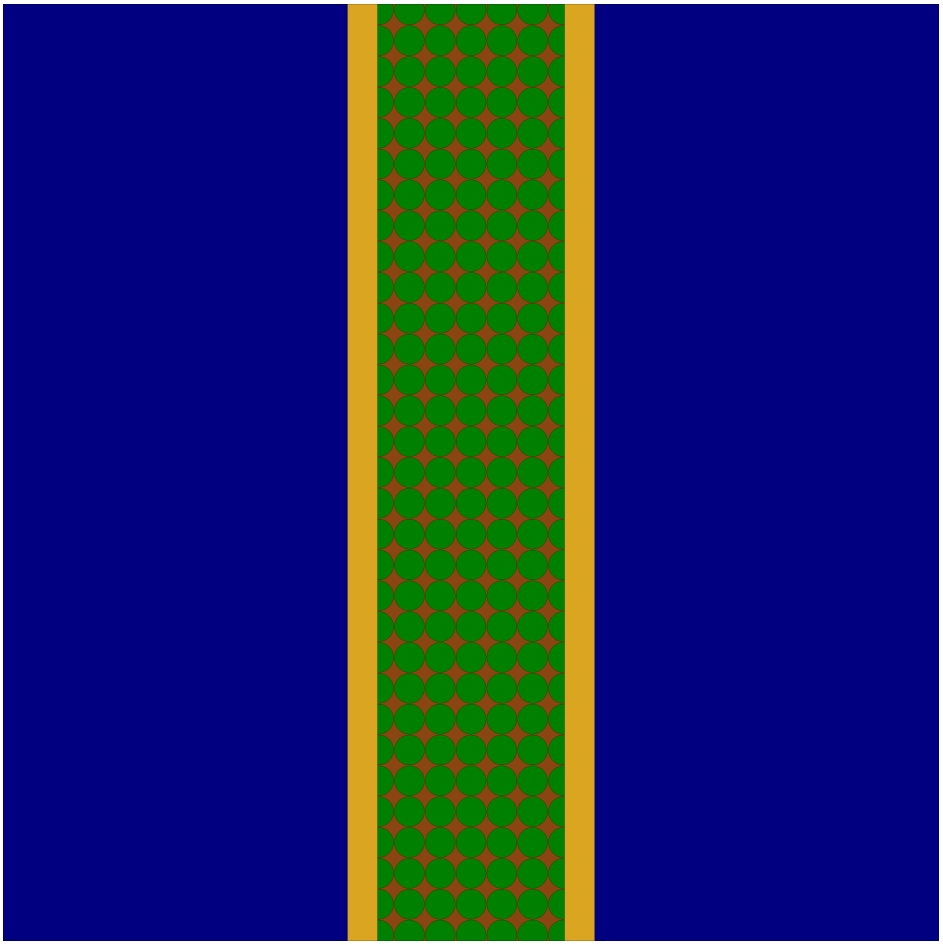

Figure 4.12. This figure shows what the fuel plates look like with the uranium oxide modeled as actual grains instead of a homogeneous uranium, oxygen, and zirconium mixture. An improved simulation would use a more random dispersion of particles.

uranium oxide will lead to a temperature within the fuel particles that is greater than that predicted by the mixture thermal conductivity. These higher temperatures increase the Doppler broadening of ^{238}U, lowering reactivity.[14] Secondly, the drop in reactivity due to the treatment of UO_2 as distinct particles is independent of particle size in the range of realistic particle sizes.[15] For the purposes of this thesis then, the exact particle size will not be identified. That decision can be based off of factors other than reactivity such as thermal properties, material strength and fatigue characteristics, or ease of fabrication.

[14] While this effect is lessened in HEU, due to the low concentration of ^{238}U, it is still present.

[15] When fabricating uranium oxide dispersion fuels, the uranium oxide particles are kept smaller than 125 μm [111, p.13].

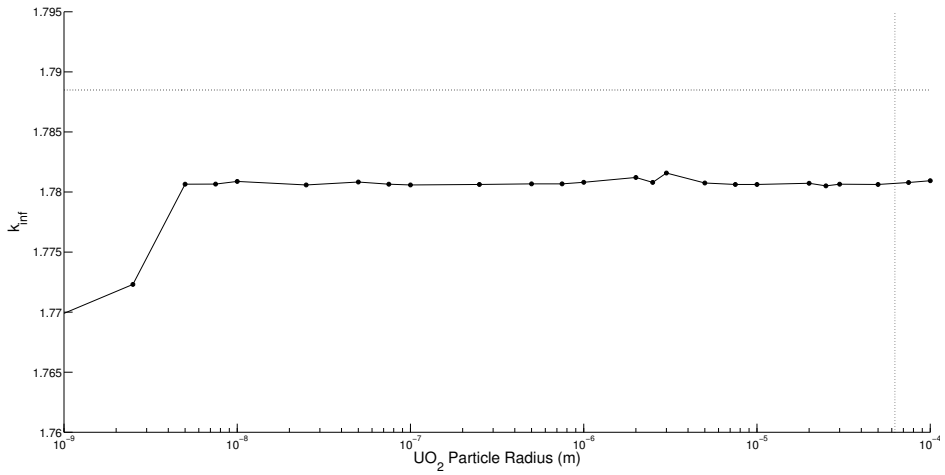

Figure 4.13. The size of the UO_2 particles within the metal fuel matrix, in the pattern of figure 4.12, was varied from a nanometer to a fraction of a centimeter. The values have a mean error of 4.8 pcm, and a maximum error of 5.7 pcm. The horizontal line shows the value of k_{inf} when the fuel is treated as a homogeneous material, while the points show k_{inf} at various particle sizes. The data show that there is a slight reactivity hit ($\approx$ 1000 pcm) once the fuel is treated as particles, but that the difference is fairly constant despite the actual size of the particles. The vertical line shows the limit of 62.5 μm, the upper limit on particle radius [111, p.13]. While the data should converge to the homogeneous case at some point, this is not seen.

4.7.2 Oxide Volume Fraction

One concern with the fuel used in this thesis is that the volume fraction of uranium oxide is extremely large. This can be shown using a simple volume ratio. If uranium oxide has a 41.8% volume fraction, and the uranium oxide particles are treated as spheres, then one has the relations:

$$0.418 = \frac{V_{\text{UO}_2}}{V_{\text{cell}}}$$

$$0.418 = \frac{\frac{4}{3}\pi r^3}{P^3} \tag{4.2}$$

$$P = 2.057 \cdot r \tag{4.3}$$

In the above equations P is the pitch between particles of UO_2, r is the radius of the particles, and V_{cell} is the volume of a particle of fuel and its surrounding zirconium. The factor of 2.058 between pitch and radius (or 1.029 between pitch and diameter) leaves a small damage zone between neighboring particles. If the fuel particles get too close to each other, these damage

areas can begin to overlap, leading to cracking of the fuel.[16] For example: the HIFR at Oak Ridge has a damage zone about 10 μm wide, while the 41.8% volume fraction used here would only provide a damage zone of 2 μm (at its narrowest), leading to significant damage to the matrix as a whole [112, p.256]. This means that an actual dispersion fuel would have to use a volume fraction less than 0.418, lowering the total weight of uranium and increasing the required burnup of the core.

4.8 Flux Spectrum

Many of the rules-of-thumb for light-water reactors are based on the assumption of a typical light-water reactor neutron flux spectrum. However, there is a reasonable expectation that the HEU core design used in this thesis will have a slightly different spectrum. The high enrichment of the uranium combined with the significant undermoderation of the core makes the reactor slightly faster than a typical LWR. The most significant result of this is its effect on xenon poisoning.

4.8.1 Thermal Spectrum Comparison

Figure 4.14 shows the flux spectrum of a normal LWR and the HEU core.[17] As shown in the figure, the HEU core has a faster spectrum than a commercial PWR. One useful measure of the spectrum is its fast-to-thermal flux ratio. For the commercial reactor, the ratio is 6.8. For the HEU reactor, the ratio is 8.5.

There will be a variety of small consequences due to the faster flux spectrum. First, the neutron damage of reactor materials will be different. Materials with larger fast-to-thermal cross section ratios will receive more damage, and vice-versa. This may affect the type of shielding used in naval reactors as opposed to commercial reactors. Additionally, the effects of Doppler broadening should be lessened, as the flux in the resonance region will be slightly more depressed, as shown in figure 4.14. Finally, moderator temperature and void coefficients of reactivity will be smaller (but still negative), as moderation is not as important for the HEU reactor to function as for a commercial reactor. Most of these effects should be relatively small, as the change in flux ratio is not very large.

[16] For a more in depth description of how dispersion fuels become damaged during burnup, see [44, p.69-71] or [112, p.256-259].

[17] The LWR spectrum is based on an infinite pin cell lattice using the Seabrook Station data contained in Appendix K of [34].

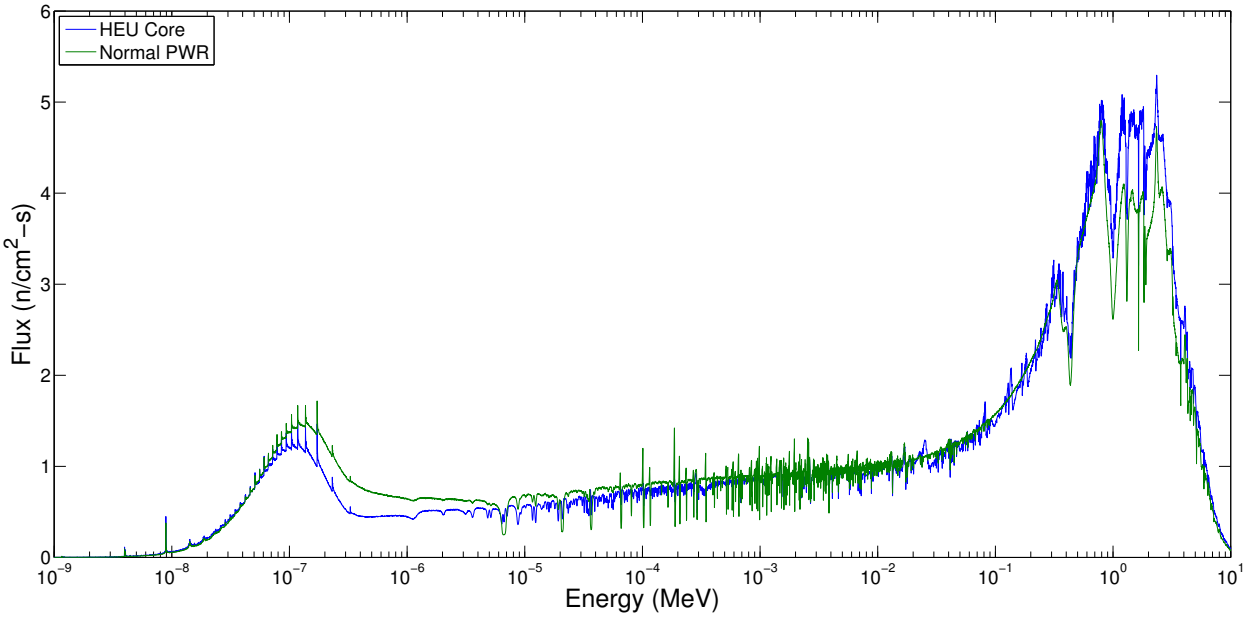

Figure 4.14. The typical PWR reactor has a larger thermal peak than the HEU core. The HEU core has a correspondingly higher fast peak than the PWR. The HEU core also has smaller resonance absorption drops due to ^{238}U than the normal PWR. The spikes in flux in the thermal range are due to the use of thermal scattering cross sections to replace low-energy free-gas elastic scattering reactions [104, p.12].

4.8.2 Xenon Poisoning Magnitude

One area where the flux spectrum causes a large effect is in the effect of ^{135}Xe as a neutron poison. Equation 2.9 shows the method of calculating xenon reactivity loss. The macroscopic cross sections of fission and absorption are reported directly by Serpent. Additionally, Serpent can report the ^{135}Xe microscopic absorption cross section. Using the constants in table 2.3, this fully defines the reactivity loss to xenon after shutdown. The results of this calculation are shown in figure 4.15.

As shown in figure 4.15, ^{135}Xe does not appear to cause a substantial negative reactivity peak in an HEU naval reactor the way it does in a commercial reactor. While the commercial model reports a ^{135}Xe spectrum-weighted microscopic absorption cross section of 5.5×10^4 b, the HEU core's spectrum-weighted absorption cross section is 1.5×10^3 b.[18]

4.9 LEU in UO_2-Zr Fuel

For completeness, a lifetime simulation of LEU in the dispersion HEU fuel design was run. The weight percentages of different isotopes are shown in table 4.7. As shown in figure 4.10,

[18]The commercial model value is from the same simulation as that used for the flux spectrum figures.

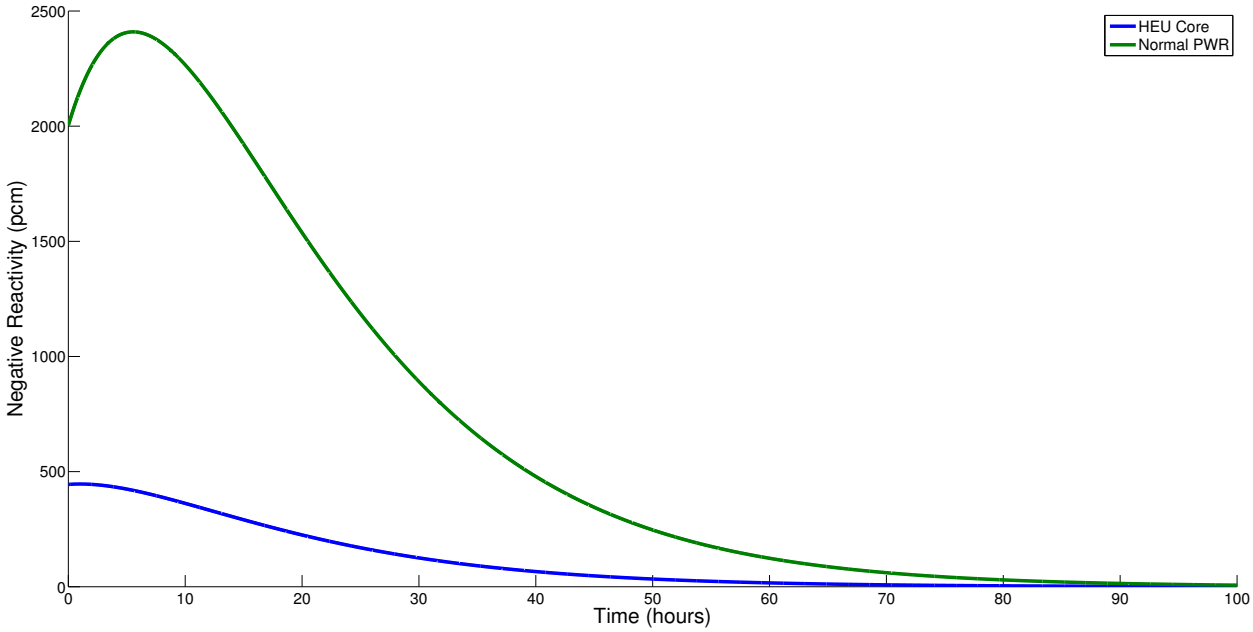

Figure 4.15. Because of the harder spectrum, ^{135}Xe has a smaller reactivity effect than normally found in a PWR.

Table 4.7. LEU Dispersion Fuel Weight Percentages

	^{16}O	Zr	^{234}U	^{235}U	^{238}U
HEU Dispersion	6.56%	45.2%	0.356%	44.8%	3.02%
LEU Dispersion[1]	6.56%	45.2%	0.260%	9.64%	38.3%

[1] The LEU dispersion fuel uses 20% enriched uranium.

the LEU UO_2-Zr fuel does not come close to meeting the 333 MWd/kg limit required for a lifetime core. k_{eff} drops below one around 125 MWd/kg, showing that the fuel would require at least two refuelings in order to reach the lifetime of the submarine. This reflects the results found in the 1995 study by Naval Reactors. The Naval Reactors followed this same method of replacing the HEU in the core with LEU, at the same core geometry and uranium density [6, p.8]. The fact that Naval Reactors concluded there would need to be three refuelings instead of two could be due to the fact that this thesis did not include reactor internals and limitations imposed by battleshock constraints, which are expected to lower the possible energy output of the core for the same size.[19]

[19]By using space in the core for other materials, the total amount of uranium in the core is lowered. If the same burnup is achieved, this leads to less total energy being pulled from the core before each refueling.

Chapter 5

Low Enriched Uranium Core

This chapter presents the results of the LEU core simulation using the U-10Mo fuel. Additionally, it discusses unexpected results of general interest. The first six sections follow the outline of chapter 3: the core's temperature profile and thermal properties, moderator-to-fuel ratio selection, coolant pressure drop estimate, Monte Carlo parameters, burnable-poison loading, and full burnup results. Section 5.7 discusses fabrication issues with the U-10Mo fuel. Section 5.8 discusses the reactor's flux spectrum and associated consequences. Table 5.1 and figure 5.1 show a short summary of the final geometry of the LEU core. The geometry of the LEU core was the same as that of the HEU core, for reasons that will be discussed in section 5.2. This led to the pressure-drop calculation being the same for both the HEU and LEU cores, as discussed in section 5.3.

Like the results of chapter 4, several thermal limits were violated over the course of the reactor's life, as shown in table 5.2. This was again due to the insufficiency of gadolinium alone as a reactivity control mechanism. Further research could focus on creating a more detailed design, which could meet thermal-hydraulic, material, and reactivity margins at all points in the burnup cycle.

5.1 Fuel Temperature and Thermal Margins

The first step of the simulation was determining the average fuel temperature of the reactor. The results of this analysis are shown in table 5.2, and are calculated using the final, poisoned, LEU core.[1] The LEU core was found to have an average fuel temperature of 382°C, with a

[1]Table 5.2 breaks the thermal results into three sections. In the first section, the temperature is reported using the average power density of the core. In the second section, the power peaking factor at beginning of core life is multiplied by the average power density, and temperatures are recalculated. In the third section, the maximum peaking factor from the depletion cycle is used.

Table 5.1. LEU Core Geometry

Fuel Plate Length	4.49 cm
Fuel Plate Width	0.25 cm
Fuel Plate Height	100 cm
Cladding Width	0.04 cm
Fuel Assembly Length / Width	5.3 cm
Core Radius[1]	55 cm
Core Height	100 cm
Uranium Weight	2,450 kg
Required Burnup	93.5 MWd/kg

[1] The core radius is equivalent to the inner radius of the core barrel or outer radius of the core shroud.

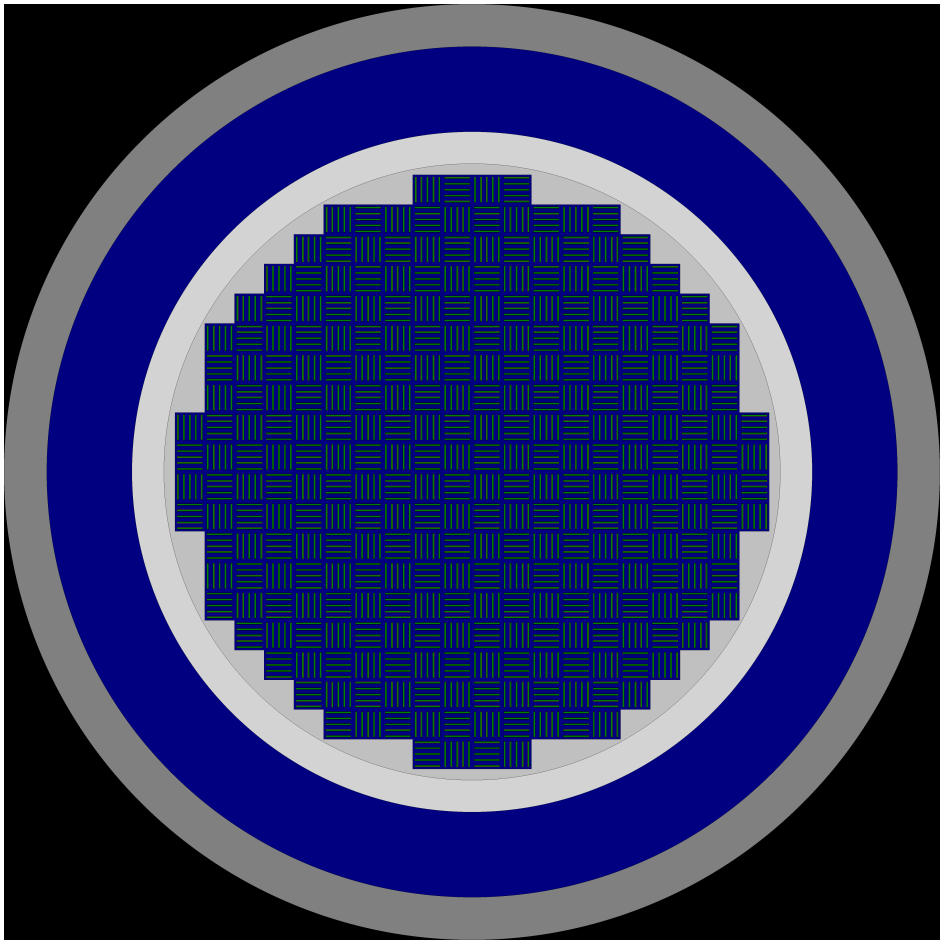

Figure 5.1. This is the final version of the LEU fueled reactor. The detailed measurements of the geometry are shown in table 5.1.

peak average centerline temperature of 423°C 3.2 cm above the center of the core. With the beginning of cycle peaking factor accounted for, the maximum temperature of the fuel rises to 439°C. With the largest power peaking factor over the life of the reactor accounted for, the maximum temperature of the fuel is 483°C. The previous chapter includes methods for increasing margin on fuel melting, departure form nucleate boiling, and cladding temperature limits. All of these are within the margins set in section 2.1. However, the cladding and MDNBR limits were violated by the end-of-life power peaking factor, which might be addressed with more sophisticated power flattening.[2]

5.1.1 Fuel Melting and Blistering Margin

The LEU core easily meets the 300°C margin to fuel melting. Section 2.6 set the estimate of the melting point of the fuel at 1150°C, determined by the uranium-molybdenum phase diagram. In order to come within 300°C of this measurement, an assembly power peaking factor of 4.2 would be required, compared to the beginning of cycle peaking factor of 1.11 and a maximum cycle peaking factor of 1.43. The fuel melting margin is easily met when using thin fuel plates. With thicker fuel plates, fuel melting would be a more sensitive margin. Figure 5.2(b) shows the fuel centerline temperature in the average fuel plate as a function of z; this plot does not reflect the peak radial power peaking, but shows that the fuel is closest to melting at the axial center of the plate, indicating that the use of axial burnable poisons could help in obtaining even more margin. The LEU fuel also meets all fuel blistering margins set in section 2.1.7.

5.1.2 DNB Margin

Section 2.1.8 set the minimum value of 1.3 for MDNBR. The LEU core meets this condition in the average assembly (MDNBR of 1.84), as well as under the power peaking factor at the beginning of the core's life (MDNBR of 1.62). However, once the gadolinium poison runs out the power peaking factor increases dramatically. This causes the DNB margin to be violated (MDNBR of 1.13). This indicates that the burnable poison loading of the reactor is very important to maintain thermal margins. Additionally, it indicates that it may not be possible to thicken the fuel plates much, as this increases the heat flux through the plates. There are two other ways to increase the DNB heat flux: first, by increasing the mass flow rate of the coolant; second, through the addition of turbulence enhancing structures.

[2]A detailed, full-core design would address these concerns. However, for this thesis they were not fully explored.

Table 5.2. LEU Core Thermal Properties

Power Density[1]	0.058 kW/g-U
Power Density[2]	0.891 kW/cm^3
Average Cladding Temperature	344°C
Maximum Outer Cladding Temperature	353°C
Outer Fuel Temperature	383°C
Average Fuel Temperature	373°C
Maximum Fuel Temperature	423°C
MDNBR	1.84
Recalculation using Beginning of Cycle Peaking Factor[3]	
Corewide Power Peaking Factor	1.10522
Average Cladding Temperature	350°C
Maximum Outer Cladding Temperature	359°C
Outer Fuel Temperature	393°C
Average Fuel Temperature	382°C
Maximum Fuel Temperature	439°C
Coolant Exit Temperature	312°C
MDNBR	1.62
Recalculation using Maximum Peaking Factor[4]	
Corewide Power Peaking Factor	1.42874
Average Cladding Temperature	367°C (350°C limit)
Maximum Outer Cladding Temperature	380°C (375°C limit)
Outer Fuel Temperature	423°C
Average Fuel Temperature	408°C
Maximum Fuel Temperature	483°C
Coolant Exit Temperature	318°C
MDNBR	1.13 (1.3 limit)

[1] The power density in kW per gram of uranium is used as the normalization factor for Serpent simulations.

[2] The power density in kW per cm^3 is used in the temperature calculations described in section 3.2.

[3] The beginning of cycle power peaking factor. This value was calculated using Serpent, and is discussed in section 5.5.

[4] The largest power peaking factor over the life of the reactor. This value was calculated using Serpent, and is discussed in section 5.6.2.

5.1.3 Cladding Margins

Like the DNB margin, the cladding temperature margins are met at the beginning of the core's life and at all times for the average assembly. However, they are violated towards the end of the core's life when the power peaking factor increases due to burnable poison depletion. The methods described in the previous section for helping with the DNB margin would also assist with the cladding temperature margins. This reinforces the importance of both burnable poison loading (to keep power peaking low), and thermal margins. The results of the cladding temperature calculations are shown in table 5.2.

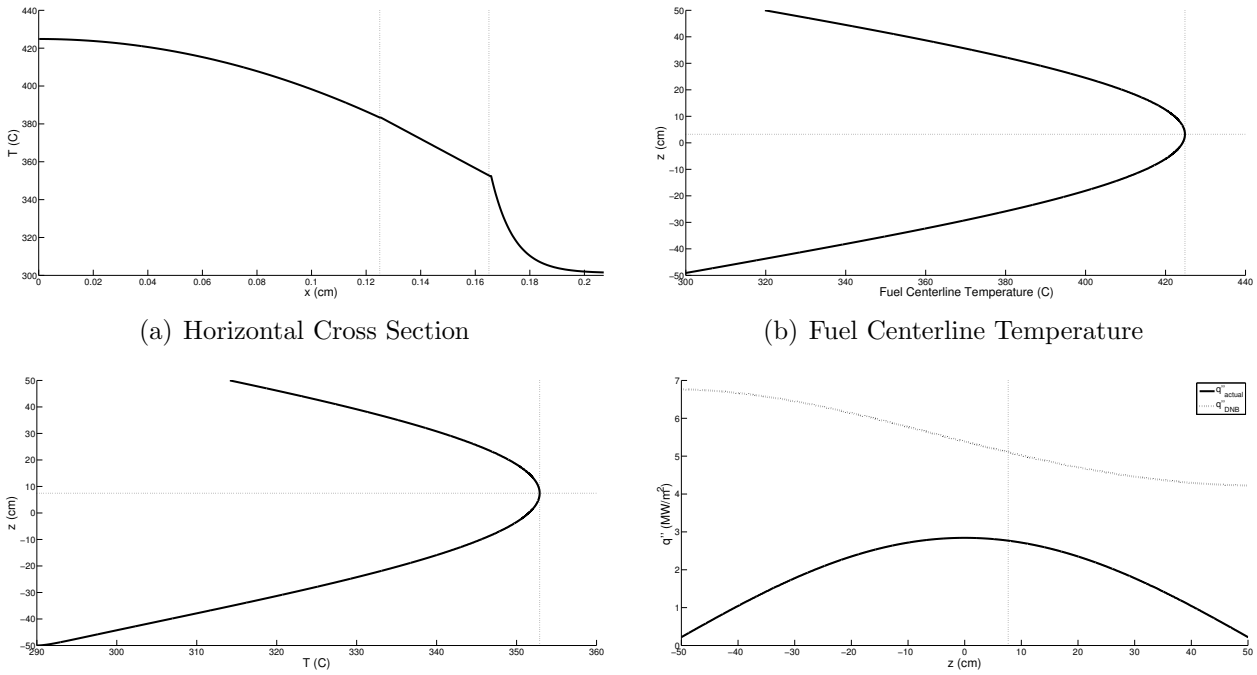

(a) Horizontal Cross Section

(b) Fuel Centerline Temperature

(c) Outer Cladding Temperature

(d) DNB Margin

Figure 5.2. Subfigure (a) shows the temperature profile of the fuel, cladding, and coolant at the point of maximum centerline fuel temperature. Subfigure (b) shows the centerline fuel temperature as a fucntion of z. Subfigure (c) shows the outer cladding temperature as a function of z. Finally, subfigure (d) shows the heat flux profile and critical heat flux profile as a function of z. The fuel power density is that of the average fuel assembly, and not of that of either beginning or end of life peak assembly.

5.2 Moderator-to-Fuel Ratio

The process of determining the moderator-to-fuel ratio and pitch is the same as that followed in the previous chapter. The LEU core also used assemblies of five plates in a pattern

of alternating orientations, as shown in figure 5.1. Therefore, figure 4.3 shows the same infinite plate fuel assembly that is used for optimizing the plate-to-plate pitch. The results of the infinite plate simulations are shown in figure 5.3. Each fuel assembly was burned to 125 MWd/kg, past the 100 MWd/kg limit discussed in section 2.6.1. The results reveal several trends. First, unlike the HEU core, the rate-change in k_{inf} with burnup seems to be independent of the pitch. Secondly, the reactivity gains due to increased moderation are more significant than in the HEU core. The slopes of the moderator-to-fuel ratio versus reactivity curves are much steeper in the LEU case, showing that moderation is more important with a lower ^{235}U enrichment. Finally, the graph shows that reactivity is less in the LEU case than the HEU case. Most of the cases have a k_{inf} of around 1.25 at 90 MWd/kg of burnup (around where the lifetime requirement is for the full core). This is lower than HEU core average of about 1.45 or higher at 330 MWd/kg (the HEU core lifetime requirement). Reactivity will be further reduced once the core is built and poisons added.

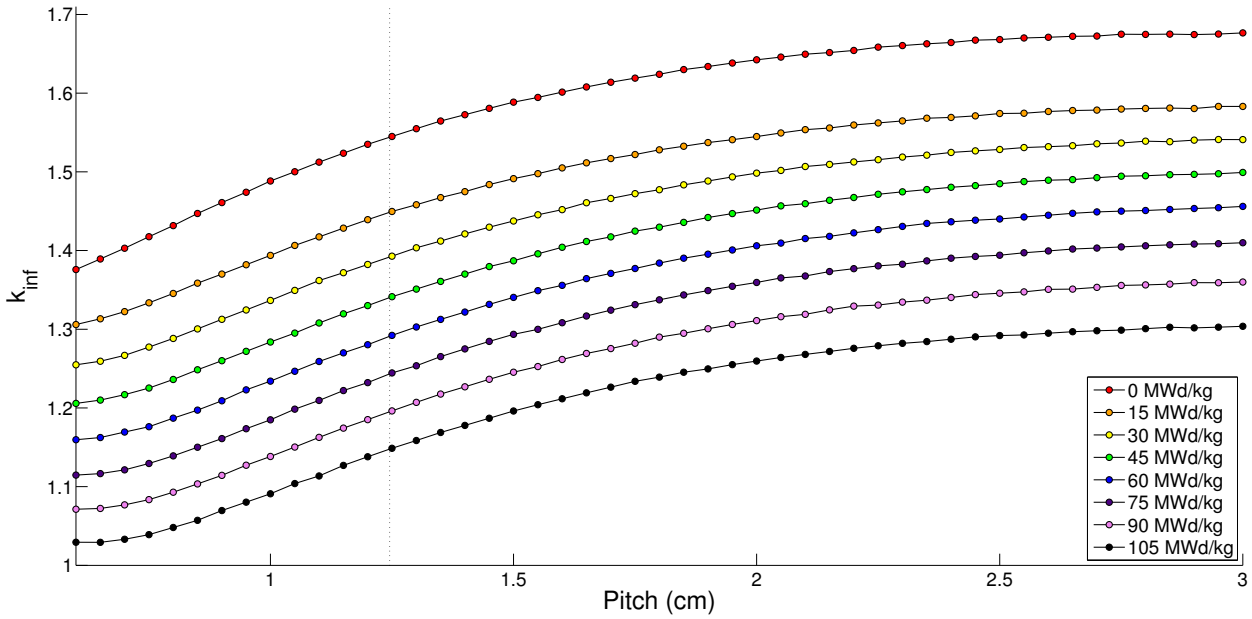

Figure 5.3. This figure shows the effect of pitch on k_{inf} throughout the burnup of the LEU fuel. Pitch is used as a stand-in for the moderator-to-fuel-ratio. Each simulation is a five plate fuel assembly, as shown in figure 4.3, and simulates 20,000 neutrons for each of 50 active cycles with 50 inactive preceding cycles. Each measurement is accompanied by an average error of 0.00035, or 3.5 pcm, with a maximum error of 0.00069, or 6.9 pcm. The line at 1.245 cm represents the final pitch chosen for use in the full reactor model.

The final value of the plate-to-plate pitch was chosen to be the same as that used for the HEU core.[3] The pitch of the infinite plates was 1.245 cm, leading to a finite length fuel

[3]This was chosen in order to maximize the amount of fuel within the core to lower required burnup.

plate with a pitch of 1.06 cm.[4] This pitch was chosen in order to maximize the fuel within the core. This lowers the average burnup required of the core, which is important for two reasons. First, the physical burnup limit of the U-10Mo fuel is low compared to the UO_2-Zr fuel used in the HEU core. This means that maximizing the fuel in the core to decrease required burnup is more important. Secondly, the reactivity limit of 1.04 is met sooner in the LEU core than the HEU core. While the HEU core never approaches a reactivity limit, the LEU core is right at the edge of being reactivity limited instead of burnup limited.

5.3 Primary Loop Pressure Drop

Because the geometry of both the HEU and LEU cores are the same, the pressure drop is identical for the two simulations. Therefore, the results in table 4.3 apply to the LEU core as well. The other results discussed in section 4.3 also apply.

5.4 Shannon Entropy / Neutrons per Cycle

The first step to estimating the neutronic aspects of the core is to determine the run parameters of Serpent. Figure 5.4 shows the results of testing a number of active and inactive cycles, as well as different neutron populations per cycle, as was shown for the HEU core in section 4.4. The convergence patterns are the same as those shown for the HEU case, so the LEU core will use the same parameters as the HEU core, shown in figure 5.5, of two million neutrons per cycle, 15 active cycles, and 15 inactive cycles. This led to an average error of less than 10 pcm in k_{eff}.

5.5 Burnable Poison Loading

The power distribution of the unpoisoned core is shown in table 5.3 and figure 5.6. These show the same pattern seen in the HEU core, with a Bessel-shaped distribution. Because of this, the core was broken into the same number and shape of gadolinium loading zones as shown in figure 4.8. However, the LEU core had significantly less excess reactivity to start with than the HEU core. This meant that the gadolinium poison loading had to be kept lower than that used in the HEU case.

The atomic densities of the elements and isotopes contained within the fuel are shown in table 5.4. Gadolinium was added to the different zones in a Bessel pattern.[5] This was then

[4]The results in fuel plates that are 4.49 cm long and fuel assemblies that are 5.3 cm square.

[5]As discussed in section 3.6.4, it is not possible to mix gadolinium into a monolithic fuel. However, for

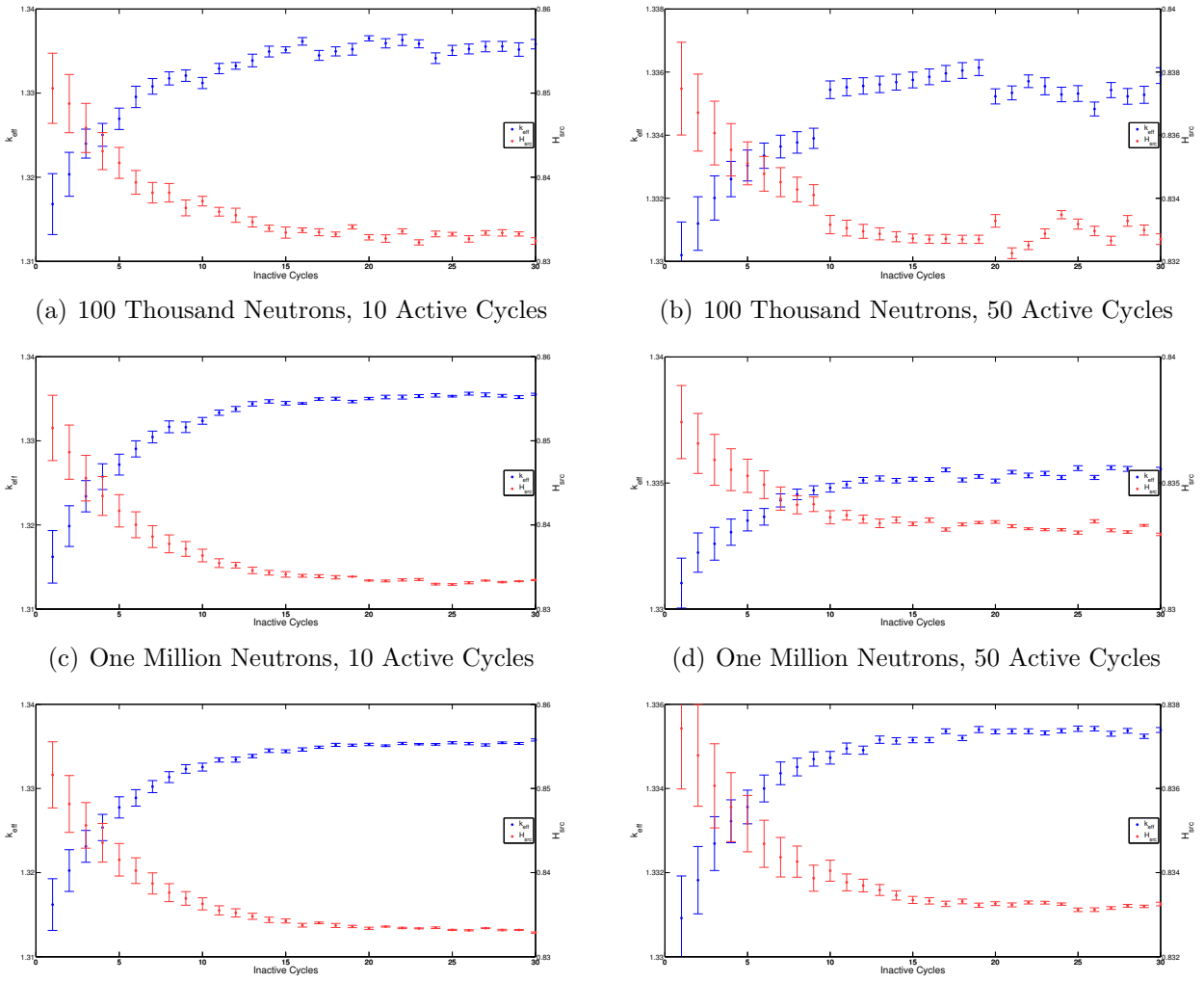

(a) 100 Thousand Neutrons, 10 Active Cycles

(b) 100 Thousand Neutrons, 50 Active Cycles

(c) One Million Neutrons, 10 Active Cycles

(d) One Million Neutrons, 50 Active Cycles

(e) Two Million Neutrons, 10 Active Cycles

(f) Two Million Neutrons, 50 Active Cycles

Figure 5.4. Subfigures (a) and (b) use one-hundred thousand neutrons per cycle. Subfigures (c) and (d) use one million neutrons per cycle. Subfigures (e) and (f) use two million neutrons per cycle. The subfigures on the left use 10 active cycles of neutrons, while those on the right use 50 active cycles. Together, these plots show the impact of an increasing number of active cycles, as well as an increasing neutron population.

refined to flatten the power density as much as possible. In the end, the gadolinium loading shown in table 5.5 was obtained. This led to the power distribution shown in figure 5.7 for the first burnup step in the core's lifetime. This distribution had a maximum power peaking value of 1.105, slightly higher than the 1.1 target. However, this was mainly an artifact of the way the power distribution was calculated. When the location with the peaking factor of 1.105 was averaged with its rotationally symmetric partners, the average power peaking

the purposes of this thesis, mixing gadolinium into the fuel will be used as a proxy for an actual burnable poison distribution within the core.

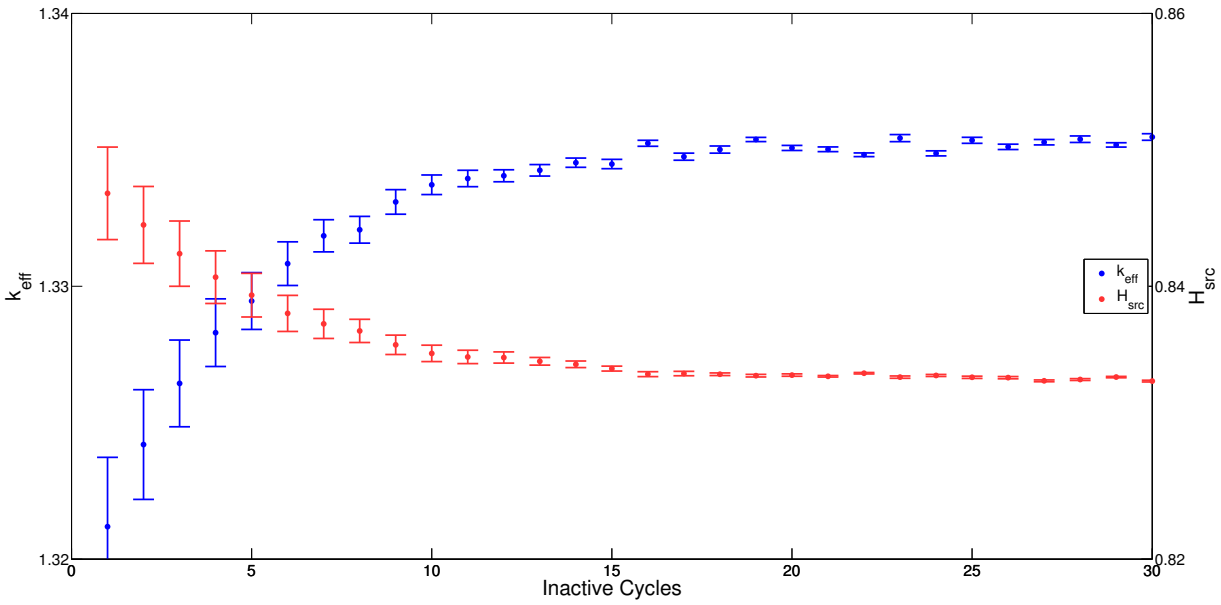

Figure 5.5. Above is the final convergence pattern for the neutron population parameters used for the LEU core. There are two million neutrons per cycle, and 15 active cycles.

factor was 1.095. Therefore, the 1.105 value was judged acceptable, as all of the reactor's thermal margins were met, and the average of the peaking factor in theoretically identical locations was less than 1.1.

5.6 Full Core Run and Results

With all of the parameters for the burnup simulation determined, the LEU core was depleted in Serpent. Though the target for the simulation was 93.5 MWd/kg (based on the energy requirement in equation 2.6), the core was burned to 120 MWd/kg in order to see the effects slightly past the end of the reactor's lifetime. This also serves to determine k_{eff} if the value in equation 2.6 were an underestimation. The results of the simulation are shown in figure 5.8.

5.6.1 Excess Reactivity

As shown in figure 5.8, the LEU core falls just short of the Ippolito limit of 1.04 for k_{eff} at the required burnup, which was judged to be conservative. This indicates two things. First, that maintaining excess reactivity is a much larger challenge in an LEU core than for an HEU core. Second, that an LEU core could potentially meet reactivity requirements if the fuel is qualified for a high enough burnup. While this model just missed the require value of k_{eff}, the unpoisoned core was able to meet the standard. Therefore, by slightly lowering the

Table 5.3. LEU Power Distribution, No Burnable Poisons[1]

0.493	0.456								
0.686	0.660	0.604	0.545	0.453					
0.864	0.843	0.796	0.725	0.638	0.507				
1.044	1.017	0.965	0.889	0.795	0.678	0.528			
1.208	1.181	1.123	1.041	0.936	0.814	0.678	0.509		
1.354	1.325	1.263	1.177	1.065	0.936	0.789	0.637	0.452	
1.477	1.444	1.387	1.296	1.177	1.035	0.885	0.722	0.539	
1.569	1.534	1.471	1.382	1.264	1.117	0.962	0.792	0.606	
1.635	1.603	1.538	1.444	1.322	1.177	1.015	0.839	0.662	0.452
1.670	1.638	1.569	1.474	1.350	1.203	1.039	0.864	0.684	0.490

[1] This table shows the power peaking factor of each assembly. Each value is an average of the position indicated and its three rotationally symmetric partners in the core.

Table 5.4. LEU Fuel Atomic Densities

Element	Weight Percent	Atomic Density[1]
Mo	10.0%	1.07×10^{-2} (barn-cm)$^{-1}$
^{234}U	0.486%	2.13×10^{-4} (barn-cm)$^{-1}$
^{235}U	18.0%	7.84×10^{-3} (barn-cm)$^{-1}$
^{238}U	71.5%	3.07×10^{-2} (barn-cm)$^{-1}$

[1] Atomic densities are given in (barn-cm)$^{-1}$, the unit used by Serpent.

[2] Atomic densities are calculated using equation 4.1, the weight fractions from table 2.9, and isotope and elemental molar masses from [77, p.138,142].

Table 5.5. LEU Gadolinium Loading

	Gadolinium Atomic Density
Zone 1	5.2453×10^{-4} (barn-cm)$^{-1}$
Zone 2	5.0404×10^{-4} (barn-cm)$^{-1}$
Zone 3	4.9284×10^{-4} (barn-cm)$^{-1}$
Zone 4	4.5291×10^{-4} (barn-cm)$^{-1}$
Zone 5	3.9309×10^{-4} (barn-cm)$^{-1}$
Zone 6	3.1809×10^{-4} (barn-cm)$^{-1}$
Zone 7	2.2654×10^{-4} (barn-cm)$^{-1}$
Zone 8	7.1564×10^{-5} (barn-cm)$^{-1}$

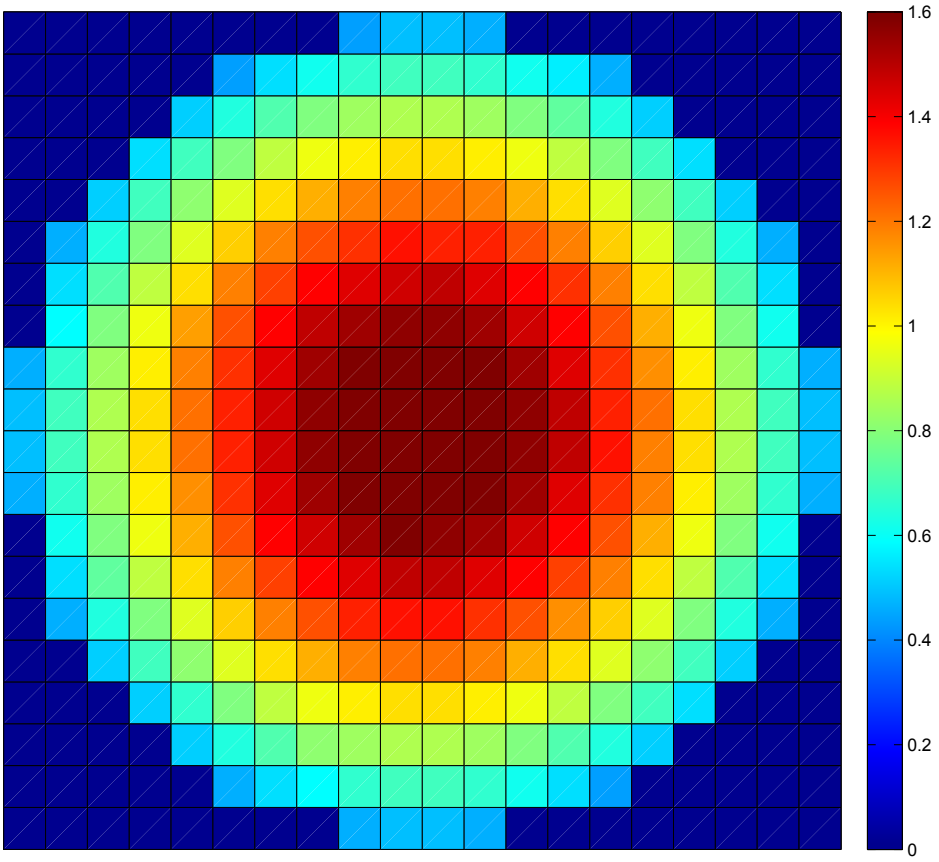

Figure 5.6. Above shows the power distribution of the HEU core at the first burnup step of the simulation without gadolinium.

burnable poison loading at the beginning of the reactor's life, the reactivity margin could be met.

5.6.2 Power Distribution

As seen in table 5.2, the LEU core violated several thermal margins at the end of core life. Once the gadolinium burnable poison had mostly burned off, the core power distribution reverted back to a similar pattern to the unpoisoned one, as shown in figure 5.9. This indicates that a more complicated burnable poison loading is required for the core in order to ensure that power peaking factors stay low for the reactor over its life.

5.7 Fuel Fabrication

There has not been a great deal of experience with the creation of monolithic fuels. To date, fabrication efforts have focused on monolithic fuel foils about 0.04 cm thick and 1.2 m long

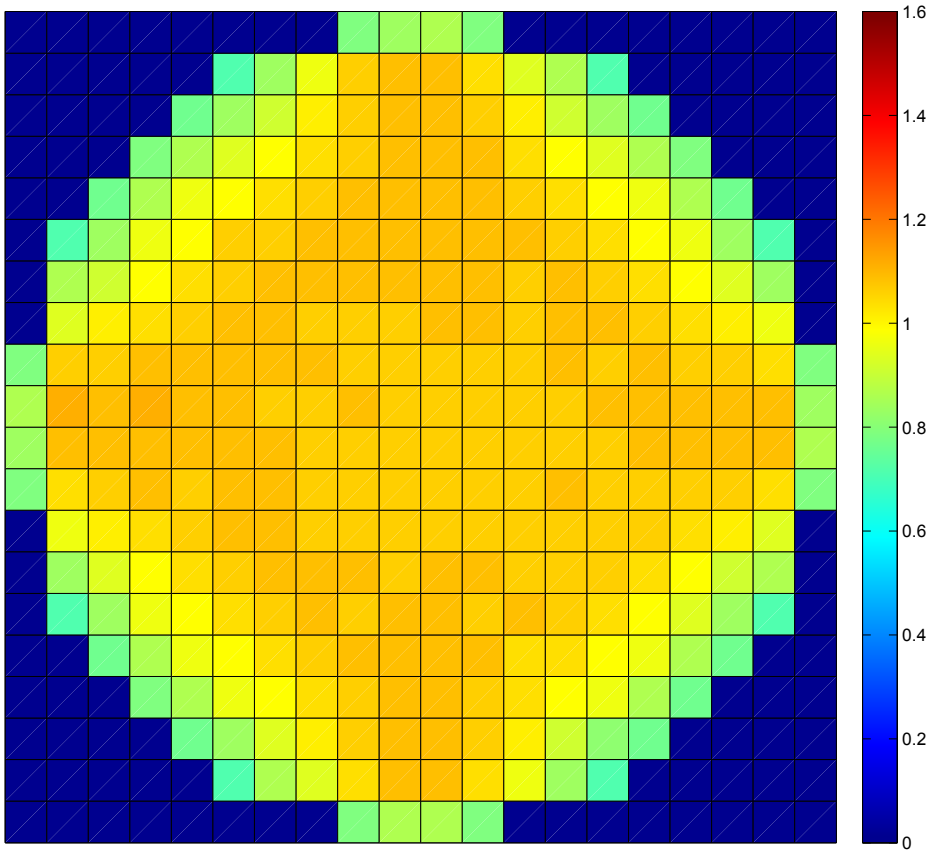

Figure 5.7. Above shows the power distribution of the poisoned HEU core at the first burnup step, 0 MWd/kg, of the simulation.

[86, p.8]. The thicknesses currently under study range from 0.01 to 0.05 cm [86, p.8]. All of these foils are much thinner than the 0.25 cm assumed in this thesis. However, fabrication methods are continually improving and a focus on thicker plates by the Department of Naval Reactors might overcome existing limitations [86, p.1].

5.8 Flux Spectrum

It is important to analyze the flux spectrum of the LEU core for two reasons. First, if the spectrum is radically different from that of a commercial PWR, different limits on the materials used in the core may have to be enforced. Secondly, the precise flux spectrum has a large impact on how ^{135}Xe behaves once the reactor is shut down. This section analyzes both of these effects.

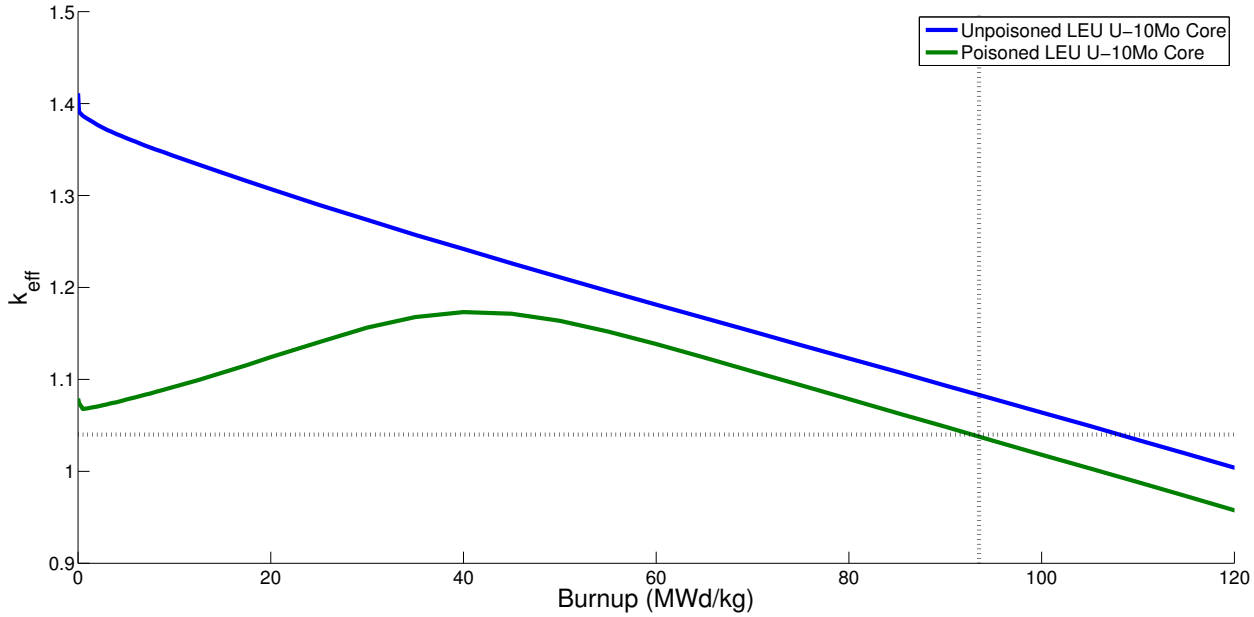

Figure 5.8. This figure shows k_{eff} vs burnup for two cases. The first is the unpoisoned LEU core, while the second is the poisoned LEU core. The vertical line shows the required burnup limit. The horizontal line shows the Ippolito reactivity limit of 1.04.

5.8.1 Thermal Spectrum Comparison

Figure 5.10 shows a comparison between the flux spectrum of a commercial PWR and that of the LEU core. As seen, the LEU core has a slightly depressed thermal peak compared to the commercial PWR, and a slightly higher flux at higher energies. This shows that the naval reactor model has a slightly faster spectrum than a commercial reactor, but not by much. While the commercial PWR had a fast to thermal flux ratio of 6.8, the LEU core had a ratio of 7.7.[6] This ratio difference was judged to be small, as commercial LWRs are typically have a fast to thermal flux ratio of five to ten [52]. Therefore, the materials used in naval reactors face a similar flux spectrum as those in commercial reactors.

5.8.2 Xenon Poisoning Magnitude

While the difference in fast to thermal flux ratio is generally small, it has a significant effect on the behavior of ^{135}Xe after the reactor shuts down. Using equation 2.9 to calculate the poisoning effect of ^{135}Xe gives results shown in figure 5.11. The LEU core spectrum-weighted absorption cross section is 5.3×10^3 b, which is higher than the HEU value of 1.5×10^3 b, but still an order of magnitude lower than the commercial PWR value of 5.5×10^4 b. Combined

[6]Serpent reports a one group flux estimation, as well as a two group estimation. By dividing the fast neutron flux by the thermal flux, an estimation of how fast the reactor operates can be obtained.

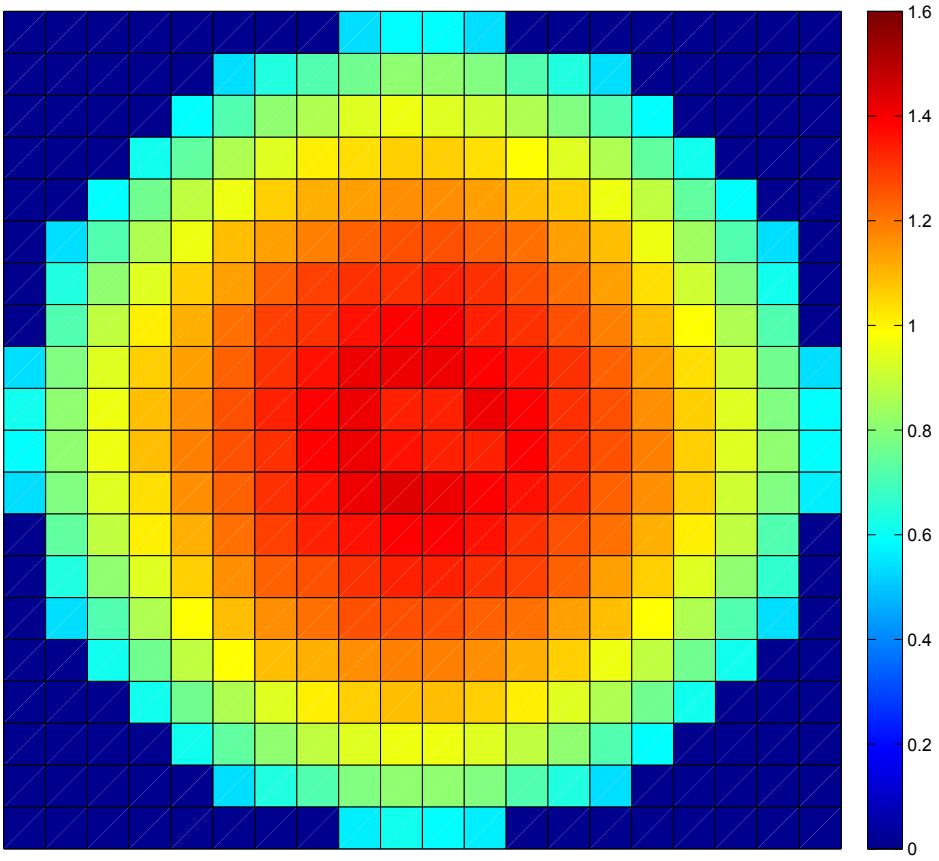

Figure 5.9. Above shows the power distribution of the poisoned LEU core 50 MWd/kg into the burnup cycle. At this point, the maximum power peaking factor reaches 1.43, the highest of any point in the cycle.

with the results from figure 4.15, this indicates that naval reactors designed to use space for fuel while sacrificing moderation can avoid significant problems with xenon poisoning after shutdown. Neither case had a significant increase in negative reactivity after shutdown, or the "xenon pit" behavior shown in figure 2.2(a).

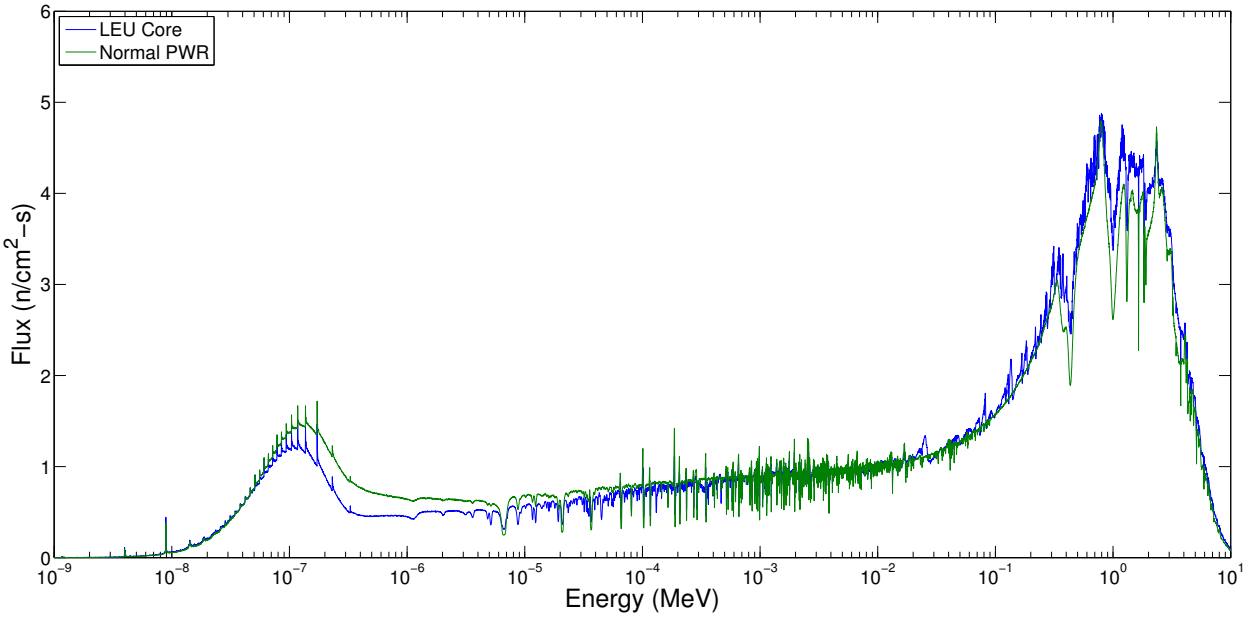

Figure 5.10. The typical PWR reactor has a larger thermal peak than the LEU core. The LEU core has a correspondingly higher fast peak than the PWR. The spikes in flux in the thermal range are due to the use of thermal scattering cross sections to replace low-energy free-gas elastic scattering reactions [104, p.12].

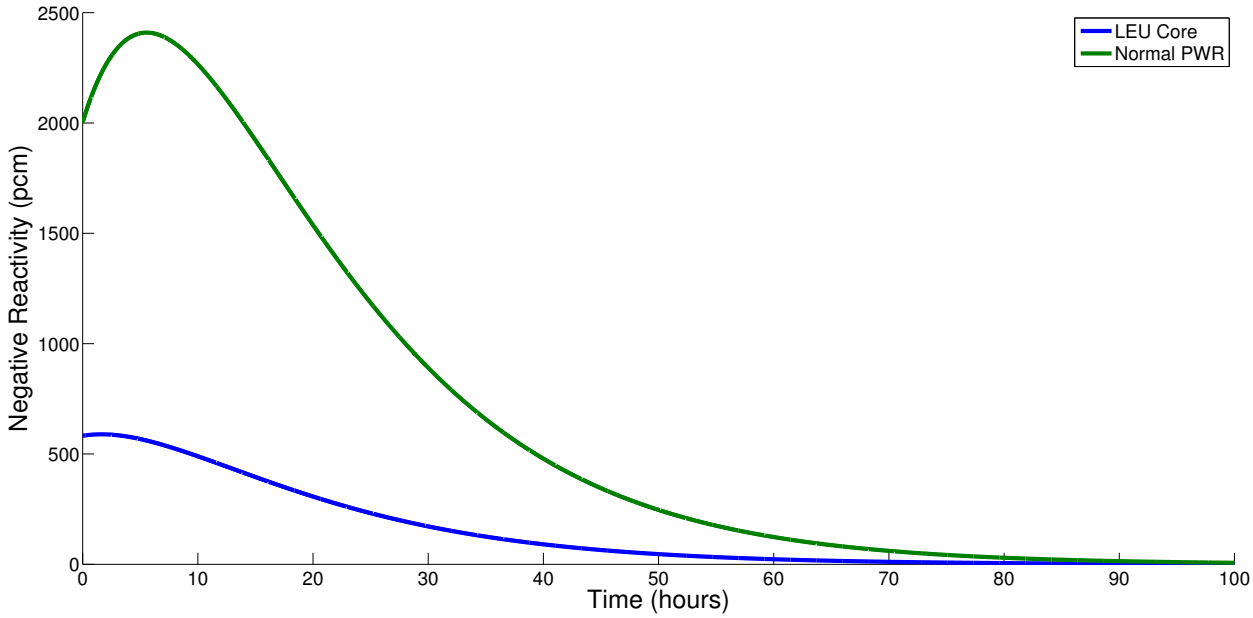

Figure 5.11. Because of the harder spectrum, ^{135}Xe has a smaller reactivity effect than normally found in a PWR.

Chapter 6

LEU Impact

This chapter analyzes the impact of using an LEU core on U.S. submarine availability and fleet size. The previous chapter found that LEU might be able to provide a life-of-the-ship core. If LEU were able to provide a lifetime core, then there would be no impact on current size or fleet availability. However, because of modeling limitations, a single refueling may still be required, resulting in a decrease in fleet availability. Furthermore, refueling affects shipyard radiation and nuclear waste. In this chapter, a refueling timetable is determined and the implications of refueling on fleet size and availability discussed.

6.1 Reasons Refueling may be Required

Though the LEU simulations suggest that a lifetime core is plausible, there are a few reasons that it might not be possible. First, U-10Mo might be unable meet the physical burnup required for a lifetime core. Secondly, there is uncertainty in the reactivity corresponding to end of core life. Finally, the core may not be able to contain as much uranium as the simulation.[1]

Physical Burnup

Some studies of U-10Mo irradiation resistance indicate that the fuel swells at roughly the same rate as dispersion fuels [84, p.7].[2] This would indicate that U-10Mo LEU fuel could go to burnups similar to that of dispersion fuels.[3] Other studies of uranium molybdenum alloys

[1] If the weight of uranium in the core is decreased, then a higher average burnup would be necessary.

[2] This theory is based on measuring burnup in fissions/cm^3. The caption of figure 2.14 explains what these measurements mean in MWd/kg.

[3] Figure 2.14 is measured in fissions per cm^3, so, due to the difference in uranium density, the burnup in MWd/kg for a monolithic fuel would be about a quarter that of a dispersion fuel.

test burnups up as high as 200 MWd/kg [88, p.3]. However, none of these studies indicate when swelling becomes unsustainable. The department of Naval Reactors surely has a series of standards for what swelling is allowable. Without knowing this, it is difficult to estimate the maximum burnup allowed.

Reactivity

There is additional uncertainty in the reactivity cutoff requirement for naval reactors. In the Ippolito study, a k_{eff} value of 1.04 was used to indicate end of life due to xenon poisoning [44, p.81]. Other studies have indicated that naval reactors must be required to overcome a reactivity drop of ρ = -0.5, or a minimum k_{eff} value of 2.1 [22, p.51][59, p.21]. However, this study found that the excess reactivity required of naval reactors may be significantly lower than either of the published estimates, as shown in section 5.8. Uncertainty in reactivity cutoff is another reason that an LEU-fueled core may not be able to meet life-of-the-ship requirements.

Uranium Loading

Finally, the simulation completed for this thesis was close to a best-case scenario from a uranium loading perspective. First, U-10Mo provides the highest possible uranium density of a practical nuclear fuel. Secondly, the simulation contains no structural materials, no space for control rods, no dedicated burnable poison elements, and expands the diameter of the core 10% beyond what is estimated to be the size of a naval reactor.[4] Once all of the additional parts of a reactor are included, the total amount of uranium will drop, increasing the required burnup of the fuel.

Though these uncertainties cast doubt on a life-of-the-ship LEU core, the prospects for a single refueling over the 33-year life of an attack submarine are good. With the required burnup halved by the refueling, physical burnup limitations become much easier to meet, and the reactivity required should exceed even conservative estimates. The remaining analysis in this chapter assumes that the use of LEU requires a single refueling in a submarine.

6.2 Refueling Strategies and Timeline

There are two methods used for naval nuclear refueling. The first, more traditional method, is the reason many have resisted refueling. The pressure hull of the submarine is cut to

[4]Naval reactors are generally believed to cylinders with a height and diameter of about 1 m.

access the reactor compartment, and the ship is put back together at the end of the shipyard overhaul. In the second method, a specially built hatch is installed over the core, allowing for a refueling similar to that of a commercial reactor. Each refueling method has advantages and disadvantages.

6.2.1 Traditional Refueling

Traditionally, nuclear submarines have been refueled during a long shipyard overhaul. The outer and pressure hulls are cut through to reveal the reactor. Then, the reactor is disassembled (similar to a commercial reactor), so that the fuel can be reached. Once it is replaced, the ship is rebuilt [20, p.93]. This is a complex and time consuming process, and was part of the impetus for moving from the two-year core of the USS *Nautilus* (SSN-571) to the lifetime cores of the Virginia class [6, p.3]. In estimating the effect of a single refueling on future attack submarine fleet size, it is necessary to estimate the time a refueling takes. This was done by analyzing records from the Los Angeles class submarines.

The Los Angeles class is generally divided into two groups. The first group comprises hull numbers 688 through 718 (USS *Los Angeles* through USS *Honolulu*). These are referred to as "688" submarines, after the lead ship in the class. Hull numbers 751 through 773 (USS *San Juan* through USS *Cheyenne*) are referred to as the "Improved Los Angeles class," or "688i" submarines. Hull numbers 719 through 725 and 750 (USS *Providence* through USS *Newport News*) are known as the "Flight II" Los Angeles class, and have characteristics of both the 688s and 688is. The 688is incorporated a number of major design changes to make them quieter and more heavily armed, as well as advanced electronics and sensors [113]. More importantly, while the 688s required an "engineered refueling overhaul" roughly one-third of the way through their life, the 688is only had an "engineered overhaul," without a refueling [114]. By comparing the length of these two types of overhauls, an estimate of the time needed for refueling a nuclear submarine can be determined.

The USS *Los Angeles* (SSN-688) completed the first refueling overhaul of the class in 1995 after 31 months in drydock [113].[5] The USS *Philadelphia* (SSN-690) completed its own engineered refueling overhaul in December 1994 after entering drydock in October 1992, a 26 month overhaul [117, p.2][118, p.2]. With lessons learned from the initial submarines, the average engineered refueling overhaul was 24 months by the completion of the program [114]. The 688is engineered overhauls were much shorter. USS *Pittsburgh* (SSN-720) began a 16-month engineered overhaul in April 2005 [119].[6] USS *San Juan* (SSN-751) completed

[5]This is confirmed by Command History Reports, which show the *Los Angeles* entering drydock in September, 1992 and completing post-overhaul sea trials in March, 1995 [115, p.4][116, p.3].

[6]The *Pittsburgh* is one of the Flight II Los Angeles class submarines. Judging from its history, it has the

a 16-month engineered overhaul between April 2010 and August 2011 [120][121]. The USS *Miami* (SSN-755) was undergoing a 20-month engineered overhaul when it was damaged by arson [122].[7] Based on these data, the average length of an engineered overhaul is 18 months.

No two submarine overhauls are the same. However, the 62 boat Los Angeles class provides the largest sample size of comparable overhauls in the U.S. fleet. The comparison of 24 months for an engineered-refueling overhaul in contrast to an 18-month engineered overhaul indicates that, as long as the boat is already scheduled for an extended drydock period, refueling should only add about six months of unavailability. This is lower than that indicated by Naval Reactor's 1995 report to Congress. In the report, it was stated that three refuelings would add two and a half years of unavailability to a submarine's lifetime, or ten months per refueling [6, p.22].[8] Therefore, for this thesis, it will be assumed that a refueling takes between six and ten months long, provided it is being done concurrently with other overhaul work.

6.2.2 Hatch

When France designed the Rubis class submarine, it included a specially designed reactor access hatch [20, p.93]. Refueling of the submarine took five months when the class was new, and was reduced to three months once shipyard "lessons learned" were applied [20, p.100]. The hatch was included partially due to the submarine's use of LEU in its fuel. This led to the submarine having a seven-year core lifetime [124]. The replacement for the Rubis class, the Barracuda class, includes fuel advancements that increase the refueling interval to ten years [124]. However, the hatch comprises a permanent cut in the submarine's pressure hull. This causes a decrease in the submarine's "crush depth," reducing the depth at which the submarine would be allowed to operate [22, p.86]. While a hatch could be incorporated into US submarines, this thesis will focus on more traditional refueling methods that do not require compromising performance characteristics. If LEU can be shown to be usable without a decrease in submarine performance, it would be much easier to convince the Navy to switch to LEU.

---

overhaul pattern of a 688i.

[7] On May 23, 2012 a civilian worker set fire to the submarine to get out of work early. Twelve hours later, the resulting blaze was finally extinguished. Estimated costs of repair rose from $450 to $700 million before the project was canceled in light of sequestration [123]. The *Miami* was decommissioned and disposed of in 2014.

[8] Part of this disparity may come from the fact that the report assumes that the HEU fueled submarine would only have two major overhaul periods [6, p.21]. It can be fairly assumed that completing a refueling during a major overhaul would take less time, as other repairs could coincide with reactor work.

6.3 Fleet Size Requirements and Availability

One of the most important questions about the use of LEU is how it will affect the required submarine fleet size and individual submarine availability. This section addresses two related topics. First, it analyzes the requirements and availability of the current submarine fleet. This will be used as a baseline for comparison. The second subsection addresses how the fleet size and availability would change if a single refueling were required.

6.3.1 Lifetime Core Force Requirements

The Navy currently estimates that a minimum of 48 attack submarines is required to meet the day-to-day peacetime requirements of the United States [125, p.10]. This estimate represents a decrease from a requirement of 62 attack submarines in 1997 [125, p.15].[9] Some, including retired Vice Admiral Albert Konetzni Jr. (former US Pacific Fleet submarine force commander), have argued that the Navy's SSN force-level analysis reflects "reverse engineering," where the force-level is set based on affordability reasons and then assumptions in studies are created to produce the figure [126, p.CRS-25].

The Navy requirements go on to say that the fleet has a day-to-day requirement of ten deployed submarines, and 35 submarines capable of being deployed at any time (known as the "wartime surge" requirement). This implies that total submarine availability is roughly 0.73.

$$\text{Availability} = 0.73 = \frac{35}{48} \tag{6.1}$$

The fleet availability can be used to determine how many years of an individual submarine's life is spent in major maintenance periods.[10]

$$1 - 0.73 = \frac{\text{Maintenance}}{33 \text{ years}} \tag{6.2}$$

$$\text{Maintenance} = 8.9 \text{ years}$$

This seems to be significantly longer than the maintenance patterns of the USS *Virginia* (SSN-774). The boat went in for its first major overhaul on September 1, 2010, and was redelivered to the Navy on May 5, 2012 [127]. This gives a maintenance time of 20 months. When that time period is applied to the four expected major maintenance periods of the Virginia class, the total maintenance time is 6.7 years [128].[11] This indicates that the Navy has

[9] The 1999 Joint Chiefs of Staff review of the 1997 Quadrennial Defense Review estimated that the Navy would require 55 submarines in 2015 and 62 in 2025 [125, p.15].

[10] This analysis will use the 33 year expected lifetime of the Virginia class as a basis.

[11] This pattern for the Virginia class throws further doubt on the fleet size estimates produced by Naval

significantly invested in methods to decrease selective availability periods for submarines.[12] Continued investment is indicated by plans for the Block IV Virginia submarines, which are expected to require only three major maintenance periods. This would give the Virginia class an availability of 0.80 for Blocks I-III, and 0.85 for Block IV.[13]

Unfortunately, there is a great deal of uncertainty about the future operations of the Virginia class. While availabilities of 0.80 and 0.85 would greatly assist with the Navy's predicted submarine shortfall between 2025 and 2041, the Navy has yet to prove this schedule possible [125, p.9]. Therefore, for this analysis, the lower value of 0.73 will be assumed.

6.3.2 Traditional Refueling Force Size

A single refueling would add six to ten months to the major maintenance period closest to the middle of the submarine's life. This would mean that the total maintenance time over the submarines life would increase to between 9.4 and 9.7 years. This would give a new fleet-wide availability of between 0.70 and 0.72.

$$\text{Availability} = 1 - \frac{[9.4 \text{ to } 9.7 \text{ years}]}{33 \text{ years}} \tag{6.3}$$

$$\text{Availability} = 0.706 \text{ to } 0.715$$

One way to use this new availability would be to recalculate the required submarine fleet size. Using the low estimate of 0.70, this would give a new fleet size of 50 submarines.[14] However, due to the constantly changing fleet-size requirements, it is probably more useful to compare the two availability factors. This shows that requiring a single refueling would require an increase in fleet size of 3.5% over current estimates.[15]

In the current era of budget cuts and sequestration, arguing for an increase in shipbuilding budget would be difficult [123]. However, a conversion of the nuclear fleet to LEU is a major strategic decision. The project requires millions in fuel development alone [7, p.5]. This would have to be accompanied by investments in uranium enrichment capabilities.

Reactors' 1995 report. The report not only indicated that three refuelings would be required, but that future attack submarines would only require two major maintenance periods [6, p.21].

[12]The Navy uses the phrase "selective availability" to refer to shipyard periods when ships are unavailable.

[13]This is also consistent with estimates based on the *Virginia's* actual schedule. The *Virginia* was commissioned on October 23, 2004, began major maintenance on September 1, 2010, and finished on May 5, 2012. This gives 70 months of operation and 20 months of maintenance in one full cycle. With four full cycles, and an additional 70 months of operation after the last yard work before decommissioning, the submarine would have 350 months of operation out of 430 months in service. This gives an availability of 0.81.

[14]Calculated by taking the wartime surge requirement of 35 and dividing by the availability of 0.70.

[15]Calculated by dividing the current availability (0.729) by the lowest estimate of the new availability (0.706). This gives a worst possible case of fleet size increase of 3.28%.

Additionally, the actual construction of submarines would not have to begin until at least 2032 [129, p.11]. The long timeline of this project means that there would be ample time for the Navy to build a small, 3% increase for shipbuilding into their budgets.[16] Additionally, the arguments for nonproliferation should be helpful in convincing Congress to release slightly more money.

A 3.5% increase is also small compared to the typical cost overrun for a Navy program. A study has shown that Navy programs typically run between 16–17% over the life of the program [130, p.9]. Additionally, the current Virginia program has shown that economies of scale can lead to savings of over 30% per boat once about 20 boats have been completed.[17] While preventing an additional increase in cost would be desirable for the Navy, it is small compared to existing cost variation.

6.4 Shipyard Radiation and Waste Impact

Two of the secondary concerns cited by Naval Reactors in their 1995 report to Congress are that the use of LEU would increase the radiation exposure of shipyard workers and increase the amount of nuclear waste generated. However, these concerns are very clearly of secondary importance to the Navy.

First, refueling has been required in every class of nuclear ship in the Navy other than the Virginia class submarines.[18] This indicates that while the Navy would prefer not to have to refuel their submarines, they are fully capable and willing to accept a certain amount of radiation exposure if it is required to service their vessels.

The 1995 report from Naval Reactors attempts to estimate the dose from refueling an LEU SSN fleet, and compare it to that of an HEU SSN fleet. Table 6.1 shows these estimates, as well as new estimates for a single refueling. The single refueling estimate attempts to determine how much of the Navy's estimate was due to refueling as opposed to decommissioning, as the operations are slightly different. In the end, this was done by using the "HEU Baseline" case as representative of the defueling process, and dividing the rest of the rem in the "Existing Design Ships" category equally between the three refuelings. This leads to an estimate of 123 average annual man-rem for the single LEU refueling.

[16] Additionally, this value is smaller than the 1995 Naval Reactor report estimated. That report indicated that an 8% increase in attack submarine fleet size would be required [6, p.22].

[17] USS *North Dakota* (SSN-784), the first block III Virginia class, came in at a cost of $2.6 billion [128]. The 10 submarine block IV contract was awarded to General Dynamics Electric Boat in April 2014 for 17.8 billion [128]. This represents a savings of $820 million per submarine, or about 30% of the total original cost.

[18] Some sources say that the improved Los Angeles class (688i) submarines do not require refueling either [114].

Table 6.1. Refueling Radiation Exposure[1]

	HEU Baseline	LEU in Existing Design Ships[2]	One Refueling[3]
SSN	60	249	123[4]
SSBN	21	93	-
CVN	63	198	-
Total	144	540	-

[1] This table is adapted from Table 6 in [6, p.17]. All values are in annual average man-rem.

[2] The "Existing Ship Design" estimate is based on 3 refuelings for an SSN, 3 refuelings for an SSBN, and 2 refuelings for a CVN, along with radiation due to decomissioning.

[3] The "One Refueling" option is only calculated for the SSN case, as the refueling patterns of SSBNs and CVNs are beyond the scope of this thesis.

[4] This value is equal to (249-60)/3 + 60. This attempts to maintain the radiation exposure during decommissioning and that due to refueling as separate entities.

The report also claims that the high neutron radiation emitted from spent LEU fuel would require expensive and complex neutron shielding and dosimetry that are currently not required in shipyard operations [6, p.18]. As shown in figure 6.1, decay activity is clearly dominated by fission products for the first few hundred years after reactor shutdown. Therefore, the increased radiation requirements are likely due solely to an increase in neutron generation from fissile and fertile isotopes due to spontaneous and background fission. A full analysis of fuel would require the determination of activities of all the transuranics possible, along with their spontaneous fission rates. As HEU is composed of mostly ^{235}U and LEU is composed mostly of ^{238}U, it is credible that LEU will have a much higher neutron activity.

This is not an unmanageable amount of radiation. The NRC proscribes that radiation workers be kept below 5 rem per year [132, p.8-3]. As long as the number of workers is more than 30, the yearly dose due to refueling runs little risk of putting workers over radiation limits. While the Navy's commitment to ALARA (As Low As Reasonably Achievable) radiation limits is commendable, it should not be an exclusive driver of ship construction policy.

The 1995 report also went into detail discussing the waste impact of LEU fuels. While a single refueling still increases the amount of waste that is required to be processed, the situation is much less dire than the 1995 report makes it seem. Additionally, the report makes much of having to renegotiate the current agreement on nuclear waste with the state

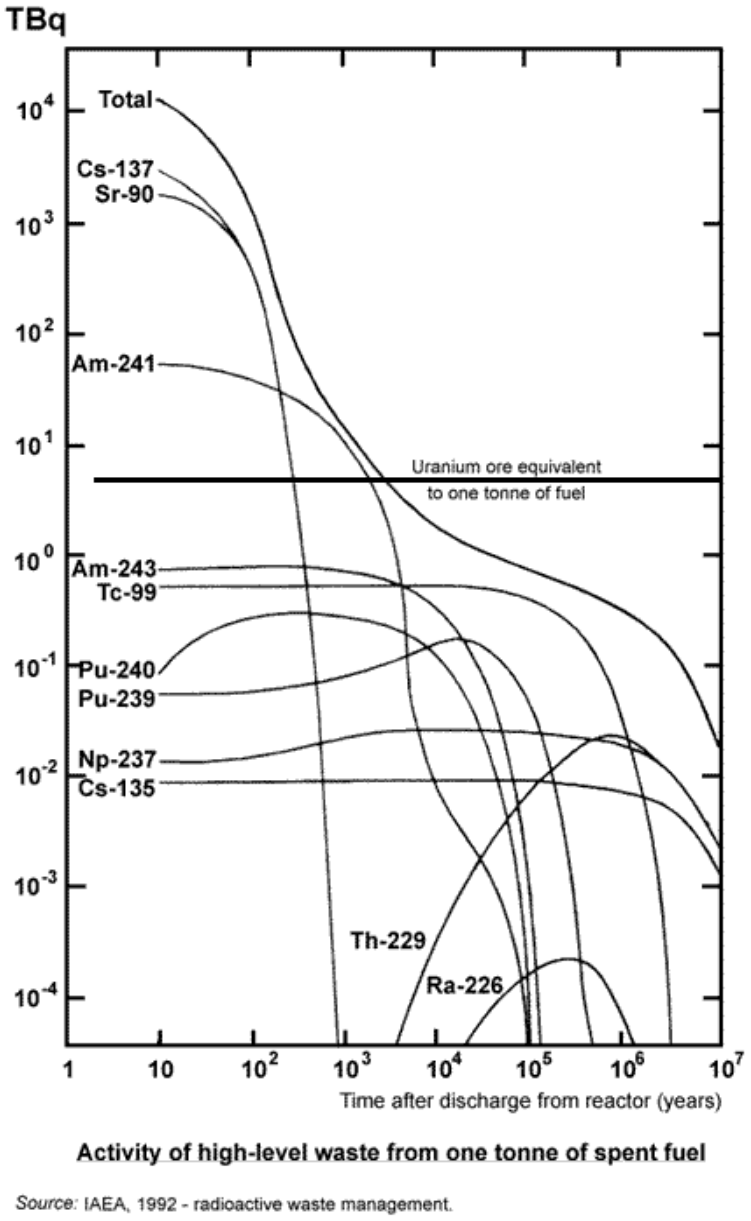

Figure 6.1. This figure is taken from [131]. It shows the activity of the most important radioisotopes in spent nuclear fuel. While the activity of the fuel is not equal to the dose received by workers, it can be used as a weak proxy in the absence of detailed information about naval reactor shielding.

of Idaho [6, p.16]. The agreement in question already requires renegotiation, as it currently states that all nuclear waste be removed from Idaho by 2035 [37, p.2]. There is currently no progress on removing waste, as the national repository at Yucca Mountain has been canceled, and so renegotiation seems to be necessary anyway. The long time line for adopting LEU fuel (following the retirement of the first Virginia class submarines after 2030) means that a federal waste repository may have been opened by then that could accept naval nuclear

waste.

Chapter 7

Conclusions

This thesis has shown that while LEU may not be usable in current naval fuel, the serious problems anticipated by Naval Reactors in their 1995 report could be avoided through the use of a new fuel material. While the U-10Mo fuel used in this thesis requires a significant experimental program to determine if it can reach the required burnup, the analytical results show that a single refueling core is almost certainly possible.

7.1 Key Findings

The primary difference between the results from the HEU and LEU cores is the amount of excess reactivity present at the end of the core's lifetime. The HEU core has about 30,000 pcm of excess reactivity present at the end of the burnup cycle. This indicates one of two possibilities. First, that the core simply operates in a manner in which no amount of xenon poisoning or reactivity limits are ever an issue. Second, that a smaller amount of uranium is used (lowering the oxide volume fraction in the fuel). This increases the required burnup of the core, decreasing end of life excess reactivity. This also lowers the initial excess reactivity, as there is less fissile material present in the core. Either way, excess reactivity is the norm in an HEU fueled reactor, regardless of lifetime. However, the LEU core faces reactivity challenges near the end of core life. The model used here falls about 250 pcm short of meeting the minimum k_{eff} requirement of 1.04 at the end of core life. This factor would only become worse as the amount of fissile material in the core is decreased to account for structural materials in the core. Therefore, if an LEU fueled reactor is capable of providing a lifetime core; it would do so by coming close to reactivity margins at the end of the core's life.

This leads to the main conclusion of the thesis: while a lifetime core may be possible using an LEU fuel, it is likely that a submarine would require a single refueling during its

midlife overhaul. This would simplify the design of the core and improve margins against a lifetime core. However, this refueling would require less time than estimates in the 1995 report by Naval Reactors. Specifically, past history has shown that engineered refueling overhauls are only about six months longer than overhauls without refueling. Consequently, a submarine fleet requiring a single refueling would only have to be about 3.5% larger than a fleet with lifetime cores.

Additionally, naval reactors may have to use a slightly faster flux spectrum than commercial PWRs. Section 4.8 and section 5.8 show that if this is true, then xenon poisoning may not be as significant a factor as some studies of naval reactors have indicated. This would be useful, as it decreases the requirement for an end of life k_{eff}, as well as ensuring that the reactor can restart at any time.

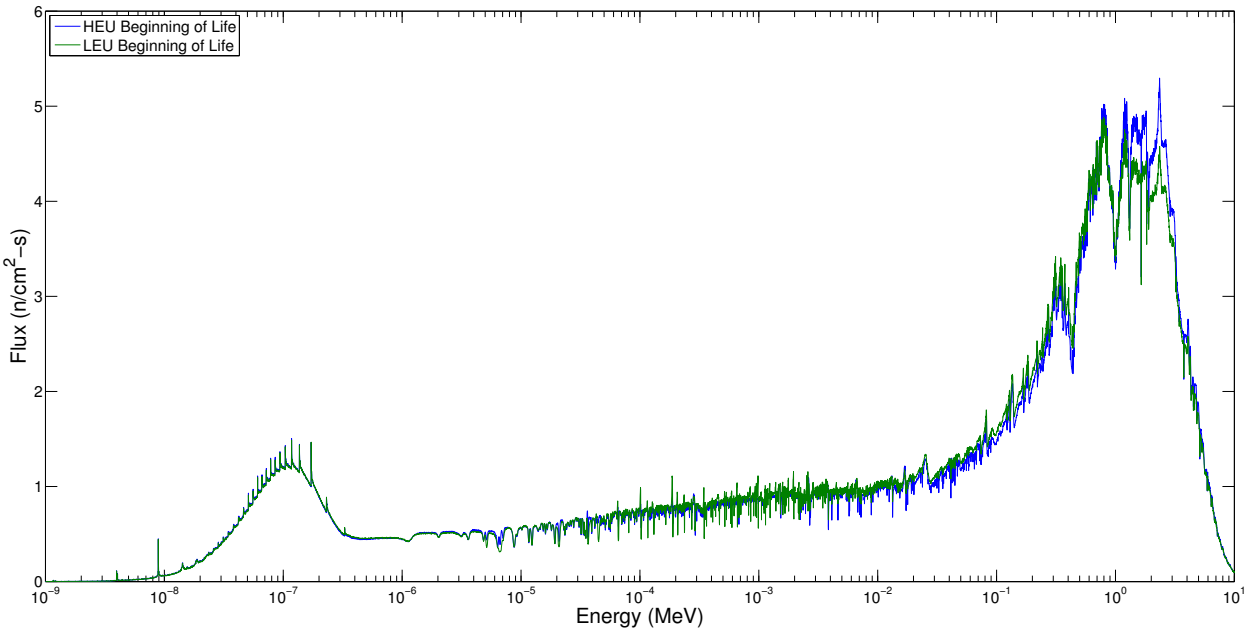

Figure 7.1. This plot shows the flux spectra of both the HEU and LEU cores at the beginning of core life.

Finally, comparing figures 7.1 and 7.2 shows that there is little difference in the flux spectra between the HEU and LEU fuels. This means that the materials in and surrounding the core should undergo neutron damage in similar ways if the fuel were shifted. This, however, does not address the concern expressed by Naval Reactors in their 1995 report that the use of LEU creates a much larger inventory of transuranic actinides in waste [6, p.17]. This seems to be a valid concern.

A program for developing an LEU fuel for the Navy's next attack submarine would have to begin within the next few years [129, p.12]. The first replacement SSN for the Virginia class will need to begin construction in 2032 in order to preserve fleet size [129, p.11]. Therefore,

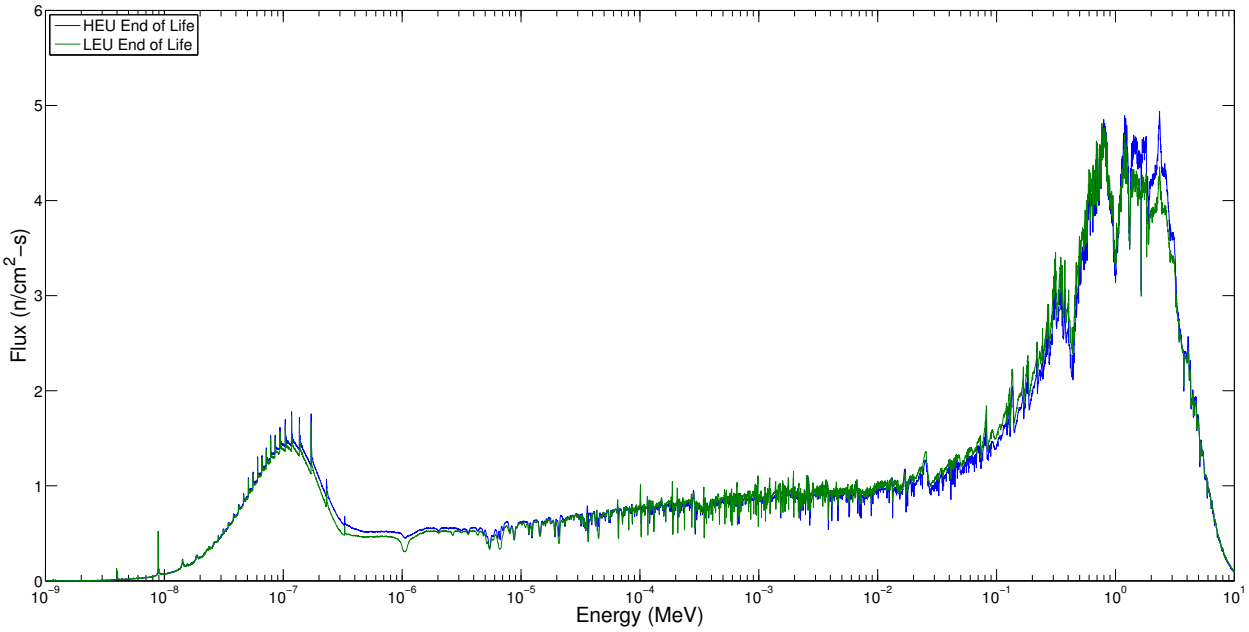

Figure 7.2. This plot shows the flux spectra of both the HEU and LEU cores at the end of core life. For the HEU core, this is the 333 MWd/kg plot, while for the LEU fuel it is 95 MWd/kg.

judging by Naval Reactors' own estimate of a 15-year design program for an LEU fuel, fuel testing would have to begin in fiscal year 2017 [7, p.5]. Initial lobbying and planning for the program would have to begin now in order to provide adequate time for qualification of a new fuel.

7.2 Uncertainty Issues

The high degree of classification and secrecy surrounding naval reactors makes many parameters of the core hard to estimate accurately. First of all, the composition of the fuel is kept highly classified [45, p.12-8]. This makes it difficult to estimate the parameters of current naval reactors. Lack of knowledge about the burnup required or achievable by naval reactors also makes it difficult to determine the mass of fissile materials within the core, the neutron flux, and the energy required from the core over the boat's lifetime. Core design and geometry is also highly classified, and restricts the accuracy of core estimates. The actual refueling process that would be used, if required, is classified, so the effects of refueling on fleet size are difficult to estimate [45, p.12-4]. Finally, there are a series of core requirements that are classified, which are highly influential on core design. This includes design requirements, such as the 50g battleshock condition, as well as lifetime requirements, such as uncertainty

about the end of life k_{eff} due to xenon poisoning.[1] These uncertainties limit the analysis that can be completed in unclassified studies.

7.3 Future Research Opportunities

There are a variety of places where the basic model used in this thesis can be improved. This section will describe a few of these methods, including adding structural components to the fuel, improving the correlations used throughout the model, and refining the estimation of the required lifetime of the core. Other methods could be used to extend core lifetime through a more complicated core design. This includes a higher degree of zoning throughout the core, or more complex materials used to provide structure to the reactor.

7.3.1 Missing Structural Components and Internals

The model used in this thesis was very basic. It modeled only the fuel, cladding, and coolant within the core, in addition to the core shroud, barrel, and pressure vessel. An improved model would incorporate the rest of the materials that make up the interior of a reactor core. First, there are the structural components that tie the core together. This could mean tie plates that connect the fuel plates directly, or a larger internal structure that connects the entire core together. Additionally, space would have to be made for control rods, and control rod reactivity worth would be simulated to ensure that the reactor could be shut down at any point. Finally, burnable poisons could be loaded in a more realistic manner. While gadolinium oxide can be mixed with uranium oxide in dispersion fuels, it cannot be mixed into monolithic metal fuels. Additionally, poisons must be managed in a way that ensures that the volume fraction of oxides within dispersion fuels, such as the UO_2-Zr HEU fuel used here, be kept low.

7.3.2 Improved Thermal-Hydraulic Correlations

A future model should use more appropriate thermal-hydraulic correlations. First, the pressure drop calculation could be significantly improved. The calculated friction factor was based on a single-phase correlation, which is inappropriate when sub-cooled nucleate boiling is present. The method of calculating the pressure drop of the primary loop was coarse. An improved estimate would model the piping and steam generator that are also part of the loop. Secondly, the heat transfer correlation could be improved. While it accounts for the

[1] While the battleshock condition (50gs of force) has been defined by Naval Reactors, the actual limits (maximum stress or strain, maximum warping of materials, etc.) have not been released.

lack of fully-developed flow, it is still a single-phase correlation, which does not account for sub-cooled nucleate boiling. As a consequence, many of the temperature calculations may be inaccurate.[2]

7.3.3 Improved Energy Requirement Estimation

The estimated energy required for a lifetime core can be improved with further research. The duty cycle estimation is the place where improvement is least likely. Open source, unclassified documentation does not seem to contain an accurate estimate of the average steaming power and speed of an attack submarine. However, the estimation of maximum power could be improved. Currently, it is based off of a scaling factor from the Seawolf and Los Angeles classes. A more accurate estimate would attempt to calculate the power required for maximum speed due to drag forces, and include an additional factor based on the hotel power of a submarine.[3] Additionally, the approximation of how long the boat spends at sea could be greatly improved. A factor of 0.5 was used in this thesis. However, by searching records of boat schedules from the Naval History and Heritage Command, a much more precise estimation of the average time spent at sea could be calculated.[4] This may be one of the most important areas for study, as the lifetime energy requirement determines the burnup required of the fuel.

7.3.4 Battleshock Requirement

The Navy has indicated that naval fuel must be capable of withstanding up to 50g ($\approx$ 500 m/s^2) of battleshock acceleration [22, p.14]. Little was done in this thesis beyond ensuring that the fuel was thicker than that proposed by Ippolito in his thesis [44, p.78]. Further studies must take this requirement into account, as it will have a large impact on the structural components used in the core, as well as the geometry in which they are arranged. A more accurate model would test the stress and strain applied to the core under large forces, and check for permanent deformation of the fuel. Damage limits would have to be set, and if they were exceeded then further strengthening of the fuel or its supports would have to be added.

[2]Subcooled boiling should increase the heat transfer coefficient beyond what is estimated by the single-phase correlation. This means that errors likely make the model more conservative, due to an overestimation of temperatures.

[3]This would be similar to the procedure used by Cameron McCord in his MIT thesis, but with the addition of a "required electrical power" term [22, p.76].

[4]The Command History Reports this refers to can be found at: `http://www.history.navy.mil/research/archives/command-operations-reports/ships.html`.

7.3.5 Fuel Material Selection

Further research should also focus on fuel qualification and testing. The U-10Mo fuel used in this thesis has not been qualified for use, nor has it been manufactured in plates as thick as those used here. There is a possibility that it might be unsuitable for use in a naval reactor. High-density, metal fuels are prone to swelling from both temperature and burnup. This may make U-10Mo unsuitable. Additionally, the melting point of U-10Mo is relatively low (1150°C), which may not provide enough margin during accident conditions. Future research should consider several of the other fuels described in figure 2.12 to determine which offers the best balance between burnup resistance and uranium loading.

7.3.6 Isotope Enrichment

The development of centrifuge and laser enrichment technologies provides significant opportunities for naval reactors. First, the burnable poisons used in reactors could be improved. Experiments have shown that boron can be enriched from 25% ^{10}B to 90% [133, p.154]. Furthermore, the odd isotopes that make gadolinium a useful poison (^{155}Gd and ^{157}Gd) naturally exist as 30% of the element, but can be enriched up to about 70% using current methods [134, p.344]. This would allow for the total weight and volume of burnable poisons in the core to be decreased. Secondly, enrichment technology could be used to enhance structural materials. Historically, nickel based super alloys under the Inconel and Hastelloy brands have suffered from significant helium embrittlement that precludes their use in some parts of the reactor [135, p.342]. This is due to the ^{58}Ni (n,γ) ^{59}Ni (n,p or n,α) chain that is favored at thermal energies [136, p.118]. It is possible that separating out ^{58}Ni could allow these alloys to be used as structural materials within the core, helping to achieve the battleshock requirement. This could also be used as the start of a more selective process for steel selection in the core, and to decrease parasitic absorption within the zircaloy cladding.

7.3.7 Optimization for Breeding

The long life of the core makes fissile isotope breeding an opportunity. This could be done in a few ways. One would be through enrichment zoning. By reducing the enrichment in some zones, the reactor could have preferential breeding in these areas. Additionally, the amount of moderation in different parts of the reactor could be varied by changing the plate-to-plate pitch in different areas of the core. Finally, breeding could be enhanced by mixing heavy water into the coolant. This would increase the conversion ratio across the entire core. Breeding could also be enhanced through the use of thorium in some areas of the core.

This would require a larger commitment to breeding within the reactor, while other methods would only require small modifications. However, breeding leads to higher power peaking factors within the core.[5] This would further lower MDNBR, which is already high due to the naturally high power density already used in naval reactors.

7.3.8 Improved Power Flattening

While this thesis made an effort to flatten the power distribution early in the core's life, the use of only gadolinium as a poison tended to be ineffective at the end of the core's life. Because gadolinium burns out fairly quickly, power distributions which, at first, were limited by a peaking factor of 1.1, increased to have peaking factors of 1.4 or greater. The peaking factor proved to be incredibly important, as the average power densities are already very large, and threaten thermal margins. Power peaking must be kept very low in naval reactors to ensure that thermal limits are met. Future work should focus on using a mix of burnable poisons that burn out at different rates to ensure that reactivity and power peaking are held down at all points through the reactor's lifetime. Additionally, while this thesis made an effort to flatten the radial power distribution in the core, it made no effort to work with the axial power distribution, which was left as a simple cosine shape. This results in an axial power peaking factor of about 1.57. Decreasing the power peaking factor over the life of the core would assist with margins to melting and departure from nucleate boiling and possible extend reactivity.

7.3.9 Cladding Thickness

The cladding thickness used in this thesis may be too low. While it is greater than that used by Ippolito, it is still lower than the average used in commercial reactors [44, p.78][75, p.1]. The long life of naval reactors may require a thicker cladding than this. Additionally, if naval reactors pulse their pumps to high power to clear crud from fuel plates then a thicker cladding may be required to continually renew the protective oxide layer [22, p.65]. Future studies could calculate the average cladding oxidation rate, as well as the maximum crud thickness that can be tolerated before an unacceptable increase in cladding temperature.

[5] Dedicating certain areas of the core to breeding lowers the power density early in the core's life, increasing the power required elsewhere. Once time has progressed and new fissile material has been bred, the power density in these areas increases to compensate for depleted zones.

Bibliography

[1] Robert Pool. *Beyond Engineering: How Society Shapes Technology*. Oxford University Press, 1997.

[2] George Schneiter. Comments from the Department of Defense to GAO draft report "Navy Aircraft Carriers: Cost-Effectiveness of Conventionally and Nuclear Powered Carriers", March 1996.

[3] International Panel on Fissile Materials. Global Fissile Material Report 2013: Increasing Transparency of Nuclear Warhead and Fissile Material Stocks as a Step toward Disarmament, October 2013.

[4] Eric Loewen. The USS Seawolf Sodium-Cooled Reactor Submarine. ANS Conference Address, May 2012.

[5] Richard Hewlett and Francis Duncan. *Nuclear Navy: 1946-1962*. University of Chicago Press, 1974.

[6] Director, Naval Nuclear Propulsion. Report on Use of Low Enriched Uranium in Naval Nuclear Propulsion, June 1995.

[7] Director, Naval Nuclear Propulsion. Report on Low Enriched Uranium for Naval Reactor Cores, January 2014.

[8] United States Government Accounting Office. Navy Aircraft Carriers: Cost-Effectiveness of Conventionally and Nuclear-Powered Carriers, August 1998.

[9] Frank Bowman. Statement of Admiral F.L. "Skip" Bowman, U.S. Navy, Director, Naval Nuclear Propulsion Program Before the House Committee on Science. Speech, October 2003.

[10] International Panel on Fissile Materials. Global Fissile Material Report 2008: Scope and Verification of a Fissile Material (Cutoff) Treaty, October 2008.

[11] James Clay Moltz. Closing the NPT Loophole on Exports of Naval Propulsion Reactors. *The Nonproliferation Review*, Fall 1998:108–114, 1998.

[12] Greg Thielmann and Serena Kelleher-Vergantini. The Naval Nuclear Reactor Threat to the NPT, July 2013.

[13] Greg Thielmann and Wyatt Hoffman. Submarine Nuclear Reactors: A Worsening Proliferation Challenge, July 2012.

[14] International Panel on Fissile Materials. Global Fissile Material Report 2006: Developing the Technical Basis for Policy Initiatives to Secure and Irreversibly Reduce Stocks of Nuclear Weapons and Fissile Materials, September 2006.

[15] Barack Obama. Remarks by President Barack Obama. Speech Hradcany Square, Prague, Czech Republic, April 2009.

[16] International Panel on Fissile Materials. Global Fissile Material Report 2010: Balancing the Books: Production and Stocks, December 2010.

[17] International Panel on Fissile Materials. Global Fissile Material Report 2007, October 2007.

[18] International Panel on Fissile Materials. Global Fissile Material Report 2009: A Path to Nuclear Disarmament, October 2008.

[19] International Panel on Fissile Materials. Global Fissile Material Report 2011: Nuclear Weapon and Fissile Material Stockpiles and Production, January 2012.

[20] Chunyan Ma and Frank von Hippel. Ending the Production of Highly Enriched Uranium for Naval Reactors. *The Nonproliferation Review*, Spring 2001:86–101, 2001.

[21] Deputy Chief of Naval Operations (Integration of Capabilities and Resources) (N8). Report to Congress on the Annual Long-Range Plan for Construction of Naval Vessels for FY2014, May 2013.

[22] Cameron McCord. Examination of the Conversion of the U.S. Submarine Fleet from Highly Enriched Uranium to Low Enriched Uranium. Masters thesis, Massachusetts Institute of Technology, May 2014.

[23] Brendan McGarry. Navy to Begin 8-month Carrier Deployments. *Military.com News*, 24 Jan 2014:1, January 2014. URL `http://www.military.com/daily-news/2014/01/24/navy-to-begin-8-month-carrier-deployments.html`.

[24] Thomas J. Moore. Q&A: Rear Admiral Thomas J. Moore. Interview, Aug 2013.

[25] Ronald O'Rourke. Navy Ford (CVN-78) Class Aircraft Carrier Program: Background and Issues for Congress, April 2014.

[26] United States Department of Defense. Navy to Christen Aircraft Carrier Gerald R. Ford. Press Release, November 2013.

[27] Ronald O'Rourke. Navy Trident Submarine Conversion (SSGN) Program: Background and Issues for Congress, May 2008.

[28] Matthew Wald. Company Struggles to Keep U.S. in the Uranium Enrichment Game. *New York Times*, 28 January 2014:B1, 2014.

[29] Participating Governments. Agreement between the Government of the United States of America and the Four Governments of the French Republic, the United Kingdom of Great Britain and Northern Ireland, the Kingdom of the Netherlands, and the Federal Republic of Germany regarding the Establishment, Construction and Operation of Uranium Enrichment Installations using Gas Centrifuge Technology in the United States of America, February 2011.

[30] R. Scott Kemp. Gas Centrifuge Theory and Development: A Review of U.S. Programs. *Science and Global Security*, 17:1–19, 2009.

[31] R. Scott Kemp. Centrifuges: A new era for nuclear proliferation. *Nonproliferation Policy Education Center*, -:1–32, 2012.

[32] The White House. National Security Strategy, May 2010.

[33] United States Department of Defense. Quadrennial Defense Review 2014, March 2014.

[34] Neil E. Todreas and Mujid S Kazimi. *Nuclear Systems Volume I: Thermal Hydraulic Fundamentals, Second Edition*. CRC Press, 2011.

[35] Oregon Department of Energy. Naval Nuclear Reactor Compartment Shipments on the Columbia River, September 2013.

[36] Paul Menser. Site of Impact: Clearning house and charting a future at INL. *Post Register*, January 27, 2008:1–5, January 2008.

[37] State of Idaho, US Department of Energy, and Department of the Navy. 1995 Settlement Agreement, 1995.

[38] U.S. Nuclear Regulatory Commission. Nuclear Regulatory Legislation: 112th Congress; 2nd Session, 2012.

[39] Savannah River Nuclear Solutions. Facts About the Savannah River Site: H Canyon, December 2010.

[40] Charles Messick, Charles Massey, and Tracy Mustin. U.S. Department of Energy Operational Experience with Shipments of Foreign Research Reactor Spent Fuel. Presented at 1998 International Meeting on Reduced Enrichment for Research and Test Reactors, October 1998.

[41] Nuclear Engineering Division at Argonne. Currently-Qualified Fuels : HEU Fuels in Use when the RERTR Program Began in 1978. URL `http://www.rertr.anl.gov/QualFuel.html`.

[42] Gerard Hofman and Mitchell Meyer. Design of High Density Gamma-Phase Uranium Alloys for LEU Dispersion Fuel Applications. *1998 International Reduced Enrichment for Test Reactor Conference*, Sao Paulo, Brazil:1–12, 1998.

[43] T.H. Newton, M.S. Kazimi, and E.E. Pilat. Development of a Low-Enriced-Uranium Core for the MIT Reactor. *Nuclear Science and Engineering*, 157:264–279, 2007.

[44] Thomas Dominic Ippolito. Effects of Uranium Enrichment on Nuclear Submarine Reactor Design. Masters thesis, Massachusetts Institute of Technology, May 1990.

[45] United States Department of Energy. Historical Records Declassification Guide: CG-HR-3, October 2005.

[46] Ronald O'Rourke. Navy Aircraft Carriers: Proposed Retirement of USS John F. Kennedy - Issues and Options for Congress, August 2006.

[47] Emilio Baglietto. Advanced LWRs Discussion. Class Lecture, November 2014.

[48] Ronald O'Rourke. Navy Arttack Submarine Force-Level Goal and Procurement Rate: Background and Issues for Congress, June 2004.

[49] Rick Grantom. Operational Risk Management for Nuclear Utilities. Class Lecture, June 2014.

[50] Ronald O'Rourke. Navy Virginia (SSN-774) Class Submarine Procurement: Background and Issues for Congress, July 2014.

[51] Ronald Allen Knief. Navy Ohio Replacement (SSBN[X]) Ballistic Missile Submarine Program: Background and Issues for Congress, February 2015.

[52] Kord Smith. Personal correspondance, May 2014.

[53] V. Memoli and A. Cammi. Evaluation of the Moderator Temperature Coefficient of Reactivity in a PWR. In *Excerpt from the Proceedings of the COMSOL Users Conference*. COMSOL, October 2007.

[54] Jaakko Leppänen. Performance of Woodcock Delta-Tracking in Lattice Physics Applications Using the Serpent Monte Carlo Reactor Physics Burnup Calculation Code. *Annals of Nuclear Energy*, 37:715–722, 2010.

[55] National Nuclear Data Center, March 2015. URL `www.nndc.bnl.gov`.

[56] Paul Roggenkamp. The Influence of Xenon-135 on Reactor Operation. Westinghouse Savannah River Company, 2000.

[57] U.S. Nuclear Regulatory Commission. Reactivity Balance Calculations, December 2012. ML11216A051.

[58] James Duderstadt and Louis Hamilton. *Nuclear Reactor Analysis*. John Wiley & Sons, Inc., 1 edition, 1976.

[59] Magdi Ragheb. *Nuclear Power - Deployment, Operation and Sustainability; Chapter 1: Nuclear Naval Propulsion*. InTech, September 2011.

[60] Manson Benedict, Thomas Pigford, and Hans Levi. *Nuclear Chemical Engineering, Second Edition*. McGraw-Hill Book Company, 1987.

[61] Dan Wachs, Francine Rice, Irina Glagalenko, Adam Robinson, Barry Rabin, and Mitch Meyer. Blister Threshold Based Thermal Limits for the U-Mo Monolithic Fuel System, October 2012.

[62] Gregor Bloch. Influence of Turbulence and Secondary Flow on the Subcooled Flow Boiling in characteristical Reactor Configurations, March 2015. URL `http://www.td.mw.tum.de/tum-td/de/forschung/themen/subcooled_flow_boiling`.

[63] Jacopo Buongiorno. Boiling crises in LWRs. Class Lecture, October 2013.

[64] Emilio Baglietto. TH Design Requirements Steady State and Trainsient Design. Class Lecture, October 2014.

[65] U.S. Nuclear Regulatory Commission. Davis-Besse Reactor Pressure Vessel Head Degredation: Overview, Lessons Learned, and NRC Actions Base on Lessons Learned, August 2008.

[66] Gary Wes, Janelle Wharry, Brian Frisbie, Brian Wirth, Dane Morgan, Julie Tucker, and Todd Allen. Assessment of radiation-induced segregation mechanisms in austenitic and ferritic-martensitic alloys. *Journal of Nuclear Materials*, 411:41–50, February 2011.

[67] Gary Wes. *Fundamentals of Radiation Materials Science*. Springer, May 2007.

[68] Jianwei Hu, A. Hayes, W. Wilson, and Rizwan-uddin. Fission Gas Production in Reactor Fuels Including the Effects of Ternary Fission. *Nuclear Engineering and Design*, 240:3751–3757, August 2010.

[69] Dan Gabriel Cacuci, editor. *Handbook of Nuclear Engineering: Nuclear Engineering Fundamentals*. Springer Science, 2010.

[70] Michael Short. How Things Fail: Corrosion. Class Lecture, February 2014.

[71] Rion Causey, Donald Cowgill, and Robery Nilson. Review of the Oxidation Rate of Zirconium Alloys, November 2005.

[72] U.S. Nuclear Regulatory Commission. U.S. Nuclear Regulatory Commission Regulations: Title 10, Code of Federal Regulations, February 2013.

[73] Todd Allen, Rudy Konings, and Arthu Motta. *Comprehensive Nuclear Materials*, volume Volume 5: Material Performance and Corrosion/Waste Materials. Elsevier, 2012.

[74] Gaurav Agarwal, Manoj Moharana, and Sameer Khandekar. Thermo-Hydrodynamics of Developing Flow in a Rectangular Mini-Channel Array. In Kannan Iyer, editor, *20th National and 9th International ISHMT-ASME Heat and Mass Transfer Conference*, pages 1342–1349, 2010.

[75] Abdekkatuf Yacout. Nuclear Fuel, April 2011.

[76] James Matos. Personal correspondance, September 2014.

[77] Nicholas Horelik and Bryan Herman. Benchmark for Evaluation And Validation of Reactor Simulations, October 2013.

[78] Lothar Wolf, Mujid Kazimi, and Neil Todreas. Introduction to Structural Mechanics. Class Notes, 2001.

[79] Kord Smith. Nuclear Reactor Physics II; Lecture 8: Heterogeneous Resonance Modleing. Class Lecture, March 2014.

[80] Anatoli Diakov, Alexander Dmitriev, Jungmin Kang, Alexey Shuvayev, and Frank von Hippel. Feasibility of Converting Russian Icebreaker Reactors from HEU to LEU Fuel. *Science and Global Security*, 14:33–48, December 2006.

[81] ASM Alloy Phase Database, April 2015. URL `http://www1.asminternational.org/AsmEnterprise/APD/`.

[82] A.M. Savchenko, A.V. Vatulin, A.V. Morozov, G.V. Kulakov, S.A. Ershov, A.V. Laushkin, S.V. Maranchak, Y.V. Konovalov, and E.K. Malamanova. Zirconium alloys matrix as innovative material for composite fuel. *Progress in Nuclear Energy*, 57: 138 – 144, 2012.

[83] Tom Newton. Fuel Characteristics. Technical Report, January 2014.

[84] A. Robinson, G. Chang, D. Keisher, and D. WacD. Wachs. Porter. Irradiation Performance of U-Mo Alloy Base 'Monolithic' Plate-Type Fuel - Design Selection, August 2009.

[85] M Meyer, J Gan, J Jue, D Keiser, E Perez, A Robinson, D Wachs, N Woolstenhulme, G Hofman, and Y Kim. Irradiation Performance of U-Mo Monolithic Fuel. *Nuclear Engineering and Technology*, 46(2):169–182, April 2014.

[86] Daniel Wachs, Curtis Clark, and Randall Dunavant. Conceptual Process Description for the Manufacture of Low-Enriched Uranium-Molybdenum Fuel, February 2008.

[87] D. Burkes, G. Mickum, and D. Wachs. Thermophysical Properties of U-10Mo Alloy, November 2010.

[88] Samuel Miller and Hakan Ozaltun. Evaluation of U10Mo Fuel Plate Irradiation Behavior via Numerical and Experimental Benchmarking. In *Proceeding of the ASME2012 International Mechanical Engineering Congress & Exposition*. ASME, November 2012.

[89] AZO Materials. Zircaloy-4 (alloy zr4) (uns r60804), June 2013.

[90] Franc Incropera, David DeWitt, Theordore Bergman, and Adrienne Lavine. *Introduction to Heat Transfer, 7th Edition*. John Wiley & Sons, Inc., 20011.

[91] Su Yongkang. Heat Transfer: Chapter 8, Internal Flow. Class Notes, Shanghai Jiao Tong University.

[92] Paul Reuss. *Neutron Physics*. Édition Diffusion Presse Sciences, September 1965.

[93] Magnus Holmgren. *X Steam for MATLAB*. x-eng, January 2006.

[94] United States Department of Energy. DOE Fundamentals Handbook, Nuclear Physics and Reactor Theory, 1993.

[95] T. Kim, W. Yang, T. Taiwo, and H. Khalil. Whole-Core Depletion Studies in Support of Fuel Sepecification for the Next Generation Nuclear Plant (NGNP) Core, July 2004.

[96] Curtiss Wright Flow Control Company: Engineered Pump Division. Naval Pump Solutions, March 2015. URL `http://epd.cwfc.com/`.

[97] U.S. Nuclear Regulatory Commission. *Reactor Concepts Manual: Nuclear Power for Electrical Generation*. USNRC Technical Training Center, 2012.

[98] Matthew Hawks. Maintenance Practices for Emergency Diesel Generator Engines Onboard United States Navy Los Angeles Class Nuclear SSubmarine. Masters thesis, Massachusetts Institute of Technology, June 2006.

[99] Bruce Munson, Donald Young, Theodore Okiishi, and Wade Huebsch. *Fundamentals of Fluid Mechanics*. John Wiley & Sons, Inc., 6 edition, 2009.

[100] Donald Schroeder. A Tutorial on Pipe Flow Equations, August 2001.

[101] Hamed Akhiani and Jerzy Szpunar. Effect of surface roughness on the texture and oxidation behavior of Zircaloy-4 cladding tube. *Applied Surface Science*, pages 832–839, September 2013.

[102] Forrest Brown. On the Use of Shannon Entropy of the Fission Distribution for Assessing Convergence of Monte Carlo Criticality Calculations. In *PHYSOR-2006 American Nuclear Society's Topical Meeting on Reactor Physics Organized and Hosted by the Canadian Nuclear Society*, September 2006.

[103] Claude Shannon. A Mathematical Theory of Communication. *The Bell System Technical Journal*, 27:379–423, July 1948.

[104] Jaakko Leppänen. *Serpent - a Continuous-energy Monte Carlo Reactor Physics Burnup Calculation Code: User's Manual*. VTT Technical Research Centre, March 2013.

[105] Kord Smith. Nuclear Reactor Physics II; Lecture 11: Reactor Control, Burnable Absorbers, Introduction to Lattice Physics. Class Lecture, March 2014.

[106] Patrick M. O'Leary and Dr. Michelle L. Pitts. Effects of Burnable Absorbers on PWR Spent Nuclear Fuel. In *Waste Magagement 2001 Symposium*, 2001.

[107] Amir Mesquita, editor. *Current Research in Nuclear Reactor Technology in Brazil and Worldwide*. InTech, 2013.

[108] Masayuki Kauchi and Yoichiro Shimazu. Optimal Burnable Poison-Loading in a PWR with Carbon Coated Particle Fuel. *Journal of Nuclear Science and Technology*, 40(1): 22–29, February 2012.

[109] M. Conner, Elvis Dominguez'Ontiveros, and Yassin Hassan. Hydraulic Benchmark Data for PWR Mixing Vane Grid. In *The 14th International Topical Meeting on Nuclear Reactor Thermal Hydraulics (NURETH-14)*, September 2011.

[110] Paul Romano and Benoit Forget. The OpenMC Monte Carlo Particle Transport Code. *Annals of Nuclear Energy*, 51:274–281, October 2012.

[111] V. Sinha, P. Hegde, G. Prasad, S. Pal, and G. Mishra. Development of UO_2/PuO_2 Dispersed in Uranium Matrix CERMET Fuel System for Fast Reactors. *Journal of Nuclear Materials*, 427:12–17, 2012.

[112] Brian Frost. *Nuclear Fuel Elements: Design, Fabrication and Performance*. Pergamon, January 1982.

[113] CDR Mark Jenkins. USS Los Angeles (SSN-688) First and Finest: Welcome Aboard. Pamphlet, 1999? (Document Providable if Requested).

[114] SSN-688 Los Angeles-Class Engineered Refueling Overhaul (ERO), April 2015. URL `http://www.globalsecurity.org/military/systems/ship/ssn-688-ero.htm`.

[115] Commanding Officer, USS Los Angeles (SSN 688). Submission of Command History for 1992, March 1993.

[116] Commanding Officer, USS Los Angeles (SSN 688). Submission of Command History for 1995, March 1996.

[117] Commanding Officer, USS Philadelphia (SSN 690). Command History, March 1993.

[118] Commanding Officer, USS Philadelphia (SSN 690). Command History, March 1995.

[119] www.uscarriers.net. USS Pittsburgh SSN 720, August 2013. URL `http://www.uscarriers.net/ssn720history.htm`.

[120] Portsmouth Naval Shipyard Public Affairs Office. USS San Juan Arrives at PNSY for Overhaul, April 2010.

[121] Portsmouth Naval Shipyard Public Affairs Office. Portsmouth Naval Shipyard Undocks San Juan Early, August 2011.

[122] Fire Extinguised on Nuclear Submarine in Maine. *CBS Boston*, May 2012.

[123] Rear Admiral Richard Brekenridge. USS Miami: A Tangible Impact to Readiness from Sequestration. *Navy Life*, August 2013.

[124] Defense Industry Daily Staff. France's Future SSNs: The Barracuda Class. *Defense Industry Daily*, February 2015.

[125] Ronald O'Rourke. Navy Virginia (SSN-774) Class Attack Submarine Procurement: Background and Issues for Congress, March 2015.

[126] Ronald O'Rourke. Navy Arttack Submarine Procurement: Background and Issues for Congress, April 2008.

[127] Portsmouth Naval Shipyard Public Affairs Office. PNSY Completes FFirst Ever Virginia-class Major Maintenance Availability, May 2012.

[128] Sam LaGrone. U.S. Navy Awards 'Largest Shipbuilding Contract' in Service History. *US Naval Institute*, April 2014.

[129] Federation of American Scientists. Naval Nuclear Propulsion: Assessing Benefits and Risks, The Report of an Independent Task Force, March 2015.

[130] Joachim Hofbauer, Gregory Sanders, Jesse Ellman, and David Morrow. Cost and Time Overruns for Major Defense Acquisition Programs, April 2011.

[131] International Atomic Energy Agency. Radioactive Waste Management, 2012.

[132] U.S. Nuclear Regulatory Commission. *Reactor Concepts Manual: Dose Standards and Methods for Protection Against Radiation and Contamination.* USNRC Technical Training Center, 2012.

[133] M. Joseph and P. Manoravi. Boron Isotope Enrichment in Nanosecond Pulsed Laser-Ablation Plume. *Applied Physics A: Materials Science & Processing*, 76:153–156, June 2002.

[134] M. Santala, A. Daavittila, H. Lauranto, and R. Salomaa. Odd-Isotope Enrichment Sudies of Gd by Double Resonance Laser Ionization for the Production of Burnable Nuclear Reactor Poison. *Applied Physics B: Lasers and Optics*, 64:339–347, October 1996.

[135] A. Rowcliffe, L. Mansur, D. Hoelzer, and R. Nanstad. Perspectives on Radiation Effects in Nickel-Based Alloys for Applications in Advanced Reactors. *Journal of Nuclear Materials*, 392:341–352, 2009.

[136] Lawrence Greenwood, Frank Garner, Brian Oliver, Martin Grossbeck, and W. Wolfer. Surprisingly Large Generation and Retention of Helium and Hydrogen in Pure Nickel Irradiated at High Temperatures and High Neutron Exposures. *ASTM Inernational*, 1:117–125, April 2004.